ISTANBUL TECHNICAL UNIVERSITY ★ GRADUATE SCHOOL

MODELING, SIMULATION AND IMPLEMENTATION OF A PERMANENT MAGNET SYNCHRONOUS MOTOR DRIVE SYSTEM USING ANFIS TECHNIQUE

M.Sc. THESIS

İpek KUVVETLİ

Department of Electrical Engineering

Electrical Engineering Programme

FEBRUARY 2022

ISTANBUL TECHNICAL UNIVERSITY ★ GRADUATE SCHOOL

MODELING, SIMULATION AND IMPLEMENTATION OF A PERMANENT MAGNET SYNCHRONOUS MOTOR DRIVE SYSTEM USING ANFIS TECHNIQUE

M.Sc. THESIS

İpek KUVVETLİ
(504171067)

Department of Electrical Engineering

Electrical Engineering Programme

FEBRUARY 2022

İSTANBUL TEKNİK ÜNİVERSİTESİ ★ LİSANSÜSTÜ EĞİTİM ENSTİTÜSÜ

SABİT MIKNATISLI SENKRON MOTOR SÜRÜŞ SİSTEMİ İÇİN ANFIS TEKNİĞİ KULLANARAK MODELLEME, SİMULASYON VE GERÇEKLEME

YÜKSEK LİSANS TEZİ

İpek KUVVETLİ
(504171067)

Elektrik Mühendisliği Anabilim Dalı

Elektrik Mühendisliği Programı

Tez Danışmanı: Prof. Dr. Lale Tükenmez ERGENE

ŞUBAT 2022

Ipek KUVVETLI, a M.Sc. student of ITU Graduate School student ID 504171067, successfully defended the thesis entitled "Modeling, Simulation and Implementation of a Permanent Magnet Synchronous Motor Drive System Using ANFIS Technique", which she prepared after fulfilling the requirements specified in the associated legislations, before the jury whose signatures are below.

Thesis Advisor : **Prof. Dr. Lale Tükenmez ERGENE** ....
İstanbul Technical University

Jury Members : **Prof. Dr. Güven Kömürgöz KIRIŞ** ....
Istanbul Technical University

Prof. Dr. Kamuran Nur BEKİROĞLU ....
Yildiz Technical University

Date of Submission : 14 January 2022
Date of Defense : 10 February 2022

To my father in heaven,

FOREWORD

I would like to express my deep appreciation to my thesis advisor Prof. Dr. Lale TÜKENMEZ ERGENE who has always encouraged and guided me throughout my thesis and tough times in my life.

I would also like to express my gratitude to Assoc. Prof. Dr. Ali Fuat ERGENÇ who contributed to the experimental process. Also, I would like to thank Res. Asst. Alper TAP for his great assistance and technical support.

I would like to acknowledge Istanbul Technical University for providing comprehensive theoretical and practical knowledge during the study.

Special thanks to Veysel ÇELİK who has always supported and motivated me as a true friend.

February 2022

Ipek KUVVETLI
(Electrical and Control Engineer)

TABLE OF CONTENTS

Page

ABBREVIATIONS

ADC	**:** Analog Digital Converter
ANFIS	**:** Adaptive Neuro Fuzzy Inference System
ANN	**:** Artificial Neural Network
BP	**:** Backpropagation
DOF	**:** Degree of Freedom
DTC	**:** Direct Torque Controller
FIS	**:** Fuzzy Inference System
FLC	**:** Fuzzy Logic Controller
FOC	**:** Field Oriented Control
PI	**:** Proportional-Integral
PMSM	**:** Permanent Magnet Synchronous Motor
PWM	**:** Pulse Width Modulation
RPM	**:** Revolution Per Minute

SYMBOLS

$\boldsymbol{B}$	: Damping
$\boldsymbol{R_s}$	: Stator resistance
$\mathbf{L_s}$	: Stator inductance
$\boldsymbol{i_d}$	: d-axis current
$\boldsymbol{i_q}$	: q-axis current
$\boldsymbol{\lambda_d}$	: d-axis flux linkage
$\boldsymbol{\lambda_q}$	: q-axis flux linkage
$\boldsymbol{\lambda_{pm}}$	: PM flux linkage
$\mathbf{L}_{\boldsymbol{d}}$	: d-axis inductance
$\mathbf{L}_{\boldsymbol{q}}$	: q-axis inductance
$\boldsymbol{p}$	: Number of pole pairs
$\boldsymbol{J}$	: Inertia
$\boldsymbol{T_e}$	: Electromechanical torque
$\boldsymbol{T_L}$	: Load torque
$\boldsymbol{\omega_m}$	: Rotor mechanical speed
$\boldsymbol{\omega_r}$	: Rotor electrical speed

LIST OF TABLES

Page

LIST OF FIGURES

Page

MODELING, SIMULATION AND IMPLEMENTATION OF A PERMANENT MAGNET SYNCHRONOUS MOTOR DRIVE SYSTEM USING ANFIS TECHNIQUE

SUMMARY

The Permanent Magnet Synchronous Motors are widely used in robotics, electricity, gas, oil and transportation, etc. The PMSM drive allows adjustable speed drives and enhanced speed and torque control. Since the motor has various advantages such as higher efficiency, improved torque to inertia ratio and high power density, the PMSM drive has become very popular in aerial and electrical vehicles, as well as military applications [1-3].

Compared to the DC motors, the Permanent Magnet Synchronous Motors have distributed windings and do not have a brush-commutator system. They provide reliable operation. However, these motors require advanced control techniques to drive.

Field Oriented Control (FOC) of PMSM is the most common method for the speed control of this motor. Employing Park and Clarke transformations, the control of the torque and flux of the motor is achieved by using appropriate field orientations which are dependent on phase currents in the stator. PMSM drive based on FOC combines the d-q-axis current control in the inner loop and the speed control in the outer loop[4]. The most significant requirements for the speed control of the PMSM are improved dynamic features and high-precision tracking performance [5].

The entire PMSM drive system is modelled using mathematical expressions of a PMSM and an inverter, the system is controlled with two different controllers and implemented through code generation in MATLAB/Simulink. The speed control with FOC method generally is integrated with a PI controller because of a simple design. As a drawback of a PI controller design for the PMSM, fine tuning of PI parameters is a challenging task since the linearization is utilized to converge the value of a function at a particular point.

The parameter variations and disturbances cause undesired uncertainties in the non-linear model of the PMSM and the complexity is increased. The most of linear control methods cannot fulfill the requirements in high-performance applications of PMSM drives. To enhance the dynamic response of the PMSM control system, several advanced non-linear control methods have been studied and applied in academic and commercial fields recently, such as: linearization control [6], adaptive control [7,8], sliding mode control [9, 10], fuzzy control [11] and neural network control [12, 13].

In this study, to obtain extended dynamic characteristics for the speed control, a conventional PI controller is replaced by an Adaptive Neuro Fuzzy Inference System (ANFIS) controller. Unlike PI control, ANFIS can approximate to the whole system dynamics if it is well-trained.The ANFIS controller consists of a Neural Network and a Fuzzy Inference System and it can learn and adapt to the entire system.

In this thesis, speed control via FOC is studied using two methods; a conventional PI controller and an Adaptive Neuro Fuzzy Inference System (ANFIS) controller. The proposed ANFIS controller requires the extraction of training data from a PMSM dynamic model with a conventional PI controller. The simulation of both controllers in Simulink environment is performed.

The hardware to drive the PMSM at low voltage is chosen as a development kit which is compatible with the Simulink Code Generation. The control system implementation with an encoder sensor is also explained in this study.

Simulation and experimental results show that the speed controller of an ANFIS controller has better dynamic response compared to a conventional PI controller in terms of the settling time and overshoot. However, it is observed that the off-line training of ANFIS controller causes some steady-state error.

SABİT MIKNATISLI SENKRON MOTOR SÜRÜŞ SİSTEMİ İÇİN ANFIS KULLANARAK MODELLEME, SİMULASYON VE GERÇEKLEME

ÖZET

Daimi Mıknatıslı Senkron Motorlar (PMSM) robotik, elektrik, gaz, petrol ve ulaşım gibi birçok alanda kullanılmaktadır. PMSM sürücüsü, ayarlanabilir hız sürücülerine ve gelişmiş hız ve moment kontrolüne olanak tanır. Motorun daha yüksek verim, geliştirilmiş moment/eylemsizlik oranı ve yüksek güç yoğunluğu gibi çeşitli avantajları olduğundan, PMSM sürücüsü, askeri uygulamaların yanı sıra hava ve elektrikli araçlarda da çok popüler hale gelmiştir [1-3].

Klasik doğru akım motorlar ile karşılaştırıldığında dağıtık sargıya sahip olan Daimi Mıknatıslı Senkron Motorlar, fırça ve kollektör sistemi içermez ve güvenilir bir işletme sağlar. Ancak bu motorları sürmek için ileri kontrol teknikleri gerekir.

PMSM'nin Alan Uyarmalı Vektör Kontrolü (FOC), motorun hız kontrolü için en çok kullanılan yöntemdir. Park ve Clarke dönüşümleri ile beraber, statordaki faz akımlarına bağlı olan uygun alan yönelimleri kullanılarak moment ve akının kontrol edilmesi sağlanır. Alan Uyarmalı Vektör Kontrolü tabanlı PMSM sürücüsü, iç döngüde d-q ekseni akım kontrolünü ve dış döngüde hız kontrolünü birleştirir[4]. PMSM hız kontrolü için en önemli gereksinimler, gelişmiş dinamik karakteristikler ve yüksek hassasiyetli izleme performansıdır [5].

Tüm PMSM sürücü sistemi, PMSM ve eviricinin matematiksel ifadeleri kullanılarak modellenmiştir, sistem iki tip kontrolör ile kontrol edilip MATLAB/Simulink'te kod üretimi ile gerçeklenmiştir . Vektör kontrolü yöntemiyle hız kontrolü, basit bir tasarım nedeniyle genellikle bir PI kontrolör ile entegre edilir. PMSM için, PI kontrolörde bir fonksiyonun değerine belirli bir noktada yakınsamak için doğrusallaştıma kullanıldığından PI parametrelerinin ince ayarı zorlu bir görev olması bir dezavantajdır.

Parametre değişimleri ve dış bozucular, PMSM'nin doğrusal olmayan modelinde istenmeyen belirsizliklere neden olur ve karmaşıklık artar. Doğrusal kontrol yöntemlerinin çoğu, PMSM sürücülerinin yüksek performanslı uygulamalarında gereksinimleri karşılayamaz. PMSM kontrol sisteminin dinamik yanıtını geliştirmek için, son zamanlarda akademik ve endüstriyel alanlarda doğrusallaştırma kontrolü [6], adaptif kontrol [7,8], kayan kip kontrolü [9, 10], bulanık kontrol [11] ve sinir ağı kontrolü [12, 13] gibi birkaç gelişmiş doğrusal olmayan kontrol yöntemi geliştirilmiş ve uygulanmıştır.

Bu çalışmada, hız kontrolü için gelişmiş dinamik özellikler elde etmek için geleneksel bir PI kontrolör, Adaptif Sinir Ağları Bulanık Girişim Sistemi (ANFIS) kontrolörü ile değiştirilmiştir. İyi eğitilmiş bir ANFIS kontrolör doğrusal olmayan sistem kontrolünde daha iyi performans sonuçları verebilmektedir. ANFIS kontrolörü bir Sinir Ağı ve bir Bulanık Girişim Sisteminden oluşur ve sistem dinamiklerini öğrenip tüm sisteme uyum sağlayabilir.

Bu tezde, alan uyarma ile hız kontrolü, iki yöntem kullanılarak incelenmiştir; Geleneksel bir PI kontrolörü ve Adaptif Sinir Ağları Bulanık Girişim Sistemi (ANFIS) kontrolörü. Önerilen ANFIS kontrolörü, geleneksel bir PI kontrolörü ile bir PMSM dinamik modelinden eğitim verilerinin çıkarılmasını gerektirir. Simulink ortamında her iki kontrolörün benzetimi tamamlanmıştır.

Alçak gerilimde PMSM'yi sürebilecek donanım, Simulink Kod Üretimine uygun bir geliştirme kiti olarak seçilmiştir. Çalışmada bir enkoder algılayıcı ile ilgili kontrol sistemi uygulaması anlatılmaktadır.

Benzetim ve deneysel sonuçlar, bir ANFIS tabanlı hız kontrolörünün, yerleşim süresi ve aşım açısından geleneksel bir PI kontrolörle karşılaştırıldığında daha iyi dinamik yanıta sahip olduğunu göstermektedir. Ancak, ANFIS kontrolörünün çevrim dışı eğitiminin sürekli hal hatasına neden olduğu gözlemlenmiştir.

1. INTRODUCTION

In recent years, AC drives in aerial and electric vehicles have gained attention due to energy cost, global warming threat, high energy demand and population [14]. As the urban air mobility has been increasing day by day, environmental issues such as CO_2 emissions has emerged. Aircraft applications requires high reliability, high power density and increased efficiency with weight saving and reduced torque and CO_2 emissions [15]. The Permanent Magnet Synchronous Motors meet the requirements of the aircraft applications and electric vehicles by offering reduced fuel consumption, high power density and clean energy. The conventional propulsion systems has been declining in popularity gradually with the developing technology. Considering the technology assessment, Hybrid Electric VTOL Aircrafts in the aviation have come into prominence [16].

The Permanent Magnet Synchronous Motors enable adjustable speed drives and advanced speed and torque control. Many control techniques of the PMSM drive are proposed in academic and commercial fields. The most popular control method of the PMSM drive is Field Oriented Control (FOC). The FOC technique of PMSM drive consists of a speed controller and a d-q-axis current controller. Since the speed controller is in the outer loop, its frequency is lower than the current control. Therefore, this study is carried out with a speed control via FOC.

The FOC incorporates Park and Clarke Transformations which enable conversion from the stator frame into the rotor frame. The vector transform is explained in detail. In addition, a dynamic model of the entire drive system provides estimation of the system response before the setup. A conventional FOC methodology is based on PI controller.

This study focuses on two types of speed controllers: A conventional PI controller and an ANFIS controller. Firstly, a PI controller with FOC is designed for the high-precise speed tracking. To adjust PI parameter, design criteria are determined. Then, the ANFIS controller is introduced as a speed controller. The proposed ANFIS controller requires the extraction of training data from a PMSM dynamic model with a conventional PI controller. The simulation results are examined in terms of the overshoot, steady state error and settling time.

Implementation of the drive system requires extreme coding ability and experience. However, Mathworks developed an interface to build and deploy code into microcontrollers by using Motor Control Blockset and Embedded Coder to generate C code [17]. The experimental results are obtained with non-complex communication interface in MATLAB/Simulink. The performance results of the both controllers are illustrated, compared and analysed in simulation environment and real-time tests.

1.1 Purpose of Thesis

The goal of this thesis is to model the entire PMSM drive system using mathematical expressions of the motor and inverter, design two different controllers, which are a conventional PI controller and an ANFIS controller, and implement a drive system in MATLAB/Simulink environment.

Simulation of the drive system and code-building and deployment to the microcontroller with Serial Communication Interface through USB cable are explained.

Comparative performance analysis of two types of speed controllers is conducted. The performance results of the simulation and the real time for both controllers under various operating conditions are evaluated in MATLAB environment.

1.2 Literature Review

In [18], the authors investigated PMSM technology. Regarding the equivalent electrical circuits for PMSMs, they presented the comparison of the calculated parameters and the measured experimental parameters associated with laboratory studies.

In [19], the authors declared that IPMSMs had an advantage of an adjustable speed operation, which is distinguishable feature compared to other AC machines types. Due to high motor and inverter efficiencies, high power density of robust machines was achieved. The relationship between the buried magnet design and the motor's electromagnetic characteristics are evaluated. A reluctance torque expression are substituted into the IPM motor's torque equation and the rotor magnetic saliency led the increment in the quadrature-axis inductance. In order to design comprehensive torque control, the control of sinusoidal phase currents in magnitude and phase angle depending on the rotor orientation is studied. In this concept, the current vector torque control is integrated with a feed forward algorithm and current control structure is saturated at high speed. Simulations and measurements of this machine are shown and discussed.

In [20], the authors focused on the Permanent Magnet motor drives dividing into two groups: Permanent Magnet Synchronous Motor drives (PMSM) and Brushless DC Motor (BLDC) drives. The PMSM produces constant torque with sinusoidal stator currents and it has a sinusoidal back EMF. The BLDC produces constant torque with rectangular stator currents and it has a trapezoidal back EMF. Unlike the wound rotor synchronous motor, the Permanent Magnet Synchronous Motor is excited by a PM. By referring rotor reference frame for the PMSM, the circuit model does not include damper windings and field oriented control of a drive system is designed.

In [21] the authors continued to their studies related with modeling, simulation and analysis of a drive of the PMSM. This study consists of state space expressions of the motor and the speed control design. The models of the inverter and vector controller are implemented in real time. This PMSM model is correlative to the wound rotor synchronous motor. All the equations were expressed in the rotor reference frame. Damper windings are removed in the equivalent circuit by considering a motor driven with field-oriented control. The PWM is included in the study. In addition, the hysteresis current controller is analysed. Torque and speed characteristics are evaluated and experimentally verified.

In [22], the authors mainly interested to increase efficiency in permanent magnet (PM) synchronous motor drives. The optimal control of the current could reduce the electrical losses included copper losses and iron loss. In this control algorithm concept, the optimal current vector is determined regarding the nominal speed and the load conditions. This control algorithm is also implemented via a digital signal processor. At the final step, computer simulations and experimental results are presented.

In [23], the authors studied the both of the Surface-Mounted PMSM and interior type PMSM. According to the changes depending on the magnetic parameters and losses, the derivation of a two-axis circuit model for permanent magnet synchronous motor

(PMSM) is investigated. A method for on-line parameter identification scheme without loading is presented. To achive the high-fidelity of the dynamic parameters and saturation constants while as the dynamic parameters change, test schemes are built.

In [24], the authors worked on a flux-weakening design for an Interior type Permanent Magnet Synchronous Motor (IPMSM). It is considered that PWM inverter is cascaded with a PI current controller and the current controllers are saturated considering the rated voltage. Disregarding the machine parameters, this flux weakening mechanism provides current control at determined extended range with the good performance dynamics. Under different operation conditions, effects of tuning parameters on this control design are analysed.

In [25], the authors proposed different types of synchronous motors and distinguished them from the induction motors. The Permanent Magnet motor model is based on salient pole synchronous motor. All the equations are given in matrix form and expressed in synchronously rotating reference frame. The equivalent circuit included damper windings. A constant current source is utilized for the representation of the PM. Vector control via voltage fed inverter are also added.

In [26], the authors proposed an efficiency optimization method for vector-controlled interior type PMSM drive. A loss reduction condition that affects the optimal q-axis current is analysed theoretically. Test results are verified to improve the proposed method.

In [27], the authors presented a modular control technique to a PMSM speed control. The modular approach enabled the empowered intelligent and robust control modules to easily replace any existing module which is out of order, while as the other modules are still undamaged for the operation. The module comprises a conventional PI speed control module, reference current module and PI current control module. When PMSM is operated in high-performance servo condition the torque pulsation cannot be neglected. Therefore, the torque ripples is reduced with an internal model in the feed-through path. In this design, the reference current-generating module is replaced by an iterative learning control (ILC) module. So as to obtain better dynamics in torque response, a torque estimation module with a gain-shaped sliding-mode observer is required to provide torque learning control. Also, the real-time implementations and experimental responses are compared at the end.

In [28], a new modeling tool is invented to focus on the electrical systems simulation of the automotive industry. PSIM enables to examine the dynamics of power electronic converters and motor drives in simulation environment.

In [29], MATLAB introduced the AC6 block of SimPowerSystems library in Simulink environment. It involved a PMSM drive model with a braking chopper. A PWM voltage source inverter with universal bridge block is connected to the inputs of the PM synchronous motor. The speed control loop required a PI regulator to produce the flux and torque references for the vector control block which computed the three reference motor line currents incorporating the flux and torque references and then fed the motor with these currents using a three-phase current regulator.

In [30], MATLAB shared an example of a Permanent Magnet Synchronous Motor fed by PWM inverter. The PWM inverter is created by using Simulink library. The inverter output is directly connected to Controlled Voltage Source blocks to obtain the reference stator voltages. Two control loops are designed: The inner loop is used to control the currents. The aim of the outer loop is to control the motor speed.

In [31], the authors presented a novel based on the On-line estimation of permanent magnet flux linkage ripple for PMSM with a Kalman filter. To provide more comprehensive and robust control, the permanent magnet flux linkage value without uncertainty is required. For stator flux estimation and the observer, the rotor flux linkage is accepted as an already-known constant parameter. However, the rotor flux linkage is fluctuated in some conditions. So, Kalman filter based on a rotor flux linkage observer is proposed. A three order Kalman filter is presented. In Surface Mounted PMSM, the rotor flux linkage of the motor could be obtained by using the d-axis inductance equal to the q-axis inductance. The results of the designed observer, which are satisfactory, are compared in the simulation environment and testing.

In [32], the authors conducted a study related to the field oriented vector control for PMSM drives with space vector modulation. The field oriented vector control for the speed control of the PMSM is used to generate a q-axis current command depending on the speed control signals. The simulation allowed to examine motor dynamic behaviors under transient and steady state conditions. This study includes

MATLAB/Simulink implementations of the vector control with related current controllers. The real-time results of the Permanent Magnet Synchronous Motor control using a DSP board are given. The speed control of the PMSM is achieved in the constant torque region. All the performance results are evaluated at the end.

In [33], the authors proposed a study of a modeling method for Interior Permanent Magnet (IPM) synchronous machines. After the experimental results based on dyno-testing, a stator winding flux linkage table is filled in this modeling method. The relationship between computer simulation and dyno-testing, high fidelity nonlinear behavior of IPMSM could be analysed.

In [4], the authors studied the speed sensorless Field Oriented Control (FOC) of PMSM supplied by a space vector pulse width modulation (SVPWM). The PMSM mathematical model is combined with Adaptive Neuro-Fuzzy Inference System (ANFIS) and Model Reference Adaptive System (MRAS) algorithms under different speed and load torque conditions. The results are given and desired efficiency of the entire drive system for the different scenarios is achieved.

In 2020, Mathwork [17] introduced Motor Control Blockset enabling designs and implementations of motor control algorithms. Motor Control Blockset allows creating, tuning field-oriented control and other algorithms for BDCM and PMSMs. It is declared that verification of control algorithms in closed-loop simulation integrated with the motor and inverter models in the blockset. This Blockset gives opportunity to generate C code with appropriate execution rates for the implementation.

1.3 Hypothesis

The nonlinearity in the PMSM makes the conventional PI parameters tuning a challenging task and especially high power applications with a PI controller leads an undesired overshoot. When the non-linear motor structure is exposed to unavoidable uncertainties and external disturbances, the most linear control methods cannot meet the requirements [34]. In recent years, many advanced non-linear control methods which allow more comprehensive dynamics are proposed. One of them is an ANFIS controller. The data collected from the reference model of the PMSM is imported to the ANFIS. The well-trained ANFIS controller shows more robust performance in terms of overshoot and settling time [35].

2. PERMANENT MAGNET SYNCHRONOUS MOTOR

A Permanent Magnet Synchronous Motor (PMSM) needs permanent magnets to generate the air gap magnetic field instead of the electromagnets. According to the construction design of the PMSM rotor, permanent magnets can be located on the rotor surface (Surface mounted Permanent Magnet Synchronous Motor-SPMSM) or inside the rotor (Interior type Permanent Magnet Synchronous Motor-IPMSM).

PMSMs are also grouped by the direction of the field flux: Radial field flux and axial field flux. The radial field flux which is along the radius of the motor is mostly preferred in the motors. The axial field flux is perpendicular to the radius of the motor and this type motor technology is used rarely.

The material selection of the permanent magnet associates the performance of the motor. AlNiCo (Aluminum-nickel-cobalt), Ceramic (ferrite) and rare-earth materials are generally used permanent magnet types for the electric motors. In recent years, the rare earth magnets such as Samarium Cobalt (SmCo) and Neodymium Iron Boron (NdFeB) have been come into prominence due to their high flux density.

2.1 Mathematical Model of PMSM

PMSMs are classified into two main type: Internal-mounted magnets with saliency, and Surface mounted magnets without saliency. In the Interior type Permanent Magnet Synchronous Motors, a variable reluctance which changes with the rotor angle exists. Unlike the Interior type Permanent Magnet Synchronous Motors, the surface-mounted Permanent Magnet Synchronous Motors have a fixed reluctance for any rotor angle because of a uniform airgap and the direct axis inductance is equal to the quadrature axis inductance.

This thesis study focused on the surface mounted synchronous machine. The mathematical model of the PMSM is proposed in this section.

A cross section of the rotor and stator of a PMSM has characteristics of two-pole and three phase is shown in Figure 2.1. This representation is more simplex so two pole PMSM is preferred for the illustration. The d-q notations of a PMSM drive system represent a rotor reference frame. The angle between the rotating d-axis and the stator axis is θ_r. Since PMSM is a synchronous motor, the rotor and stator magnetomotive force rotates at the same speed.

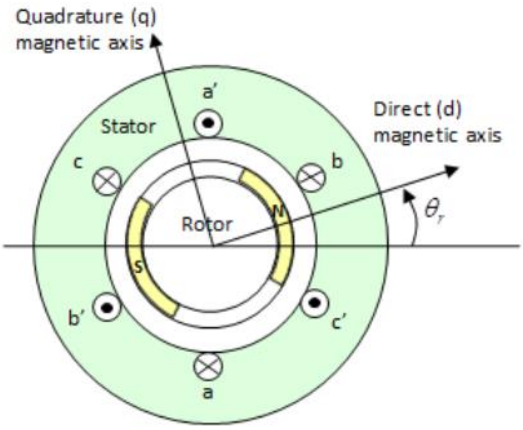

Figure 2.1: Cross section of the two pole PMSM [39].

When creating the mathematical model of the PMSM, the following assumptions are considered [40]:

-The saturation of the electric motor core is ignored.

-Turbulent flow, Eddy currents and hysteresis losses of electric motor are disregarded.

-PMSM has symmetrical three phase sinusoidal current.

-Induced EMF is sinusoidal in nature.

The main voltage expressions for the PMSM in the d-q axis is given in Equation 2.1 and Equation 2.2. The zero axis components are neglected as wye-connected stator windings are supplied with the balanced three phase.

$$u_d = R_s i_d - \omega_r \lambda_q + \frac{d\lambda_d}{dt} \tag{2.1}$$

$$u_q = R_s i_q + \omega_r \lambda_d + \frac{d\lambda_q}{dt} \tag{2.2}$$

Here, d and q stand for the direct axis and the quadrature axis component of the variables respectively.

The flux linkage expressions related d-q axis reference frame are:

$$\lambda_d = L_d i_d + \lambda_{pm} \tag{2.3}$$

$$\lambda_q = L_q i_q \tag{2.4}$$

For surface mounted PMSM, the d-axis inductance is equal to q-axis inductance.

The developed voltage expressions for the PMSM in the d-q axis are given as follows:

$$u_d = R_s i_d + L_s \frac{di_d}{dt} - \omega_r L_s i_q \tag{2.5}$$

$$u_q = R_s i_q + L_s \frac{di_q}{dt} + \omega_r (L_s i_d + \lambda_{pm}); \tag{2.6}$$

where R_s is the stator resistance, L_s is the stator inductance, ω_r is the rotor electrical speed and λ_{pm} is the permanent magnet flux.

The equivalent circuit of PMSM is illustrated in Figure 2.2.

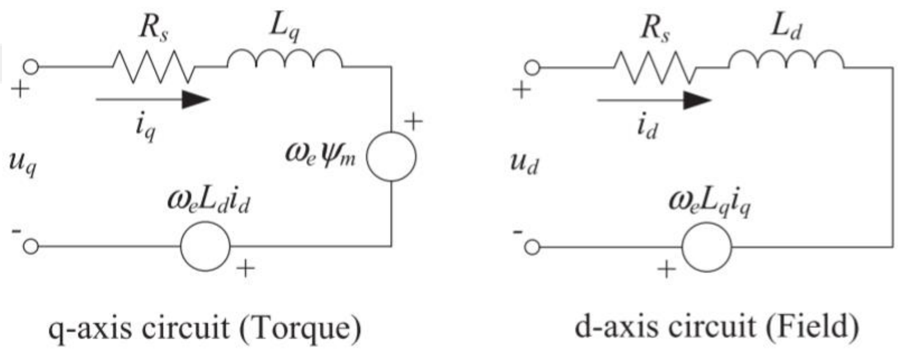

Figure 2.2 : Equivalent circuit of PMSM [41].

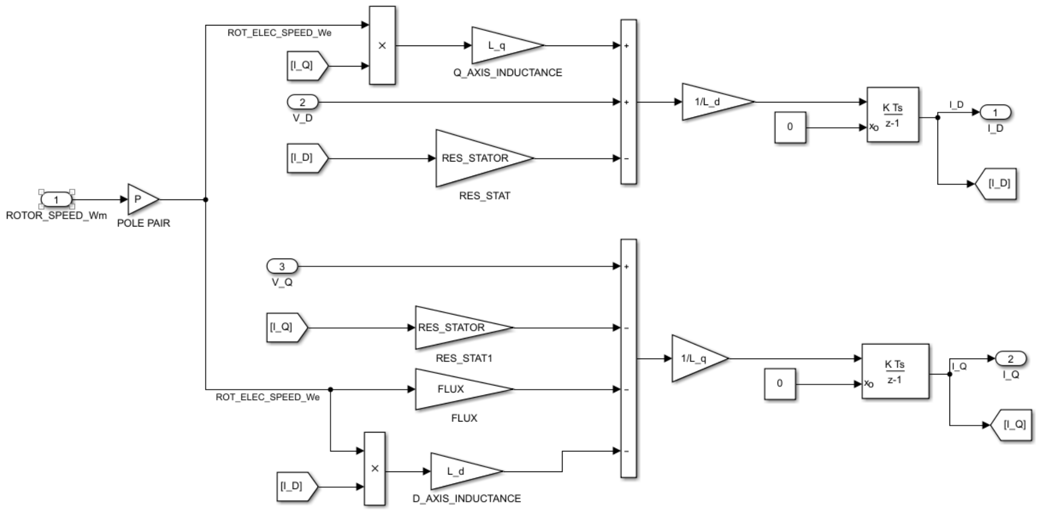

Figure 2.3 : PMSM electrical circuit model.

The PMSM electrical circuit model is illustrated in Figure 2.3. The electromagnetic torque of the machine is calculated as follows:

$$T_e = \left(\frac{3}{2}\right) p\left(\lambda_d i_q - \lambda_q i_d\right) \tag{2.7}$$

Substituting Equation 2.3 and Equation 2.4 into Equation 2.7, the Equation 2.8 is obtained. The developed electromagnetic torque modelled in Simulink is shown in Figure 2.4.

$$T_e = \left(\frac{3}{2}\right) p\left(\lambda_{pm} i_q - (L_q - L_d) i_q i_d\right) \tag{2.8}$$

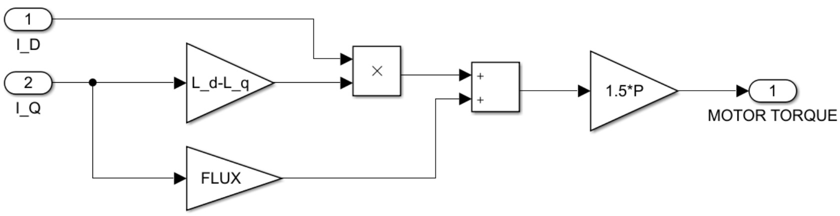

Figure 2.4 : Electromagnetic torque model.

Since this type motor has no saliency, d and q axis inductances are equal. T_L is the load torque. *B* and *J* are expressed as damping and inertia, respectively. *p* is pole pair. ω_m is motor mechanical speed. The developed electromagnetic torque expression is obtained as follows:

$$T_e = \left(\frac{3}{2}\right) p\, \lambda_{pm} i_q \tag{2.9}$$

$$T_e = T_L + B\omega_m + J\frac{d\,\omega_m}{dt} \tag{2.10}$$

$$\omega_m = \frac{\omega_r}{p} \tag{2.11}$$

The electromagnetic torque derived from ω_m, B, J and T_L is shown in Figure 2.5.

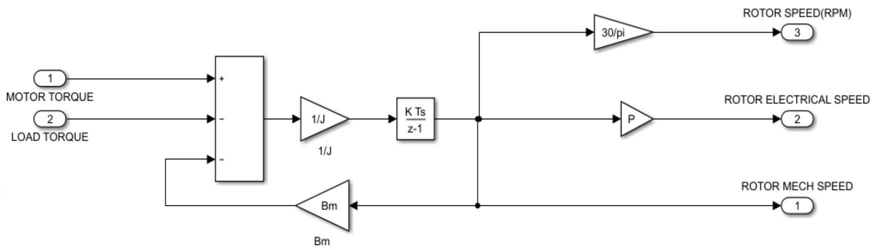

Figure 2.5 : General torque-speed model.

The electrical symbols and their SI units are given in Table 2.1.

Table 2.1 : Electrical symbols and SI units.

Symbols	Units
B	$Nm/rad/s$
R_s	$Ohm(\Omega)$
$\mathrm{L_s}$	$Henry\ (H)$
i_d, i_q	$Amper(A)$
$\lambda_d, \lambda_q, \lambda_{pm}$	$Weber\ (Wb)$
$\mathrm{L}_d, \mathrm{L}_q$	$Henry\ (H)$
p	$-$
J	Kgm^2
T_e, T_L	Nm
$\omega_m,\ \omega_r$	rad/s

The entire PMSM model is shown in Figure 2.6.

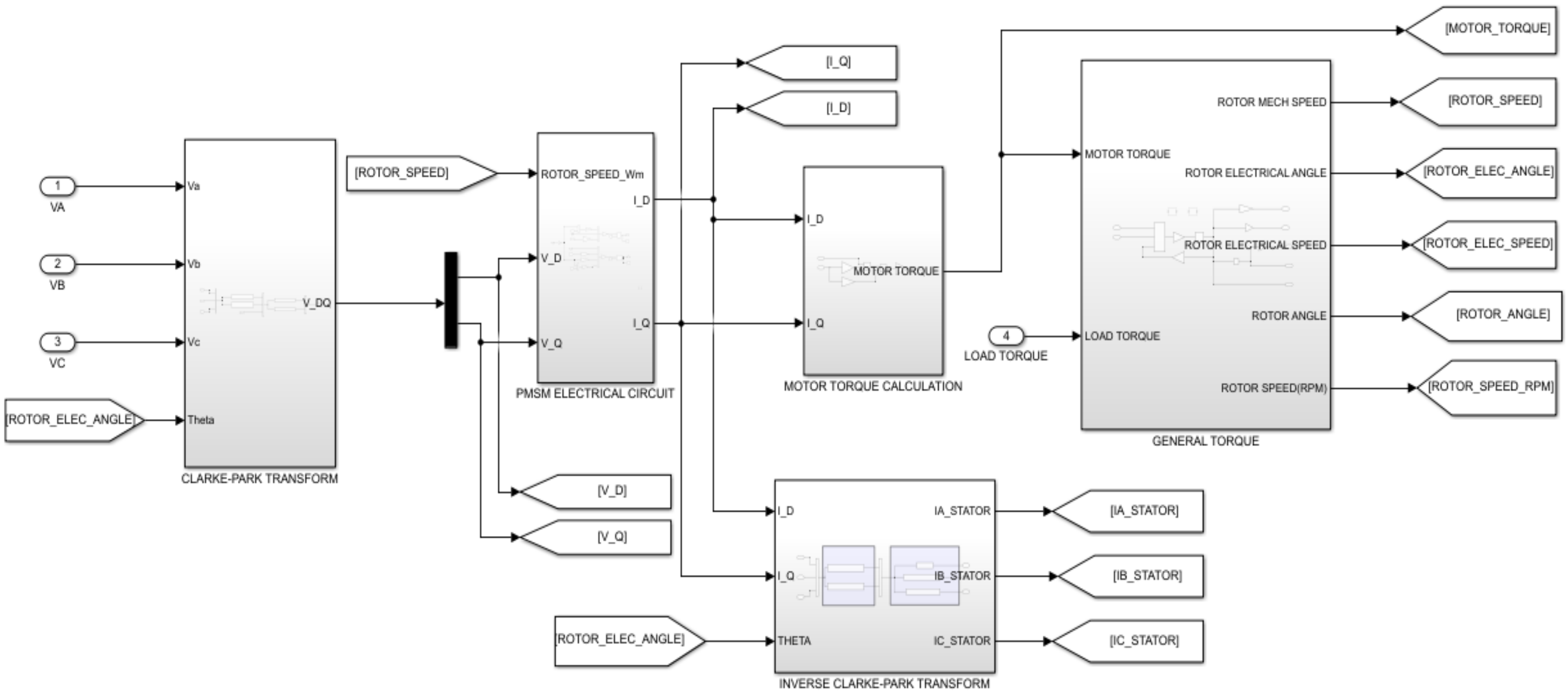

Figure 2.6 : PMSM model.

3. PMSM CONTROL ALGORITHMS

The PMSM control techniques mainly comprise scalar and vector control methods as seen in Figure 3.1.

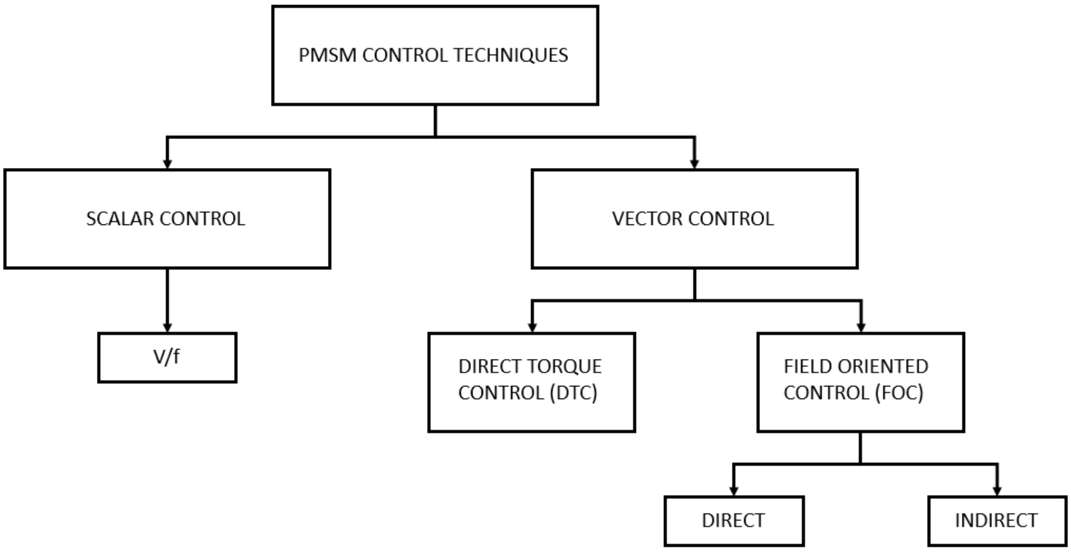

Figure 3.1 : Some common PMSM control techniques.

3.1 Scalar Control

This method is generally performed in variable speed applications where the angular speed is unknown through the open loop. This control method is typically implemented in pump and fan drives and also low-cost drives.

In the scalar control method, the magnitude of voltage is varying with the frequency in a constant ratio. The main advantage of this method is to allow the motor operation in a sensorless mode since this algorithm does not require the angular speed or the actual rotor position. However, this control technique is applied only in steady-state operation of the motor, the transition processes of the technique result in increased torque ripples and high speed fluctuations.

3.2 Vector Control

The vector control techniques enable to control the both of the motor flux and torque via stator currents. This technique ensures high accuracy, an extended speed range, fast response and minimized losses. Compared to the scalar control, these methods are much more complex as they need sensors, high measurement accuracy and many real-time calculations.

The most commonly used vector control techniques of PMSM are Field Oriented Control (FOC) and Direct Torque Control (DTC).

In Field Oriented Control, the direct axis component is adjusted to zero and this method provides to control motor flux and torque seperately and the permanent magnet magnetic field is aligned in the direction of the d-axis. This causes the linear relationship between torque and the q-axis current component. FOC is very popular method for Surface mounted PMSM. However, regarding reactive torque component, FOC algorithm may not be effective for Interior type PMSM.

Direct Torque Control does not require the coordinate system transformation and stator flux and electromagnetic torque are controlled directly. Although the DTC prevents computational burden and it can be used without a speed sensor, torque and current ripples are relatively higher compared to FOC method.

There are essentially two common methods of vector control of FOC: Direct (feed-back method) and Indirect (feed forward method). In the direct FOC, the rotor angle is obtained by the terminal voltages and currents. In the indirect FOC, the rotor angle is determined by using rotor position measurement and machine parameter estimation.

Field-weakening operation provides to increase speed range. The operation voltage of the motor is limited by the inverter and the current controller is saturated. In order to operate the motor at higher speed than the rated speed, the flux-weakening control should be performed. The d-axis current cannot be ignored for the operation principle.

The direct FOC-based vector control is suitable to a low voltage SPMSM that is studied in the thesis. Beside the conventional PI controller, the ANFIS controller can be combined with FOC to design the high-peformance speed controller.

4. FIELD ORIENTED CONTROL

Field oriented control of PMSM is extensively performed in vector control method. The purpose of FOC is to control the torque and flux using appropriate field orientations via controlling phase currents in the stator.

Field Oriented Control requires the stator currents and the rotor angle values to regulate the motor torque and the flux easily. This method mostly results in reduced torque ripple and fast response.

This technique consists of two current controllers. One of two current controllers is related to the direct axis component. Other is the quadrature axis component based. It also needs one speed controller. Speed control in FOC of PMSM can be performed by various control techniques. To drive dynamic model in Simulink, the control techniques are investigated. Two control methods are applied in the speed controller: PI controller and ANFIS Controller.

Firstly, Field Oriented Control using d-q transformation is introduced briefly. This method incorporates Park and Clarke transformations presenting how voltages and currents are transformed from one reference frame to another reference frame.

FOC diagram is illustrated in Figure 4.1.

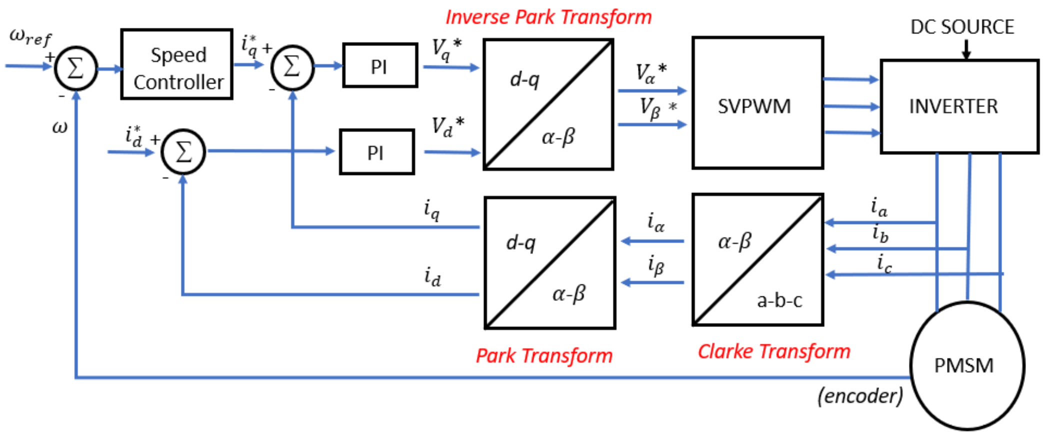

Figure 4.1 : FOC diagram.

4.1 Dynamic Direct and Quadrature Axis Transforms

In three phase motors, they have distributed windings. The stationary reference frame includes three phase quantities which are at fixed angles, despite their amplitude is changing with a time. The differential part related to the vectors varies with a time during rotation of the system. Therefore, fluxes, currents, induced voltages and flux linkages are varying and the control of the model is getting complex to model. For simplicity, a mathematical conversion is required to solve mathematical equations by using a common reference frame. Park and Clarke transformation allows study this vector control on a common reference frame [36,37].

Clarke and Park transformation is mostly used in PMSM vector control techniques.

To understand this transform, electrical quantities are interpretated and given in Table 4.1. Vector representation in different frames is shown in Figure 4.2.

Table 4.1 : Electrical quantities and interpretations.

Quantities	Interpretation
V_{abc}, I_{abc}	Three phase reference frame
$V_{\alpha\beta}, I_{\alpha\beta}$	Orthogonal stationary reference frame
V_{dq}, I_{dq}	Rotating reference frame

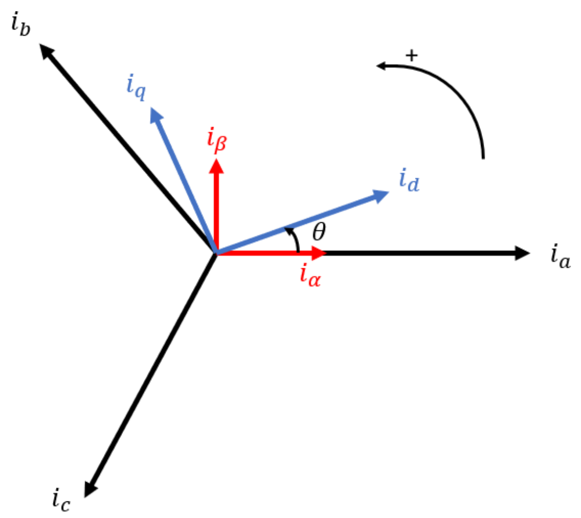

Figure 4.2 : Electrical quantities in different coordinate systems.

4.1.1 Clarke Transform

As a general operation of Clarke Transform, three phase quantities in a three phase coordinate system are converted into the two-phase quantities of an orthogonal stationary coordinate system using Equation 4.1 and Equation 4.2.

$$V_\alpha = \frac{2}{3}V_a - \frac{1}{3}V_b - \frac{1}{3}V_c \quad (4.1)$$

$$V_\beta = \frac{1}{\sqrt{3}}(V_b - V_c) \quad (4.2)$$

4.1.2 Park Transform

Two axis quantities of an orthogonal coordinate system are converted into two-axis quantities of a rotating coordinate system with Equation 4.3 and Equation 4.4.

$$V_d = V_\alpha \cos\theta + V_\beta \sin\theta \quad (4.3)$$

$$V_q = -V_\alpha \sin\theta + V_\beta \cos\theta \quad (4.4)$$

Clarke-Park transform is depicted in Figure 4.3.

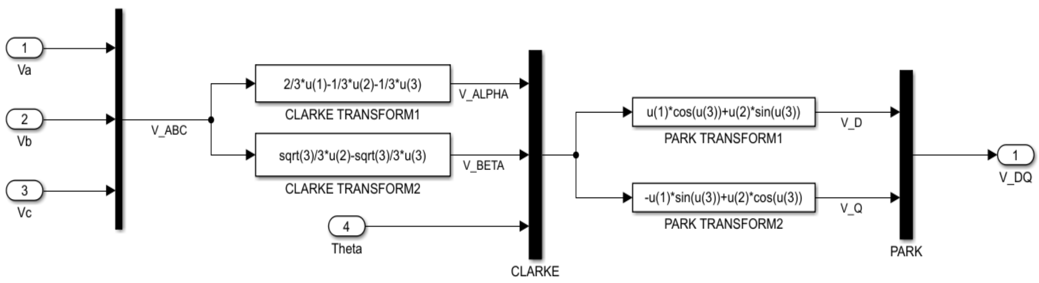

Figure 4.3 : Clarke-Park transform model.

4.1.3 Inverse Park Transform

Two axis quantities in a rotating coordinate system are converted into two axis quantities of an orthogonal stationary coordinate system using Equation 4.5 and and Equation 4.6.

$$I_\alpha = I_d \cos\theta - I_q \sin\theta \quad (4.5)$$

$$I_\beta = I_d \sin\theta + I_q \cos\theta \quad (4.6)$$

4.1.4 Inverse Clarke Transform

Two axis quantities of an orthogonal coordinate system are converted into three-phase quantities of a stationary coordinate system with Equation 4.7, Equation 4.8 and Equation 4.9.

$$I_a = I_\alpha \tag{4.7}$$

$$I_b = \frac{-I_\alpha + \sqrt{3}I_\beta}{2} \tag{4.8}$$

$$I_c = \frac{-I_\alpha - \sqrt{3}I_\beta}{2} \tag{4.9}$$

Inverse Clarke-Park transform is depicted as:

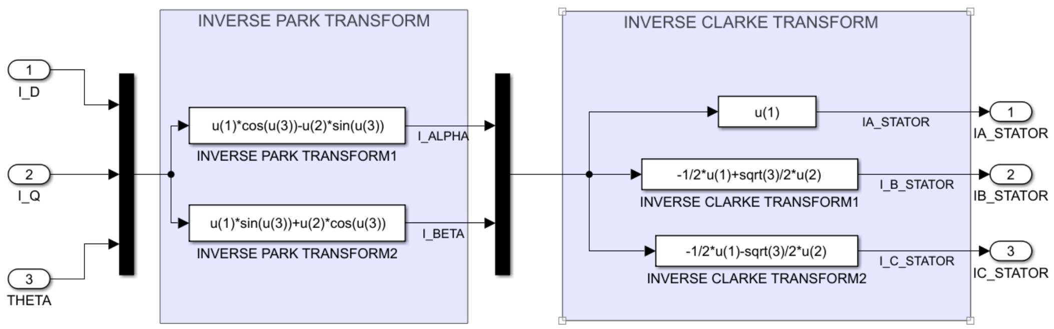

Figure 4.4 : Inverse Clarke-Park Transform model.

abc to d-q axis transformation or d-q to abc axis transformation is widely used in dynamic modelling of PMSM. The four equations mentioned above can be combined in two ways [38]:

$$V_a = V_d \cos\theta - V_q \sin\theta \tag{4.10}$$

$$V_b = V_d \cos\left(\theta - \frac{2\pi}{3}\right) - V_q \sin\left(\theta - \frac{2\pi}{3}\right) \tag{4.11}$$

$$V_c = V_d \cos\left(\theta + \frac{2\pi}{3}\right) - V_q \sin\left(\theta + \frac{2\pi}{3}\right) \tag{4.12}$$

Besides abc to d-q transformation, d-q to abc transformation can be calculated as follows:

$$V_d = \frac{2}{3}\left[V_a \cos\theta + V_b \cos\left(\theta - \frac{2\pi}{3}\right) + V_c \cos\left(\theta + \frac{2\pi}{3}\right)\right] \quad (4.13)$$

$$V_q = -\frac{2}{3}\left[V_a \sin\theta + V_b \sin\left(\theta - \frac{2\pi}{3}\right) + V_c \sin\left(\theta + \frac{2\pi}{3}\right)\right] \quad (4.14)$$

4.2 Average Value Inverter Model

An average value inverter performs the calculation of the three phase AC voltage output from the inverter DC voltage by utilizing the modulation indices that change between 0 and 1. The modulation indices are obtained by scaling Space Vector Pulse Width Modulation block output signals. The average value inverter simulates the drive system by taking average value and operates as a full wave inverter [42].

D_a, D_b and D_c represent modulation indices. V_{dc} is the DC bus voltage of the inverter. V_a, V_b and V_c denote the output stator voltages in Volts.

DC to AC conversion is done using the Equation 4.15, Equation 4.16, Equation 4.17, and Equation 4.18.

$$D_0 = \frac{(D_a + D_b + D_c)}{3} \quad (4.15)$$

$$V_a = V_{dc} \times (D_a - D_0) \quad (4.16)$$

$$V_b = V_{dc} \times (D_b - D_0) \quad (4.17)$$

$$V_c = V_{dc} \times (D_c - D_0) \quad (4.18)$$

The average value inverter model is depicted in Figure 4.5.

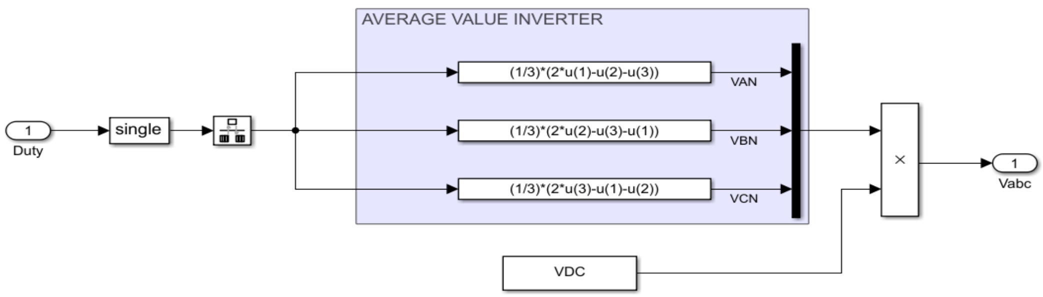

Figure 4.5 : Average value inverter model.

4.3 PI Controller Design

The PI controller illustrated in Figure 4.6 incorporates a proportional gain and an integral gain that ensure a fast response and reference tracking. A proportional gain assures a fast output and an integral gain decreases the output error.

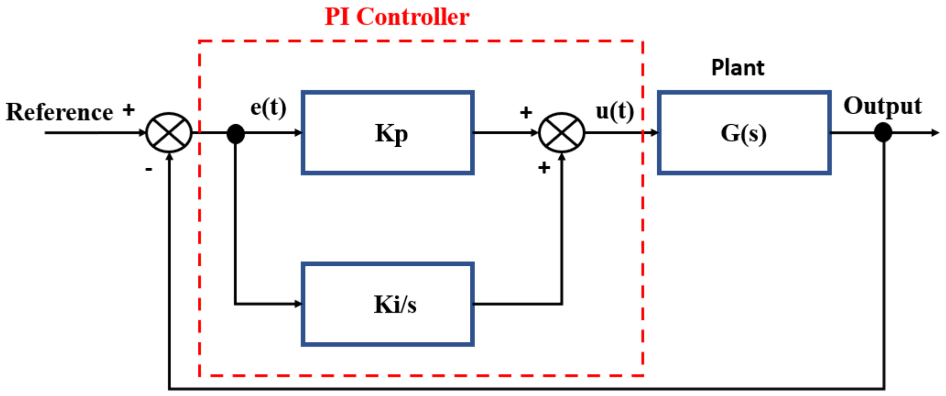

Figure 4.6 : PI controller structure.

The PID Controller block(1-DoF) in Simulink is selected to control the d-q-axis currents and speed. In constant torque region of the motor operation, the d-axis current reference is 0. The q-axis current control is cascaded with a speed control. Initially, d-q-axis current control is applied to the plant model. In order to find the parameters of the PI controller, PID Tuner that automatically tunes the parameters of PI controller for Single Input Single Output (SISO) plant to obtain good characteristics with tradeoff between robustness and performance is launched. The tuning method is Transfer Function-Based. The discrete time settings are determined. The PID Tuner provides a linearized plant model for the controller by identifying the plant input and output.

When tuning the PI controller gains at the no-load condition, the settling time of the speed response is assumed to be less than 0.30 s. Additionally, one of the design requirements for the PI controller is that the overshoot (OS) is less than 15% at no-load condition. The PI controller parameters are given in Table 4.2.

Table 4.2 : Current and speed controller parameters.

Type	Kp	K_i
d-axis control	1.7283	3466.074
q-axis control	0.6332	39.8837
Speed control	0.0223	2.2811

The Figure 4.7 shows the PMSM drive modeling in Simulink associated a microcontroller, an inverter and a PM synchronous motor.

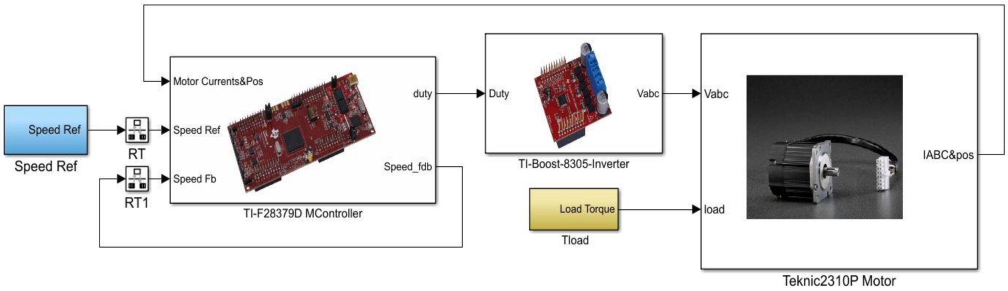

Figure 4.7 : PMSM drive complete model.

The motor is Teknic2310P low voltage motor. The control system is designed with a Texas Instruments LAUNCHXL-F28379D. The inverter module for the driver is Texas Instruments DRV8305EVM with a switching frequency of 20 kHz. DC link voltage is 24 V. The parameters of the motor and the inverter are given in Table 4.3.

Table 4.3 : Motor and inverter parameters.

Parameter	Value	Unit	Description
P	4	-	Pole pair
R_S	0.36	$Ohm(\Omega)$	Stator Resistance
L_d	$2x10^{-4}$	$Henry\ (H)$	d-axis inductance
L_q	$2x10^{-4}$	$Henry\ (H)$	q-axis inductance
λ_{pm}	0.0064	$Weber\ (Wb)$	PM flux
J	$7x10^{-6}$	Kgm^2	Inertia
B	$2.64x10^{-6}$	$Nm/rad/s$	Damping
T_{rated}	0.2724	Nm	Rated torque
I_{rated}	7.1	$Amper(A)$	Rated Current
N_{max}	6000	RPM	Max. speed
V_{dc}	24	$Volt(V)$	DC link voltage
R_{shunt}	0.007	$Ohm(\Omega)$	Inverter current sensor shunt resistor
R_{DS}	0.002	$Ohm(\Omega)$	Inverter drain-source resistance
I_{max_inv}	23.5714	$Amper(A)$	Inverter max current

The base speed is calculated as follows [43]:

$$R_{inv} = R_{DS} + R_{shunt}/3 \tag{4.19}$$

The Equation 4.19 represents the equivalent resistor of the inverter board. In the constant torque region of the motor, I_q is accepted as I_{rated}.

The maximum phase voltage of the inverter output for the Space Vector PWM is expressed as:

$$V_{phase\_max} = V_{dc}/\sqrt{3} \tag{4.20}$$

The inverter voltage constraint is found by calculating the d-axis and q-axis voltages:

$$v_{d0} = -\omega_e L_q i_q \tag{4.21}$$

$$v_{q0} = \omega_e (L_d i_d + \lambda_{pm}) \tag{4.22}$$

$$v_{max} = V_{phase\_max} - R_{inv} I_q \tag{4.23}$$

v_{d0} is the d-axis voltage when i_d is zero. v_{q0} is computed when i_q is zero. The base speed in rad/s is computed as:

$$\omega_{base} = \frac{1}{p} \frac{v_{max}}{\sqrt{{v_{d0}}^2 + {v_{q0}}^2}} \tag{4.24}$$

$$N_{base} = \frac{60}{2\pi} \omega_{base} \tag{4.25}$$

The base speed in RPM is found 4107. The component-based drive system sampling times to create a model and control are given in Table 4.4.

Table 4.4 : Drive system sampling times.

Sampling Time	Value
$T_{s_{motor}}$	25 μs
$T_{s_{inverter}}$	25 μs
T_{pwm}	50 μs
$T_{s_{current}}$	50 μs
$T_{s_{speed}}$	500 μs

5. ADAPTIVE NEURO FUZZY INFERENCE SYSTEM

The Adaptive Neuro- Fuzzy System or ANFIS is a hybrid intelligent system that combines the Artificial Neural Network (ANN) and Fuzzy Logic (FL) technology. Therefore, ANN and FL approaches should be examined separately [44].

5.1 Fuzzy Logic

The most popular fuzzy system determined by IF…THEN rules is a rule-based fuzzy system. The fuzzy systems can be used in modeling, data analysis, prediction, control and etc. A fuzzy inference system provides mapping from a given input set to an output set utilizing fuzzy logic. A fuzzy logic is divided into five essential parts: input scaling, fuzzification, rule-base inference, defuzzification and output scaling. The fuzzy inference system scheme is illustrated in Figure 5.1.

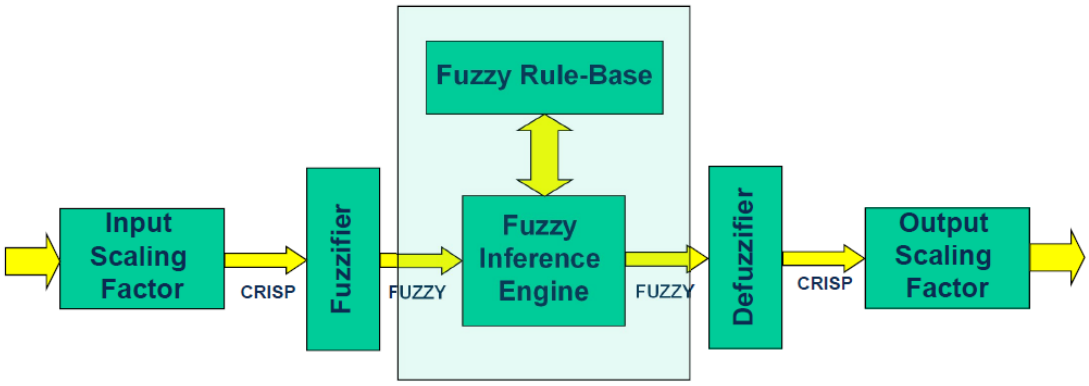

Figure 5.1: Fuzzy inference system scheme [45].

5.1.1 Fuzzy Rule Base

The Fuzzy rules represent a relationship between variables. 'If' and 'Then' define antecedent proposition and consequent proposition respectively. Linguistic variables, linguistic terms, semantic rules, membership functions and base variables are fundamentals of Fuzzy rule base.

The membership function (MF) is a function that identifies the degree to which a given input variable fits to a determined set. The degree of membership can be regarded as an output of a membership function and this value is between 0 and 1. There are many types of membership functions shown in Figure 5.2.

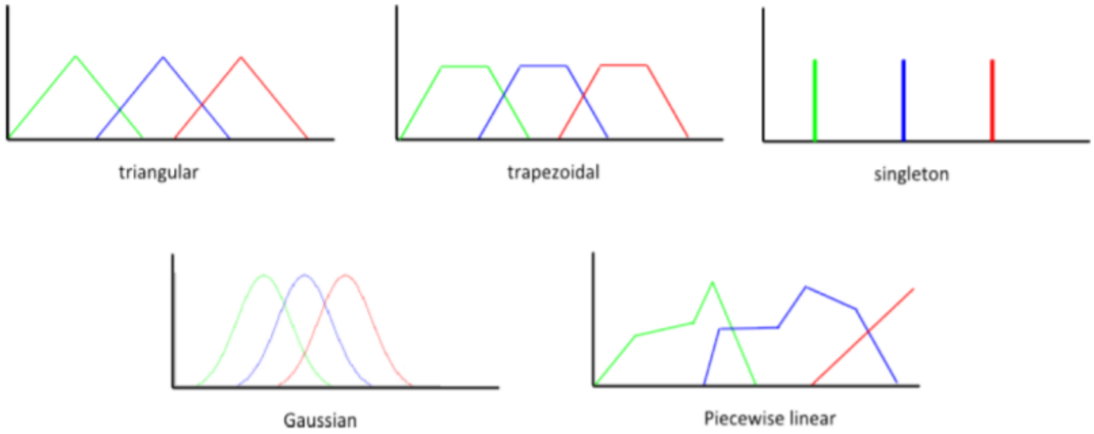

Figure 5.2 : MFs types[46].

The Rule-based fuzzy models vary according to selection of the form of the consequent. Mamdani (Linguistic) fuzzy model, Singleton fuzzy model and Takagi-Sugeno (T-S) fuzzy model are three types of the rule-based fuzzy models.

5.1.1.1 Mamdani (Linguistic) Fuzzy Model

Zadeh and Mamdani proposed the linguistic fuzzy model based on semi-qualitative knowledge with if-then rules.

$$R_i : If\ x\ is\ A_i\ then\ y\ is\ B_i \qquad (5.1)$$
$$i = 1,2, \ldots, K$$

x is the input (antecedent) linguistic variable, A_i is the antecedent linguistic terms, y is the output (consequent) linguistic variable and B_i is the consequent linguistic terms.

In the fuzzy conjunction, the minimum operator provides the relation R. The conjunction using min operator and $A \Lambda B$ implies the following expression:

$$R_i = A_i\ X\ B_i \qquad (5.2)$$

$$\mu_{R_i}(x, y) = \mu_{A_i}(x) \Lambda \mu_{B_i}(y) \qquad (5.3)$$

The disjunction or union of the rules are given in Equation 5.4, Equation 5.5 and Equation 5.6.

$$R = \bigcup_{i=1}^{K} R_i \tag{5.4}$$

$$\mu_R(x, y) = \max_{1 \le i \le R} [\mu_{A_i}(x) \Lambda \mu_{B_i}(y)] \tag{5.5}$$

$$\mu_{\acute{B}}(y) = \max_X [\mu_{\acute{A}}(x) \Lambda \mu_R(y)] \tag{5.6}$$

$\mu_{\acute{A}}$ is an input fuzzy value and $\mu_{\acute{B}}$ is an output value. The general inference mechanism is converted into Equation 5.7.

$$\mu_{\acute{B}}(y) = \max_X \{\mu_{\acute{A}}(x) \Lambda \max_{1 \le i \le R} \left[\mu_{A_i}(x) \Lambda \mu_{B_i}(y)\right]\} \tag{5.7}$$

The complete rule base is deeply related to fuzzy relation R. The output of the linguistic model can be concealed by the max-min operator. This relational calculus can be disregarded since discretization problems and retention of the relation R can be eliminated.

In max-min operator usage, their order priority can be shifted. The new form of the equation is given in Equation 5.8.

$$\mu_{\acute{B}}(y) = \max_{1 \le i \le R} \{\max_X [\mu_{\acute{A}}(x) \Lambda \mu_{A_i}(x)] \Lambda \mu_{B_i}(y)\} \tag{5.8}$$

The firing strength of the i^{th}rule's antecedent can be represented with β_i.

$$\beta_i = \max_X [\mu_{\acute{A}}(x) \Lambda \mu_{A_i}(x)] \tag{5.9}$$

The Equation 5.10 is the new form of the Equation 5.9.

$$\mu_{\acute{B}}(y) = \max_{1 \le i \le R} \{\beta_i \Lambda \mu_{B_i}(y)\} \tag{5.10}$$

The algorithm explained step by step is max-min or Mamdani-inference. After the inference process, the output should be a numeric value. This process is a conversion of a fuzzy set into a numeric value and it is termed as defuzzification. Centroid of the Area, mean of maximum, first(or last) of maxima, max-membership principal, bisector of the area or weighted average method can be selected to a defuzzifier.

Input or output scaling factors can be required for normalization of the input or the output. In fuzzy controller design, the scaling factors emulates the controller gains. They offer improved performance and stability.

5.1.1.2 Singleton Fuzzy Model

Singleton fuzzy sets can perform real numbers.

$$R_i: If\ x\ is\ A_i\ then\ y\ is\ b_i \quad i = 1,2, \dots, K \tag{5.11}$$

In singleton fuzzy model using Mamdani (max-min) inference algorithm $\mu_{\acute{A}}(x)$ is 1 for $x = x_0$ and otherwise $\mu_{\acute{A}}(x)$ is 0. The equation of firing strength β_i is $\mu_{A_i}(x_0)$. Deriving the output fuzzy sets and aggregation the output fuzzy sets are applied to the a given fuzzy model.

5.1.1.3 Takagi-Sugeno Fuzzy Model

The Takagi–Sugeno (T-S) fuzzy model requires crisp functions in the consequents. The Takagi-Sugeno rules can be shown as

$$R_i: If\ x\ is\ A_i\ then\ y_i = f_i(x) \quad i = 1,2, \dots, K \tag{5.12}$$

Mostly, f_i can be depicted as a vector-valued function. However, in order to obtain practical parameterization, the rules can be following form:

$$R_i: If\ x_1\ is\ A_{i1} and \dots and\ x_n\ is\ A_{in}\ then\ y_i = a_i^T x + b_i \quad i = 1,2, \dots, K \tag{5.13}$$

Firing strength is given as

$$\beta_i(x) = \prod_{j=1}^{n} \mu_{A_{ij}}(x_j) \tag{5.14}$$

T-S Fuzzy model output is expressed as

$$y = \frac{\sum_{i=1}^{K} \beta_i(x) y_i}{\sum_{i=1}^{K} \beta_i(x)} \tag{5.15}$$

If Takagi-Sugeno fuzzy model structure given in Figure 5.3 is examined by using 2 rules, following expressions are obtained.

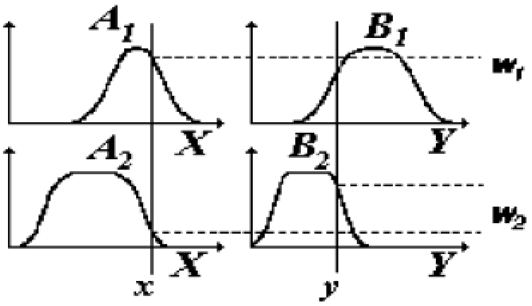

Figure 5.3 : Takagi-Sugeno fuzzy model structure [45].

Rule 1 and Rule 2 are expressed as follows:

IF x is A_1 and y is B_1 THEN $f_1 = p_1 x + q_1 y + r_1$ (5.16)

IF x is A_2 and y is B_2 THEN $f_2 = p_2 x + q_2 y + r_2$ (5.17)

With weighted average method, the following expression is derived by weighting each functions in the output by its respective maximum membership value.

$$f = \frac{w_1 f_1 + w_2 f_2}{w_1 + w_2} = \overline{w_1} f_1 + \overline{w_2} f_2 \quad (5.18)$$

5.2 Adaptive Neuro Fuzzy Inference System

ANFIS comprises the fuzzy inference system(FIS) and the neural network (NN) [4-11]. ANFIS controllers provide more robust characteristics with critically damped response [47]. Adaptive Neuro Fuzzy Inference System uses Takagi-Sugeno (T-S) Fuzzy Models. The Membership functions of the fuzzy inference systems are manually designed and generally controlled with trial-and-error method. However, FIS designer should have a sufficient knowledge on their system. Otherwise, the Neural network has a capability to learn from training data and it can also behave as a black box. Besides, the results imported to the FIS can be expressed in linguistic terms. The ANFIS architecture is illustrated in Figure 5.4. The parameters of the MFs and Sugeno outputs(f_1 and f_2)) are altered by the Backpropagation (BP) algorithm that is one of various training algorithms during the process of learning. It ended when FIS output reached the desired value [48]. For simplicity, two inputs X and Y are considered for ANFIS adaptation principles.

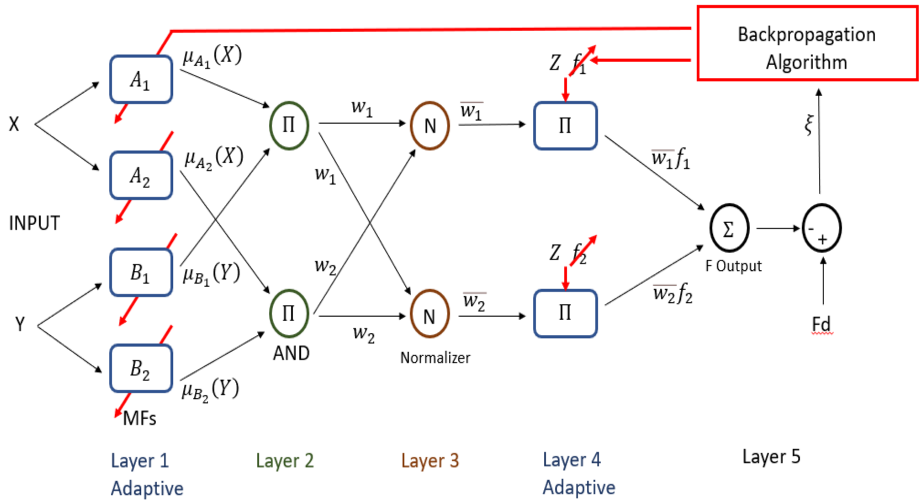

Figure 5.4 : ANFIS architecture.

At layer 1, node function is expressed as

$$O_{1,i} = \mu_{A_i}(x), for\ i = 1,2 \tag{5.19}$$

$$O_{1,i} = \mu_{B_{i-2}}(y), for\ i = 3,4 \tag{5.20}$$

x and y are inputs. A_i and B_i are labels such as small, large etc. $\mu(x)$ is membership function notation. These nodes are adaptive.

At layer 2, these are fixed nodes and T is T-norm operator.

$$O_{2,i} = w_i = \mu_{A_i}(x)\ \mathrm{T}\ \mu_{B_i}(y)\ , for\ i = 1,2 \tag{5.21}$$

Mostly, T-norm operator satisfies fuzzy AND logic, performing as minimum and product.

At layer 3, these are also fixed nodes. Normalized firing strength are obtained as outputs of this layer. To find normalized firing strength, the following formula is derived:

$$O_{3,i} = \overline{w_i} = \frac{w_i}{w_1 + w_2}\ for\ i = 1,2 \tag{5.22}$$

At layer 4, every node is an adaptive node with the function. Consequent parameters ($p_i, q_i\ and\ r_i$) are adjusted.

$$O_{4,i} = \overline{w_i} f_i = \overline{w_i}(p_i x + q_i y + r_i) \tag{5.23}$$

At layer 5, there is a single node. The total output of this layer is calculated as the sum of entire neuro signals by a single node. The weighted average defuzzification is shown in Equation 5.24.

$$O_{5,i} = \sum_i \overline{w_i} f_i = \frac{\sum_i w_i f_i}{\sum_i w_i} \tag{5.24}$$

ANFIS is based on a hybrid learning algorithm divided into forward pass and backward pass.

Table 5.1 : Hybrid learning algorithm.

	Forward Pass	Backward Pass
Premise Parameters	Fixed	Updated with Gradient Descent
Consequent Parameters	Identified by Least-squares estimator	Fixed
Signals	Node outputs	Error Signals

ANFIS should be first or zeroth order Sugeno type systems.It has a single output and all output MF functions should be linear or constant. Rule sharing is not allowed. The number of output MF functions should be equal to the number of rules. Unity weight for each rule is required.

5.2.1 ANFIS Design for PMSM Speed Control

The parameters of a conventional PI controller may not be fine-tuned due to the non-linearity and disturbance for high voltage applications [34]. In order to obtain improved performance characteristics, ANFIS controller design for PMSM speed controller is investigated [47].

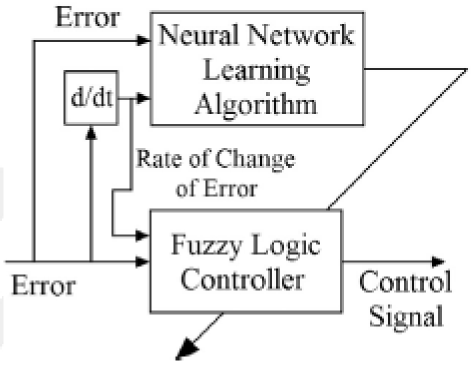

Figure 5.5 : ANFIS mechanism [49].

The design of the ANFIS controller for PMSM motors is explained in this section. Figure 5.5 represents ANFIS mechanism.

The input-output training data, which is utilized to train the FIS, are collected from the PMSM reference model. ‘Two inputs and one output’ is considered for the design of ANFIS controller. For collecting data for training, the error (e) between actual motor speed and reference speed and the change in the error (Δe) are given as inputs to the ANFIS controller. The change in control signal(du) is selected as output. The inputs for ANFIS controller, the error and the change in error is modeled using the Equation 3.25 and Equation 3.26.

$$e(k) = \omega_{ref} - \omega_m \quad (3.25)$$

$$\Delta e(k) = e(k) - e(k-1) \quad (3.26)$$

ω_{ref} is the reference speed, ω_m is the actual motor speed, ANFIS controller modeling in PMSM drive is illustrated in Figure 5.6. Input or output scaling factors emulates the controller parameters and called normalization of the input/output. They assure more comprehensive performance dynamics and stability.

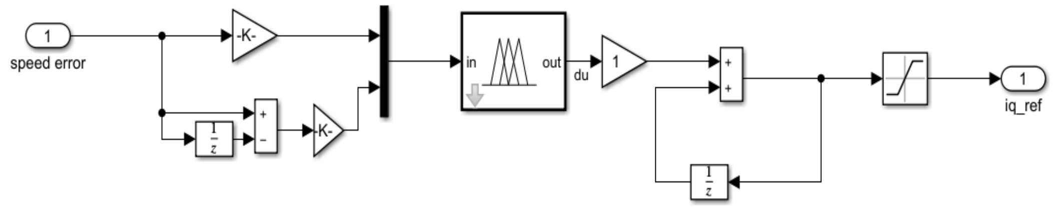

Figure 5.6 : ANFIS controller modelling in PMSM drive.

ANFIS incorporates SIMULINK in MATLAB. The flowchart of ANFIS controller design simulation process is shown in Figure 5.7.

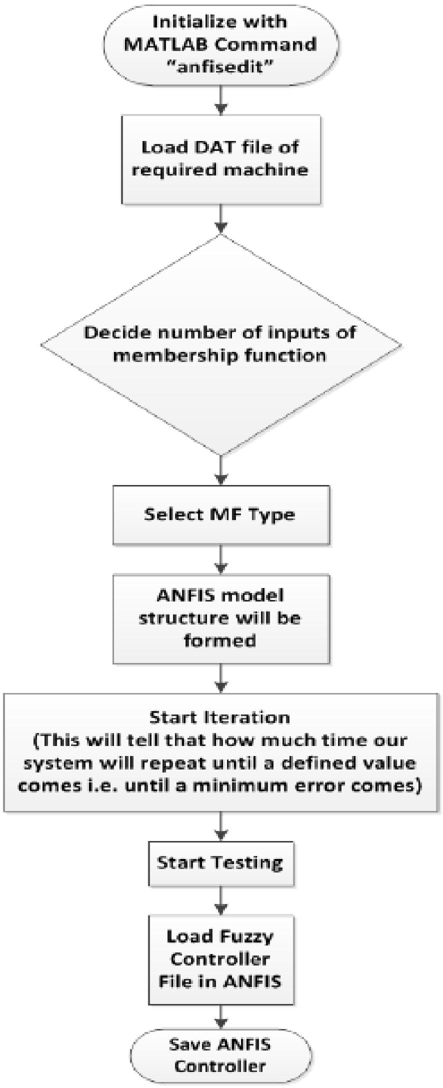

Figure 5.7 : Flowchart of ANFIS controller simulation process [50].

In training process, ‘anfisedit’ command is written in MATLAB command window to initiate ANFIS toolbox. Training data collected from the reference model is performed with appropriate sampling time. The discrete solver is chosen as ode4. In this study, sampling time is 500 μs.

To minimize the error between actual data collected dynamic model of PMSM with PI controller and ANFIS trained data, speed reference inputs, which cover the entire speed range are used by dividing all speed range into 20 sections as 10 positive and 10 negative values. Training data reference profile is given in Figure 5.8.

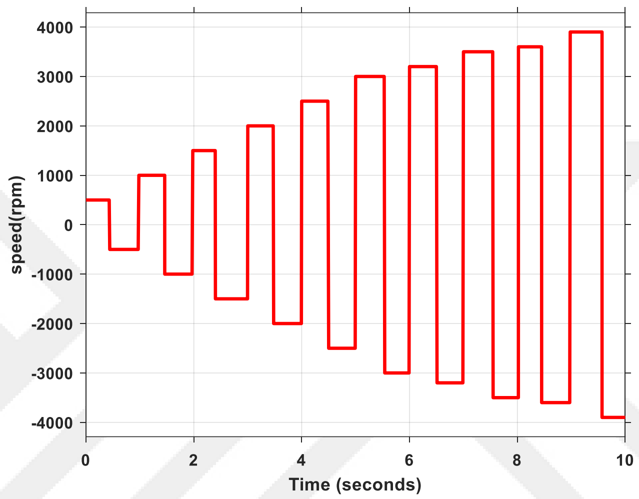

Figure 5.8 : Training data reference profile.

The data collected from the reference model of the PMSM is loaded into ANFIS from workspace or file. The next step is determination of the input/output and the MFs of the inputs.

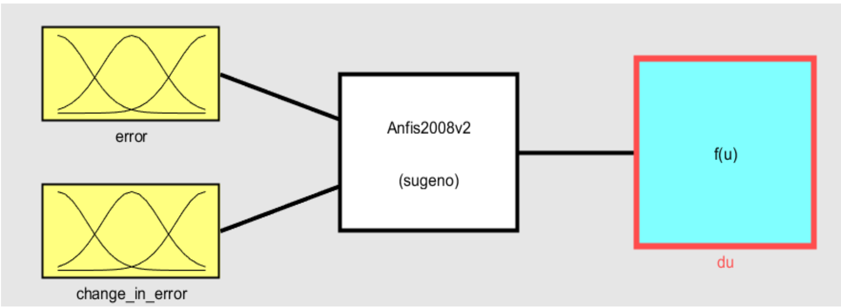

Figure 5.9 : Design of ANFIS interface.

In addition, ANFIS allows the designer to select MF type such as triangular, gauss, or etc. Design of ANFIS interface is shown in Figure 5.9. After numerous testing, the most effective adaptive speed performance is obtained with Sugeno type 5 triangular

MFs for each input. The hybrid FIS model parameter optimization technique performs to tune the parameters of the MFs, that uses least squares estimation (LSE) and back propagation (BP).The MFs of error and the MFs of change in error are shown in Figure 5.10 and Figure 5.11 respectively.

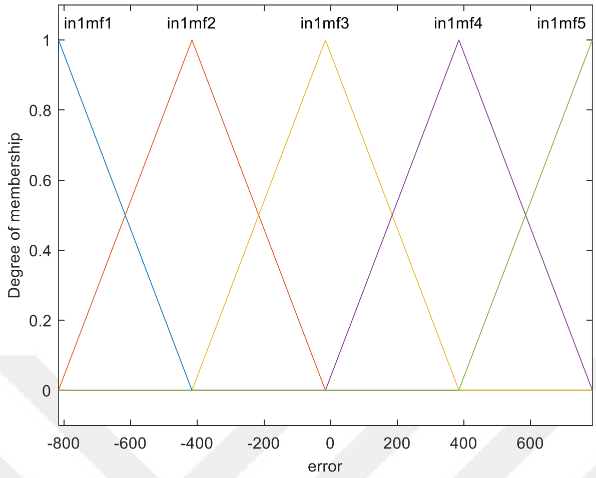

Figure 5.10 : Membership function of error.

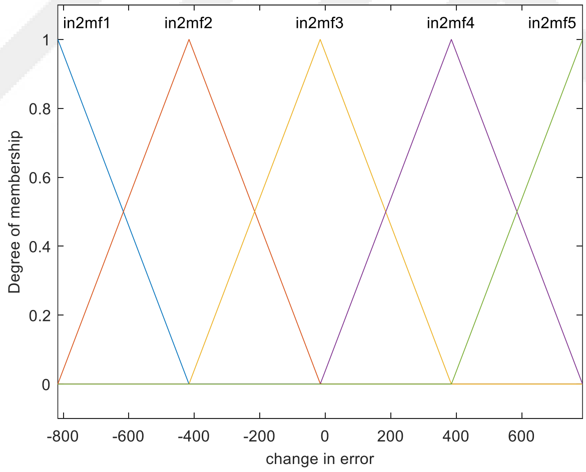

Figure 5.11 : Membership function of change in error.

The optimization method is hybrid. Iteration epochs are decided and the iteration is initiated.

Training error plot is presented in Figure 5.12. It is seen that FIS output is overlapped with the training data with the maximum absolute error of 2%.

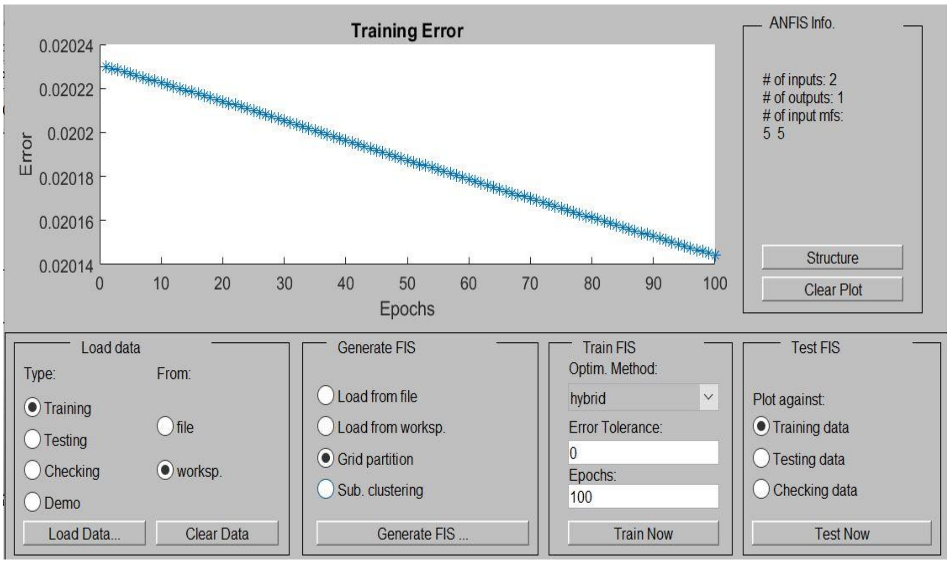

Figure 5.12 : Training error plot.

After the training process, testing data section is initiated. When the error between the training data and FIS output can be ignored, Fuzzy Controller file is saved and integrated with ANFIS controller model. Regarding the computational problem, the number of MFs should be between 3 and 6. Scaling factors are used to perform enhanced response dynamics. FIS output plotted against the training data is illustrated in Figure 5.13.

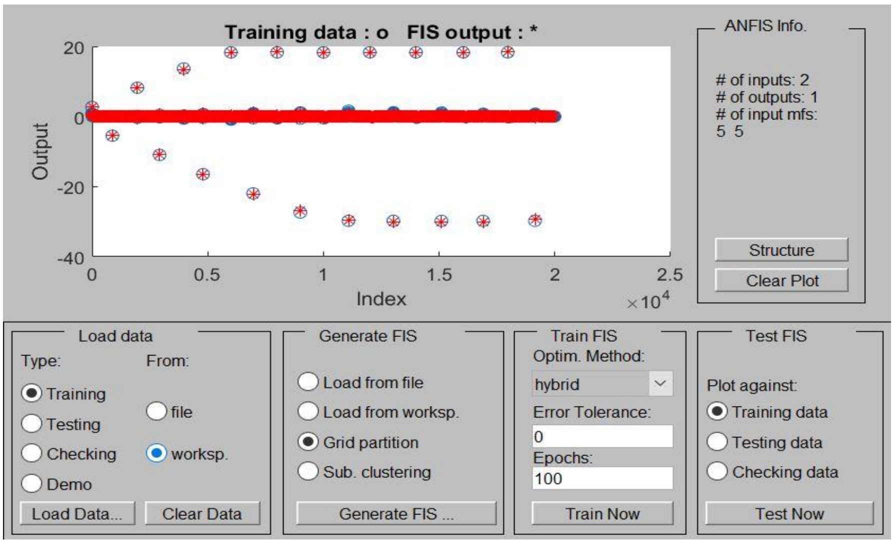

Figure 5.13 : Plot of training data and FIS output.

ANFIS rule viewer is depicted in Figure 5.14. Since the error input has 5 MFs and the change in error input has also 5 MFs, the number of ANFIS rules is 25.

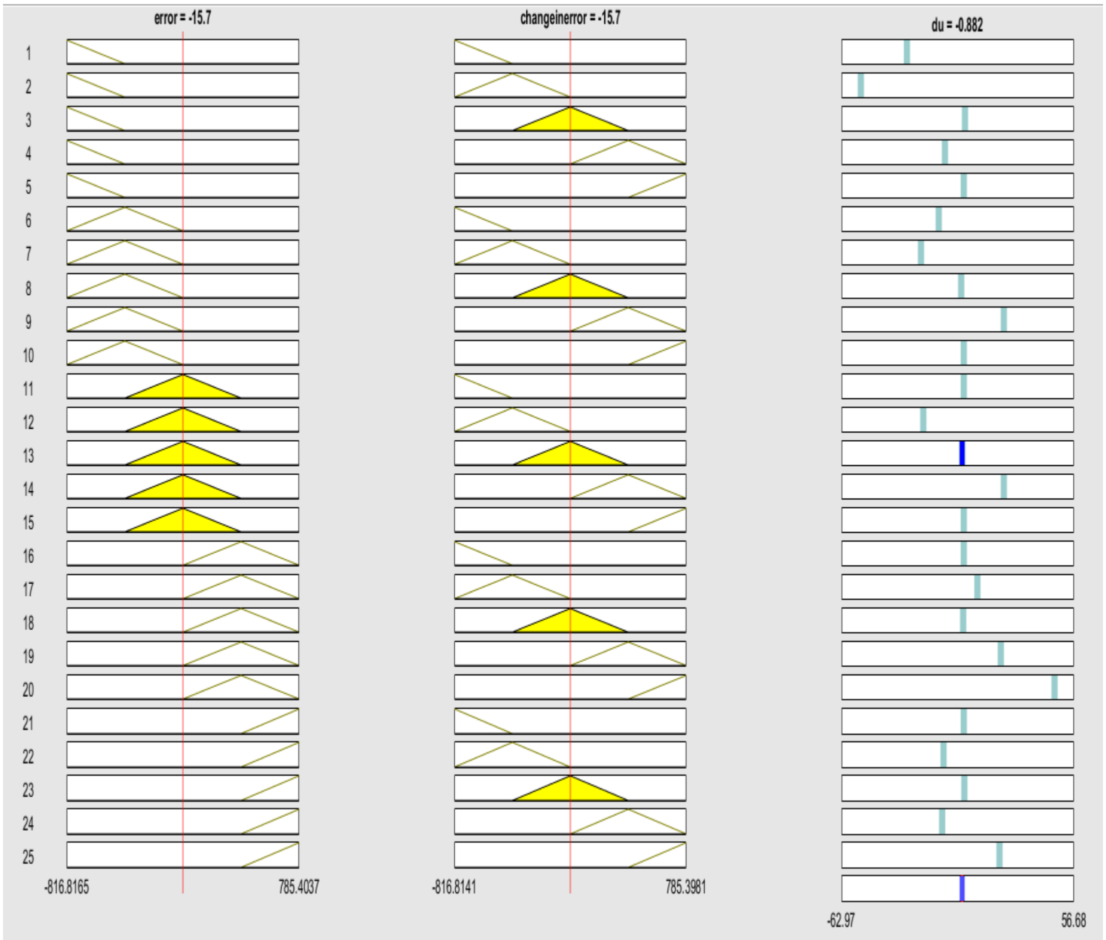

Figure 5.14 : ANFIS rule viewer.

Related ANFIS structure for a Sugeno fuzzy inference system is given in Figure 5.15.

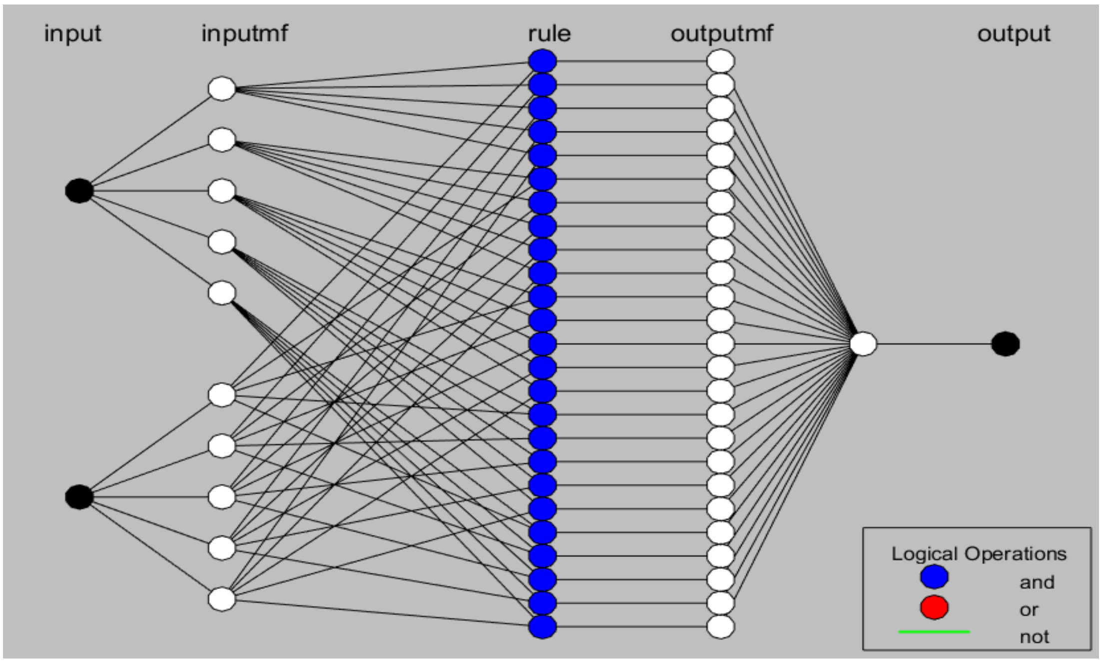

Figure 5.15 : ANFIS network structure.

The surface viewer depicted in Figure 5.16 is used for the mapping from two inputs to a single one to estimate and control the output signal of the controller.

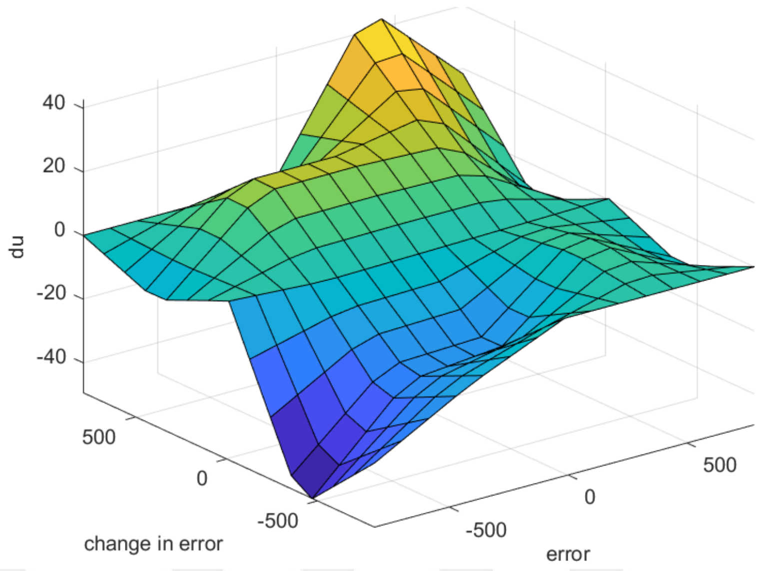

Figure 5.16 : ANFIS surface viewer.

6. IMPLEMENTATION OF A PMSM DRIVE SYSTEM

An experimental setup to implement FOC algorithm of PMSM is presented in this chapter. The system configuration is defined and afterwards, the hardware components are listed.

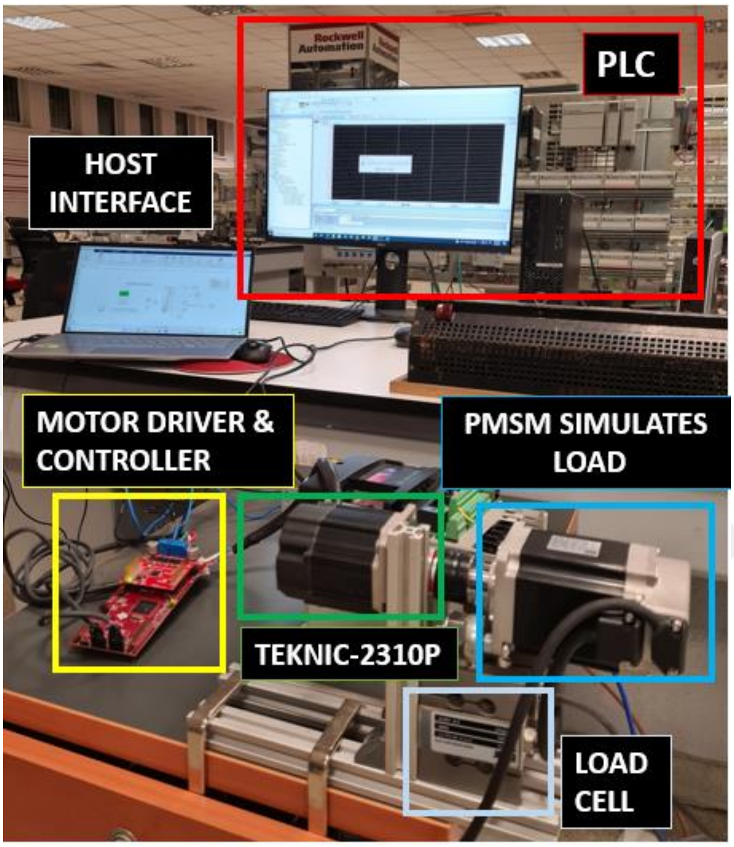

Figure 6.1 : PMSM drive implementation.

To drive a 3-phase PMSM, a driver, a microcontroller and DC Power Supply are combined in Simulink environment. All configuration features including communication interfaces, data types, sensors and delays are set by considering datasheets of the components selected.

To implement the drive system in Simulink, Motor Control Blockset providing motor control applications is integrated with Embedded Coder, Embedded Coder Support Package for Texas Instruments C2000 Processors and Fixed Point Designer.

The PMSM drive system includes the following hardware components:

- Teknic motor M-2310P supporting both Hall and quadrature encoder sensors

- BOOSTXL-DRV8305EVM driver
- LAUNCHXL-F28379D controller
- Switch Mode Power Supply (24VDC)
- Low power PMSM implemented for simulating load
- Load Cell for sensing force applied by the motor during motor operation
- Programmable Logic Controller (PLC) for measurement of motor torque via Load Cell

The test bed is shown in Figure.6.1. The Teknic 2310P motor having Neodymium-Iron-Boron magnets ensures high power density with improved performance at high thermal conditions allowing full-torque output for high-speed motor operation. Stator windings design is optimized with low inductance characteristics assuring a fast electrical time constant. The low cost Molex Mini-Fit connector of the motor supports a current rating of up to 10A per circuit and a 600 V rating. Teknic motor 2310P has built-in encoder sensors to position sensing. The low cost motor includes the type of floating optical disk of the line-driven single-ended encoders for the short transmission range of the power. The encoder density allows 4000 counts per revolution in post-quadrature. It means 0.09 degree of the resolution.

BOOSTXL-DRV8305EVM BoosterPack is an evaluation module providing evaluation of many motor drive techniques with the DRV8305 motor gate driver. It is integrated with TI LaunchPad development kits for a Motor Control Blockset as it is not a standalone motor control kit.

The BOOSTXL-DRV8305EVM combines power, control, and feedback signals and these signals are sent through the XL LaunchPad headers.

BOOSTXL-DRV8305EVM Pinout scheme is illustrated in Figure 6.2.

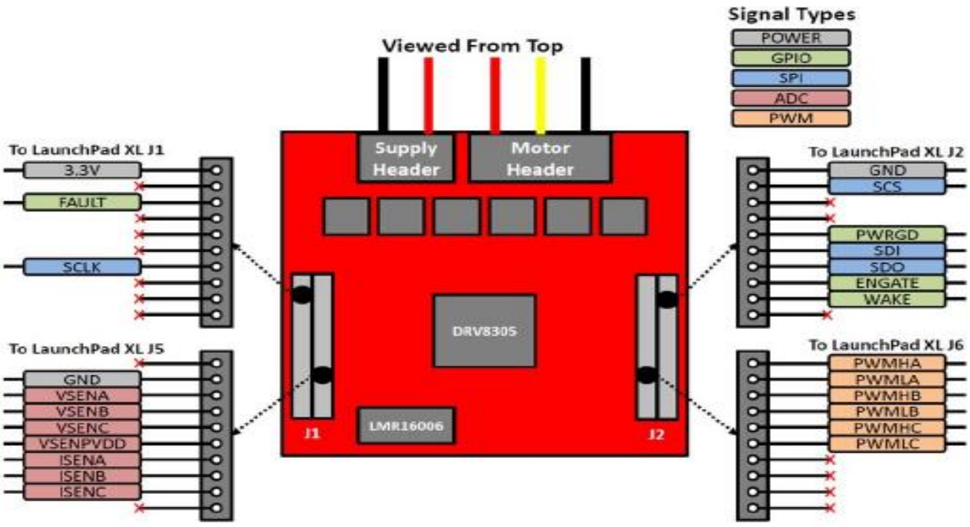

Figure 6.2 : BOOSTXL-DRV8305EVM Pinout.

LM16006 step-down buck regulator ensures 3.3V power to the LaunchPad. Fault condition is configured with the nFAULT and PWRGD signals. This board allows SPI communication for the set-up configuration, required parameters for operation of the device, and configuring device signals. In order to get voltage information from the voltage source, each phase pins support the motor operation between 4.4V and 45V. To get the low-side current information, each phase values should be between 0A and 20A (peak). The ADC structure provides the conversion of the analogue signal to the digital signal with scaling.

The module is integrated with voltage sense circuits on the DC bus (PVDD) and each halfbridge outputs of phases of A, B and C. The voltage sense circuit is shown in Figure 6.3.

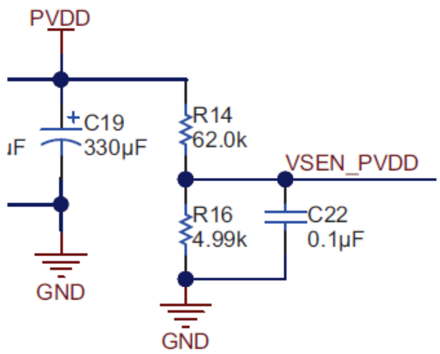

Figure 6.3 : Voltage sense circuit.

Current sense scheme is shown in Figure 6.4.

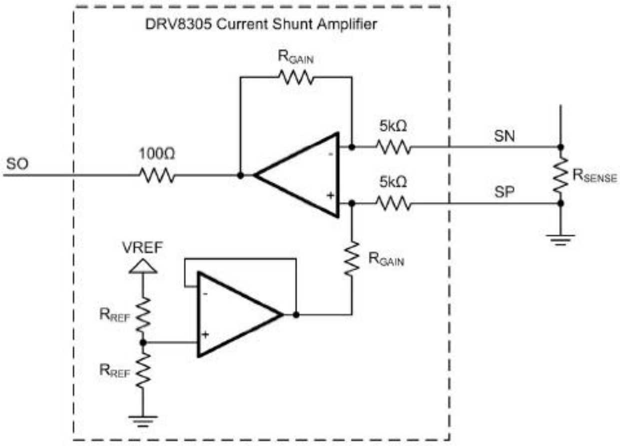

Figure 6.4 : Current sense scheme.

The differential voltage is scaled by 10 V/V and centered at 1.65 V to ensure the detection of both positive and negative currents. The resistor for sensing current is adjusted for 0A to 20A (peak).

The C2000 LAUNCHXL-F28379D LaunchPad is a low-cost development board for the Texas Instruments Delfino F2837xD devices. This board offers easy programming, debugging and evaluation with the USB interface providing a serial communication between F28379D device and the PC .

In order to deploy the model that is created in Simulink environment into the microcontroller, the configuration parameters are adjusted in the Hardware Setting tab [43]. The target hardware, which is TI Delfino F28379D LaunchPad, is determined in the Hardware Board section. All configuration settings which are compatible with C2000 MCU devices are automatically uploaded by selecting TI Delfino F28379D LaunchPad hardware board.

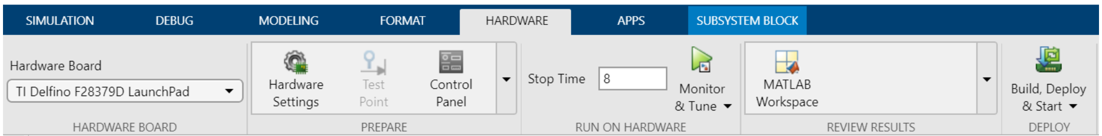

Figure 6.5 : Simulink Hardware Board section.

The solver is configured as a fixed-step discrete solver with no continuous states. For the connection of analog inputs of current or voltage sensors to hardware board, the ADC Interface Configuration settings are completed in Hardware Implementation tab regarding the ADC clock pre-scaler and ADC clock frequency. Desired CPU clock of the TMS320F28379D devices is 200 MHz. The maximum operating frequency of

ADCCLK of TMS320F28379D devices is 50 MHz. Therefore, the ADC clock frequency in MHz is 40 MHz and as it is seen, this value is less than the maximum operating frequency.

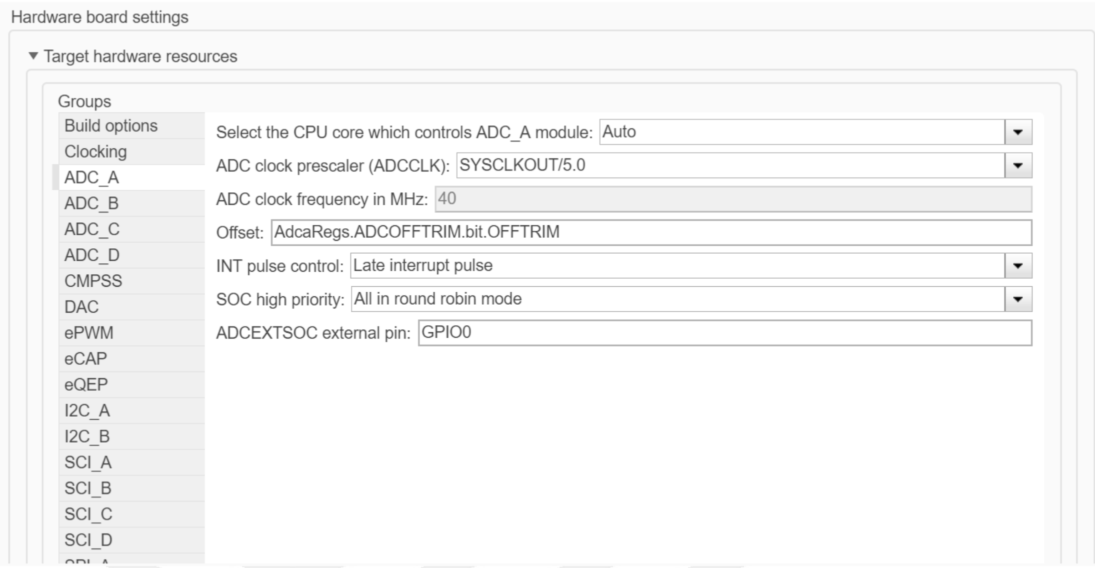

Figure 6.6 : Hardware board ADC settings.

To connect the PWM outputs of the TMS320F28379D device to the inverter, the PWM parameters are set and the PWM pin assignments are configured in the Hardware Implementation Tab.

Position sensing with a Quadrature Encoder sensor also requires assignments in the Hardware board settings. Quadrature Channel A, Quadrature Channel B and Quadrature Encoder Index are configured in the EQEP pin assignment sections.

In order to build and deploy code using serial communication via a USB cable, the Serial Communication Interface Channels settings are configured in terms of suspension mode, number of stop bits, parity mode, character length bits, desired baud rate in bit/sec, pin assignment of transmit and pin assignment of receive.

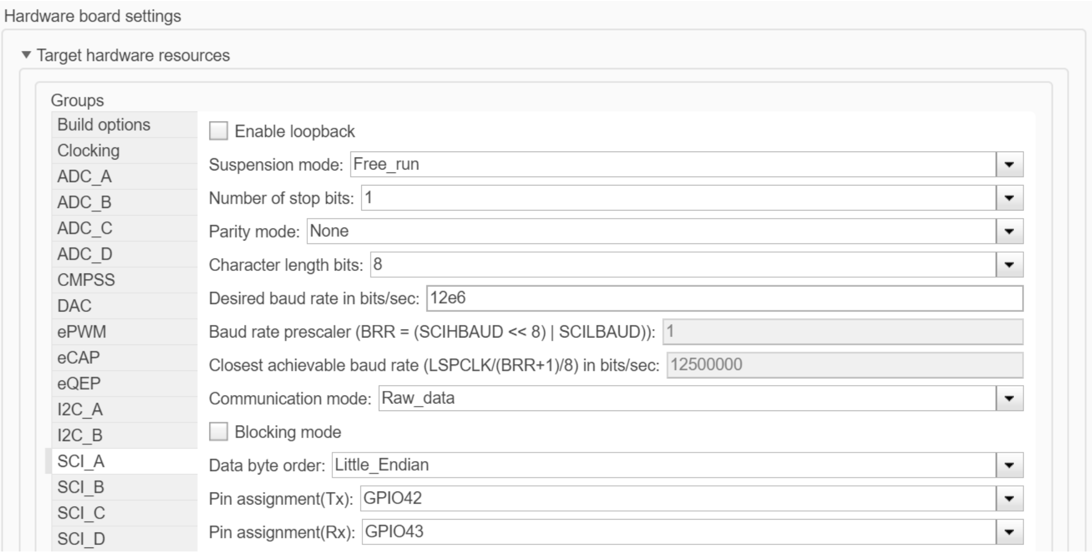

Figure 6.7 : SCI configuration panel.

The target model created in Simulink is grouped into 4 main blocks: Hardware Interrupt Block, Serial Receive, Speed Control and Current Control Block. Entire target model built and deployed to the microcontroller is shown in Figure 6.8.

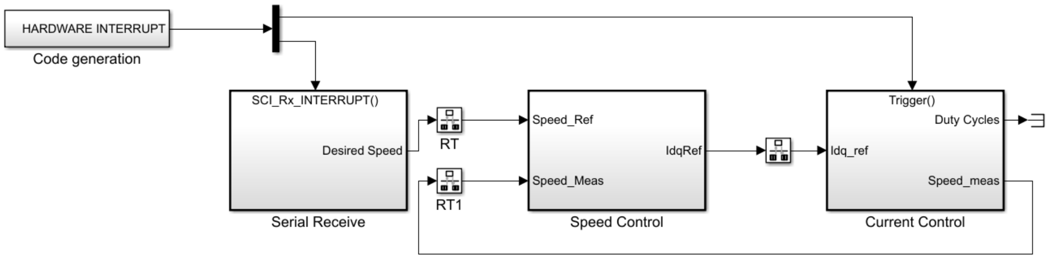

Figure 6.8 : Target model.

In the hardware interrupt block, Interrupt Service Routine that execute the model subsytem by providing asynchronous processing of interrupts triggered by events in the C280x/C2833x DSP Chip Support Library is created.

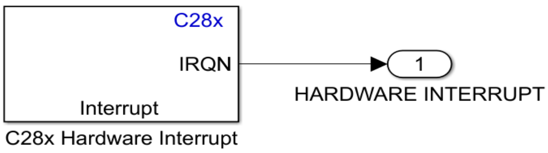

Figure 6.9 : Hardware Interrupt block.

The block output is a function call and related the number of interrupts. Each interrupt has four parameters defined as CPU interrupt numbers, Peripheral Interrupts Expansion (PIE) interrupt numbers, Task priorities and Preemption flags.

PIE and CPU Interrupt Numbers for F2837xD devices are chosen according to the Figure 6.10. There are two interrupt vectors used for the serial communication interface to transmit and reading ADC pins. The ADC for current sensing has given a priority.

PIE ⇒ / CPU ⇓	1	2
1	ADCA1	ADCB1
2	EPWM1_TZ	EPWM2_TZ
3	EPWM1	EPWM2
4	ECAP1	ECAP2
5	EQEP1	EQEP2
6	SPIA_RX	SPIA_TX
7	DMA_CH1	DMA_CH2
8	I2CA	I2CA_FIFO
9	SCIA_RX	SCIA_TX
10	ADCA_EVT	ADCA2
11	CLA1_1	CLA1_2

Figure 6.10 : Hardware Interrupt Block PIE and CPU configuration for F2837xD [42].

The SCI receive block configures the Serial Communication Interface of the C2000 MCUs to receive data from the SCIRXD pin. This block provides asynchronous serial digital communications between MCU and other connected devices.

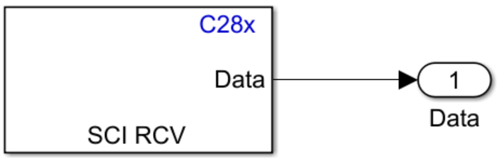

Figure 6.11 : Serial Communication Interface block.

In the speed control block, two types of the controllers already designed exist: A conventional PI controller and an ANFIS controller. The speed control block is represented in Figure 6.12.

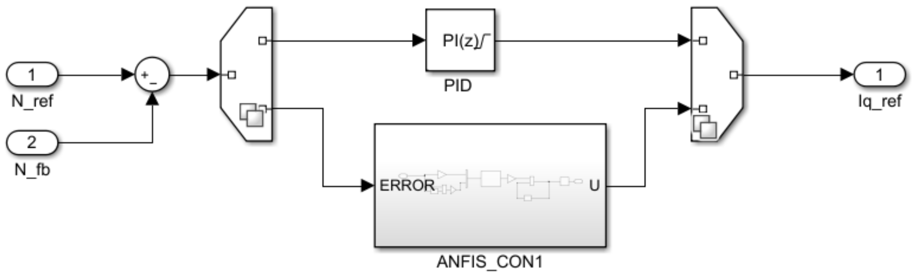

Figure 6.12 : Speed control block.

In the current control block, firstly the ADC blocks compatible with F2837xD and the enhanced quadrature encode pulse module are selected. The ADC resolution is 12 bit of single-ended input. The ADC block is used for reading one ADC channel. As a PMSM is a three-phase motor, three channels are read and therefore three ADC blocks are required.

The eQEP module enables to get the position, direction and speed information from a rotating machine for tracking speed reference. The module inputs include QEPA, QEPB and QEPI. qposcnt represents position counter signal received from the position counter and control unit. qposilat latches position counter on index event.

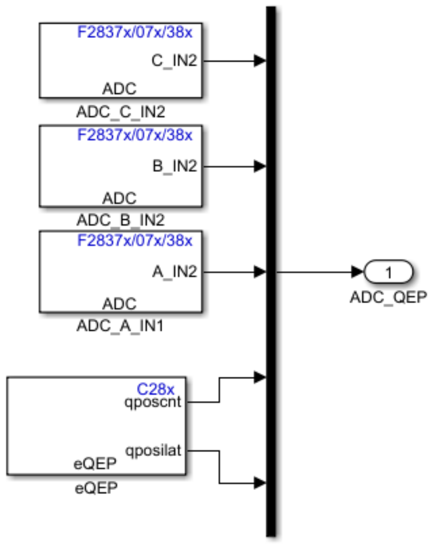

Figure 6.13 : ADC and QEP structure.

To measure the position, the quadrature decoder is applied to compute the position of the quadrature encoder. After calculating the angular position, the speed is found by mathematical expressions.

The maximum ADC count of the inverter is 4095. To get voltage at the ADC output, mid-scale 1.65/2048 is multiplied with the ADC block signal. Regarding differential voltage is centered at 1.65V, the measured stator currents are computed dividing ADC output voltage to 1.65 and multiplying with the maximum current of the inverter.

Employing Clarke and Park transform, d-q axis currents are obtained. Current controllers are located in the target model. After limiting the d-q axis reference voltage at the output of the PI current controllers, Inverse Park Transform allowing two axis quantities of an orthogonal reference frame is applied and Space Vector Generator generates the reference PWM duty cycles from α-β quantites via scaling.The d-q-axis PI current controllers are illustrated in Figure 6.14.

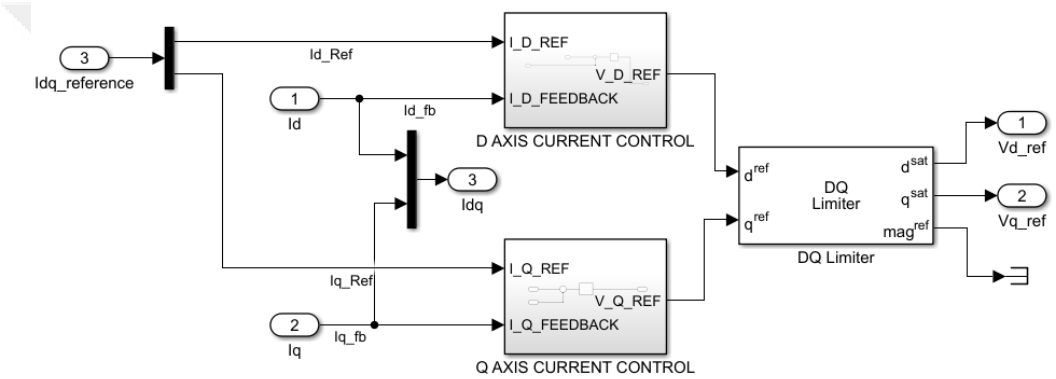

Figure 6.14 : d-q-axis PI controllers.

The PWM frequency is 20 kHz. The target PWM counter period is defined as 5000. To generate enhanced Pulse Width Modulated (ePWM) waveforms for C2000 processors, the ePWM blocks are utilized.

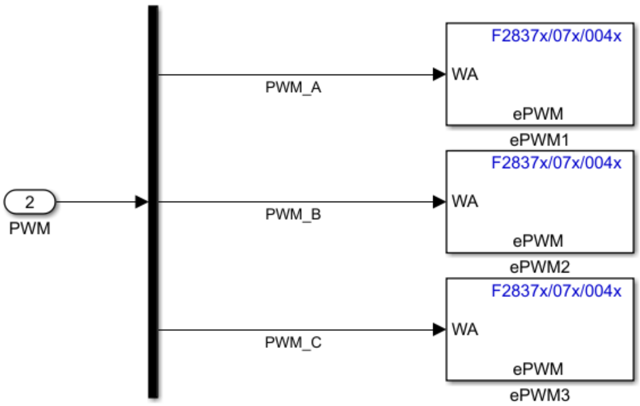

Figure 6.15 : PWM generation for C2000 processors.

The debug signals desired to monitor are selected and by using byte pack block the input data packing is implemented. The debug signals include the speed response, the stator currents, the d-q axis voltage and the currents and the rotor electrical position.

Figure 6.16 : Byte packing.

The SCI Transmit block shown in Figure 6.17 ensures Serial Communication Interface (SCI) of the C2000 MCUs to transmit data using SCITXD pin. This block provides asynchronous serial digital communications between the MCU and the other connected devices.

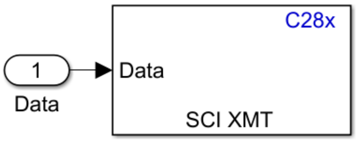

Figure 6.17 : SCI Transmit block.

To configure the Host-side serial communications interface, the Host Serial Setup block is used. This block enables user to select the port and the baud rate. The motor ON/OFF control is provided by the toggle switch. The lamp indicates the green when the motor is operating. The sliding bar or 'Reference Speed' text box is used for input speed request.

Using the Host Serial Transmit block inside the TX the requested signals data are transmitted through serial port. In the RX block, 10 debug signals are received by the Host Serial Receive block. The package received is unbuffered and observed with the scopes.

.

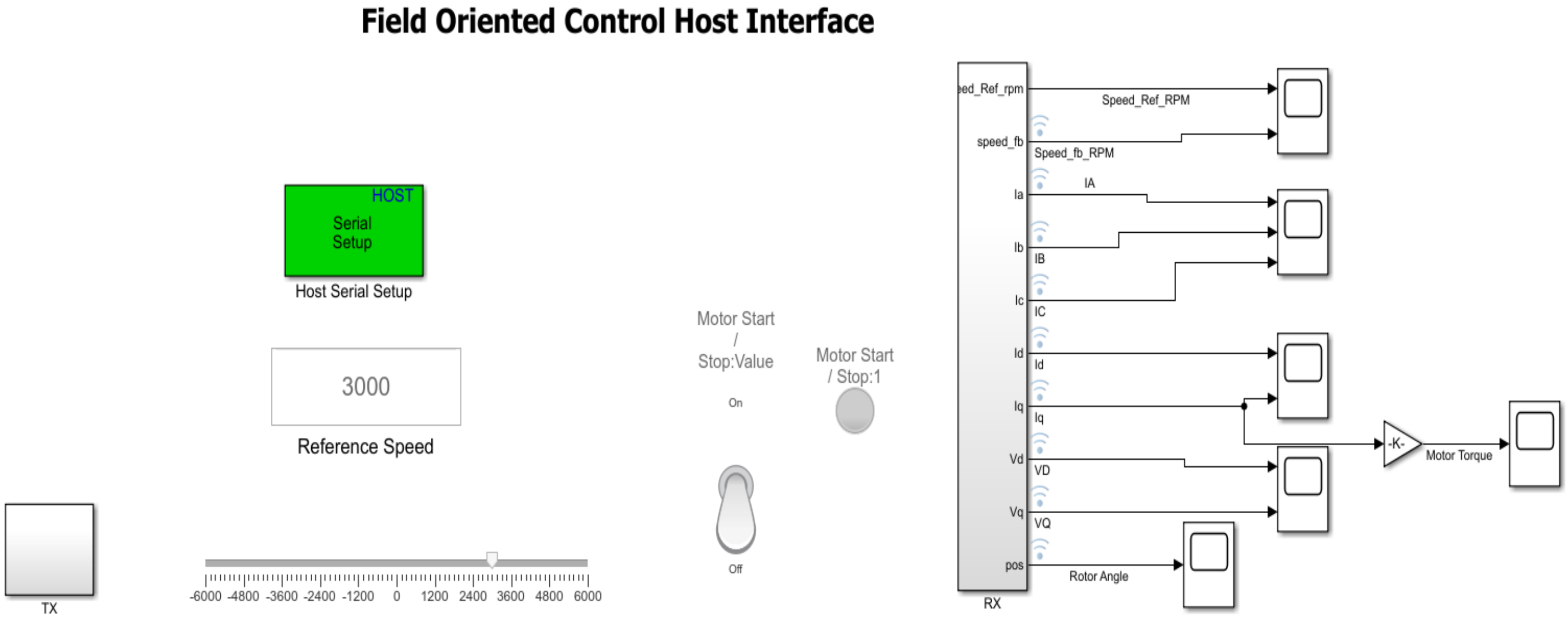

Figure 6.18 : Host model.

7. RESULTS

7.1 Simulation Results

In this section, the simulated motor performance results of the both of the PI controller and the ANFIS controller at No-Load condition are presented for 3000 rpm and 2000 rpm. Speed reversal characteristics without loading at 3000 rpm are investigated. Furthermore, the simulation of the motor operating at 3000 rpm under 0.10 Nm load is given. The step input is applied at 0.1 sec. Afterwards, two types controllers performance characteristics are compared and evaluated in terms of overshoot, settling time and steady state error. Performance results are given in Table 7.1.

7.1.1 2000 rpm without Loading

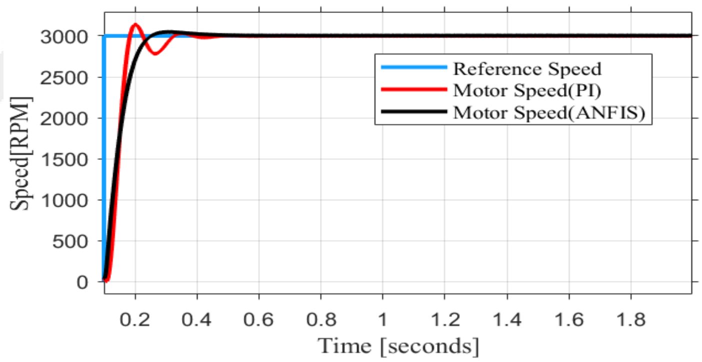

Figure 7.1 : Speed tracking at 2000 rpm without loading.

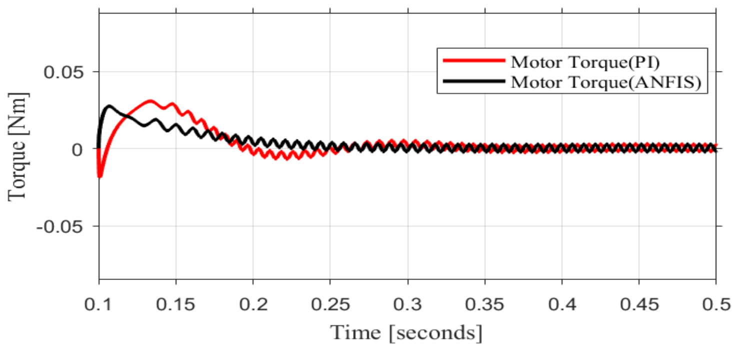

Figure 7.2 : Motor torque at 2000 rpm without loading.

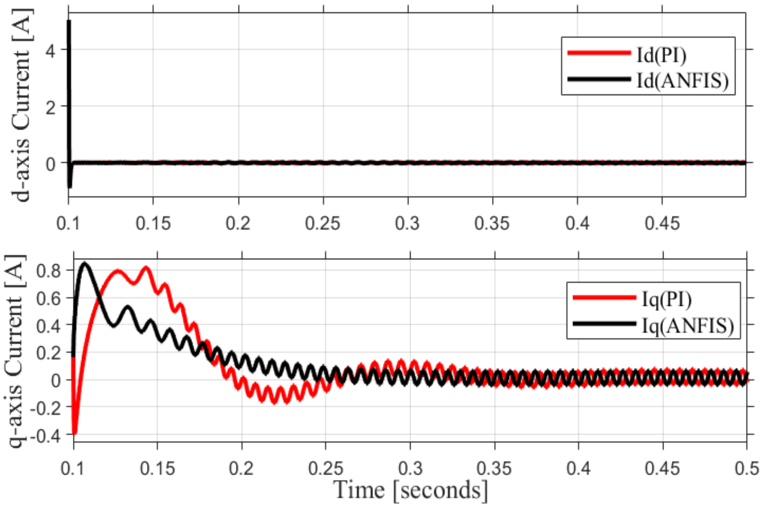

Figure 7.3 : d-q axis currents at 2000 rpm without loading.

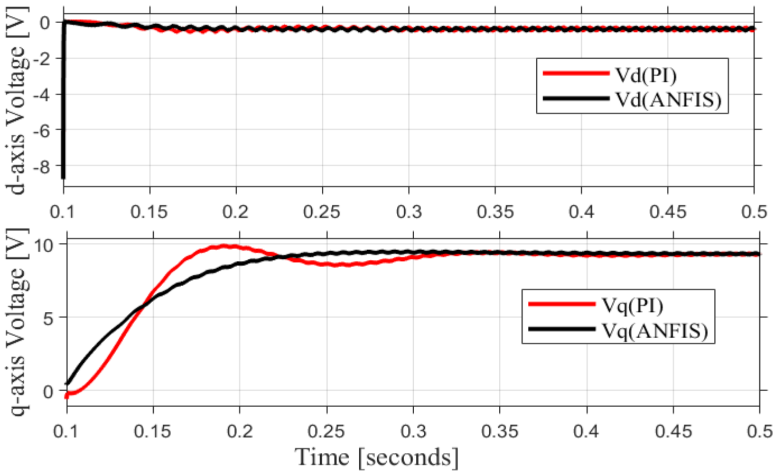

Figure 7.4 : d-q axis voltages at 2000 rpm without loading.

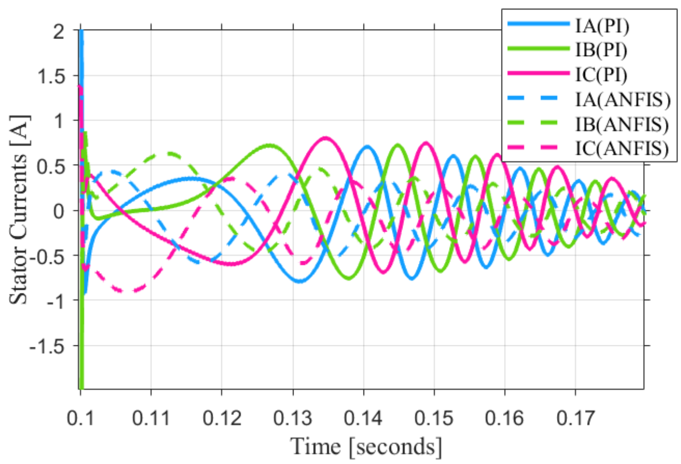

Figure 7.5 : Stator start-up currents at 2000 rpm without loading.

7.1.2 3000 rpm without Loading

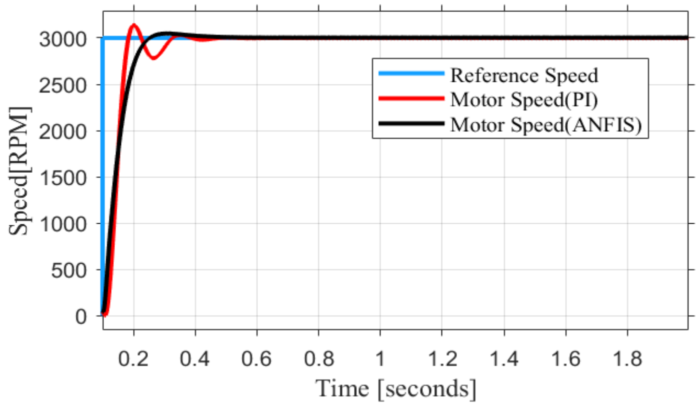

Figure 7.6 : Speed tracking at 3000 rpm without loading.

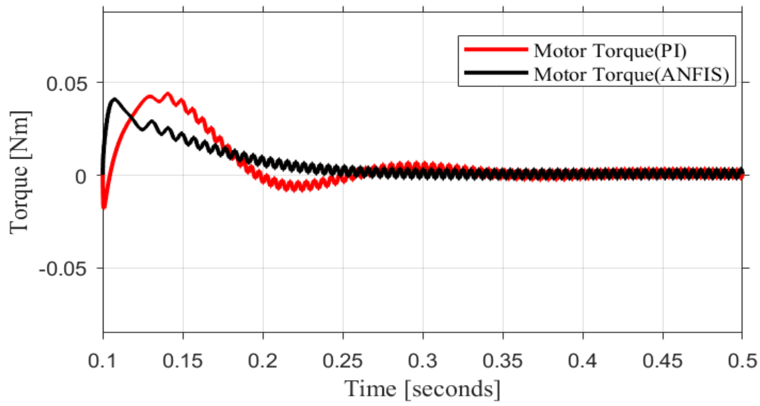

Figure 7.7 : Motor torque at 3000 rpm without loading.

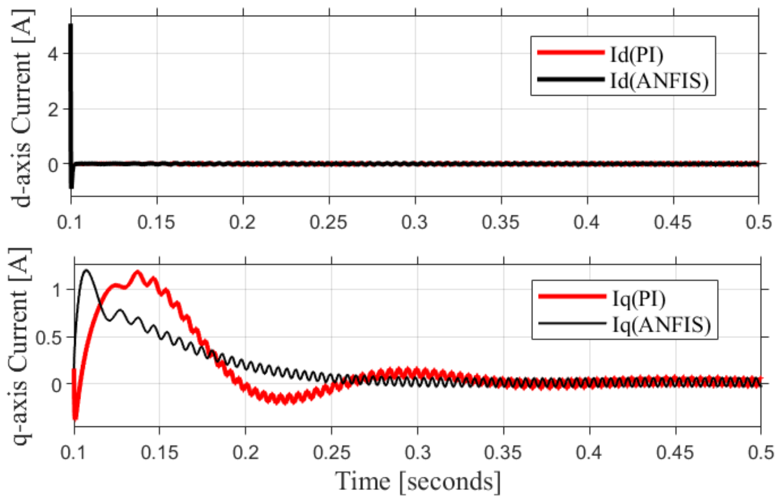

Figure 7.8 : d-q axis currents at 3000 rpm without loading.

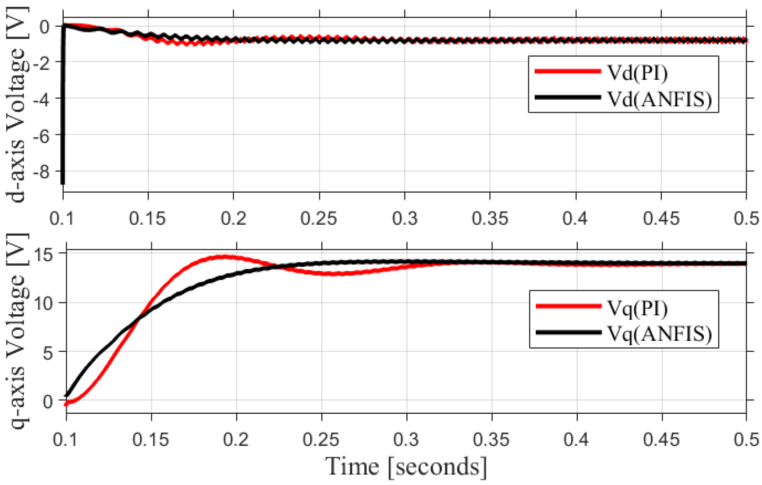

Figure 7.9 : d-q axis voltages at 3000 rpm without loading.

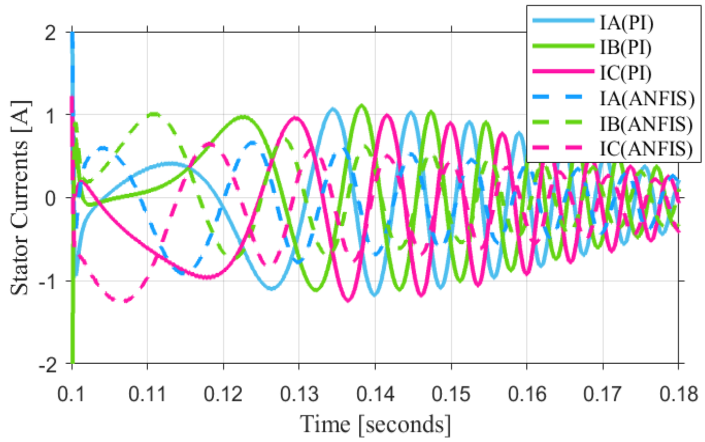

Figure 7.10 : Stator start-up currents at 3000 rpm without loading.

7.1.3 Speed Reversal for 3000 rpm without Loading

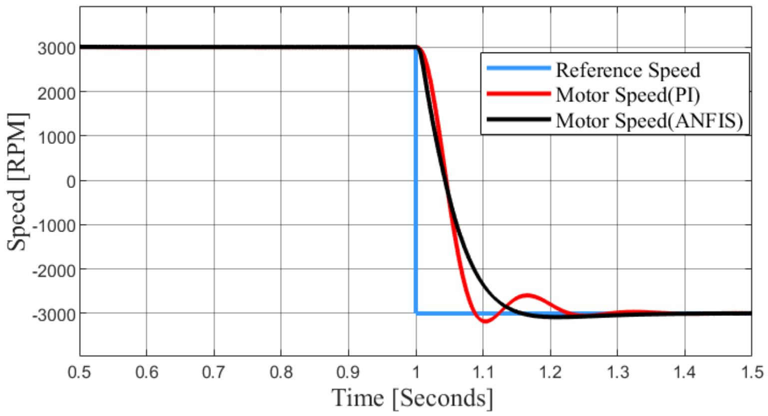

Figure 7.11 : Speed reversal response without loading.

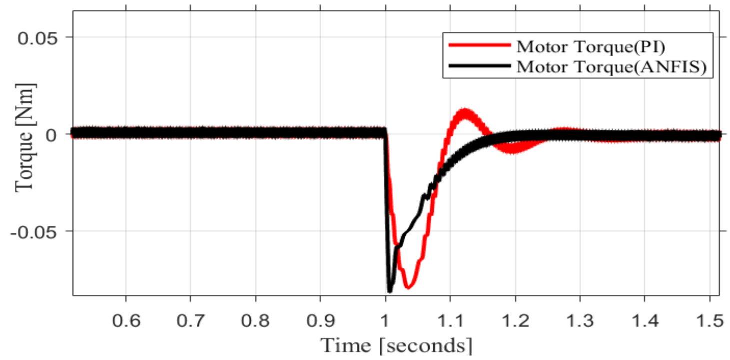

Figure 7.12 : Motor torque of speed reversal response without loading.

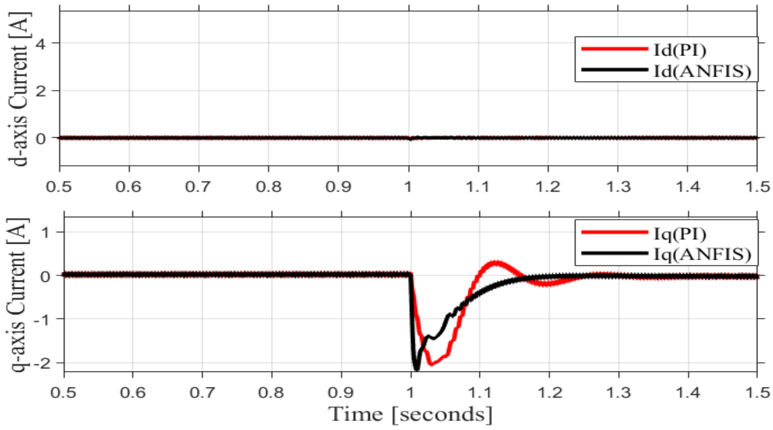

Figure 7.13 : d-q axis currents of speed reversal response without loading.

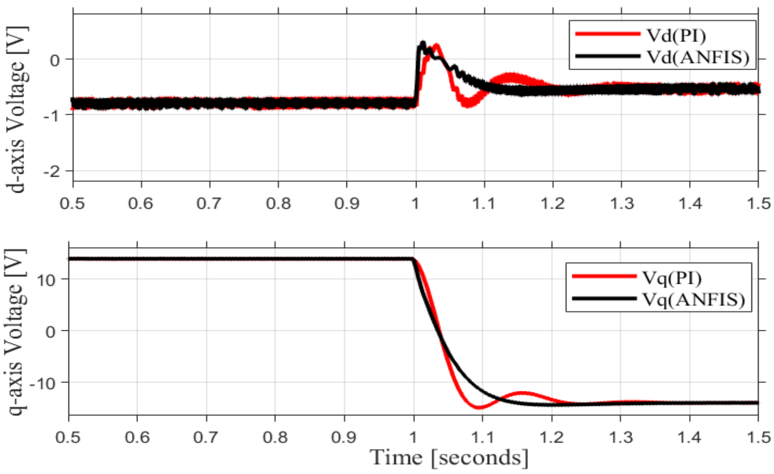

Figure 7.14 : d-q axis voltages of speed reversal response without loading.

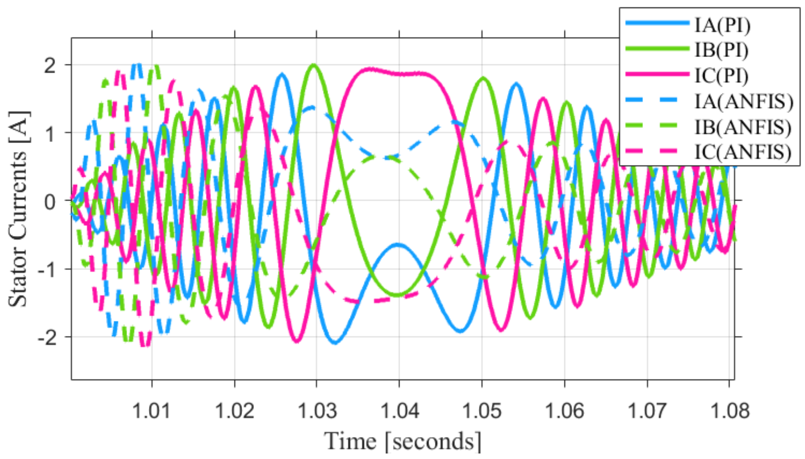

Figure 7.15 : Stator currents at speed reversal input without loading.

7.1.4 3000 rpm Under 0.10 Nm

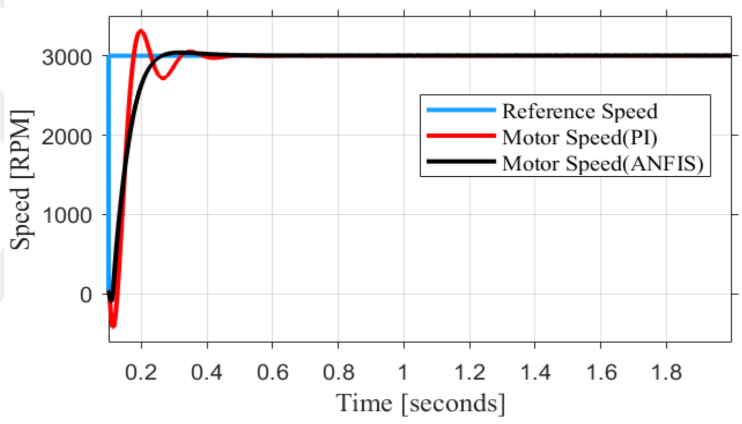

Figure 7.16 : Speed tracking at 3000 rpm under 0.10 Nm.

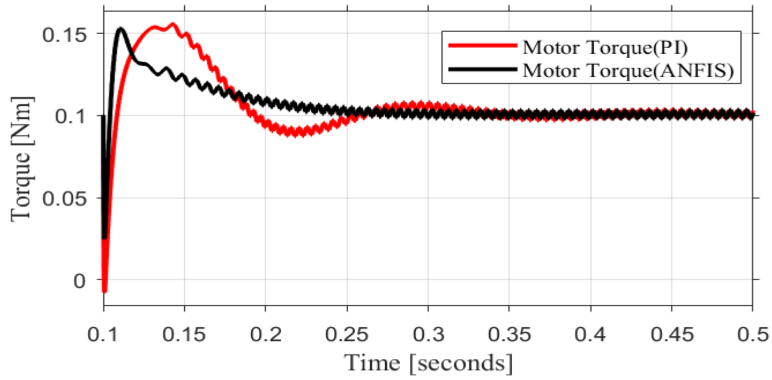

Figure 7.17 : Motor torque at 3000 rpm under 0.10 Nm.

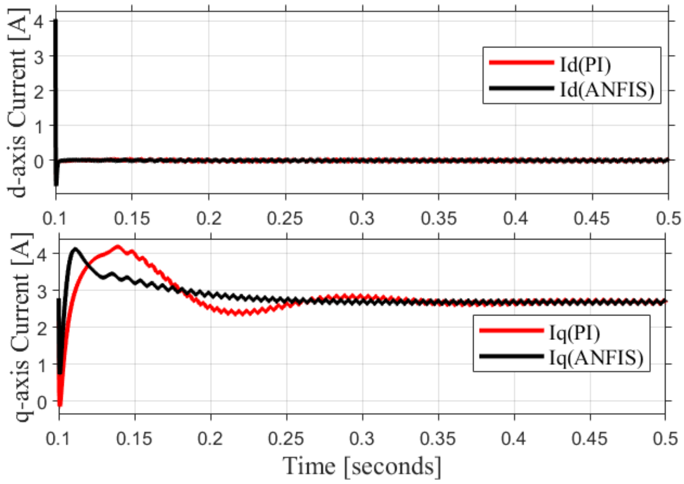

Figure 7.18 : d-q axis currents at 3000 rpm under 0.10 Nm.

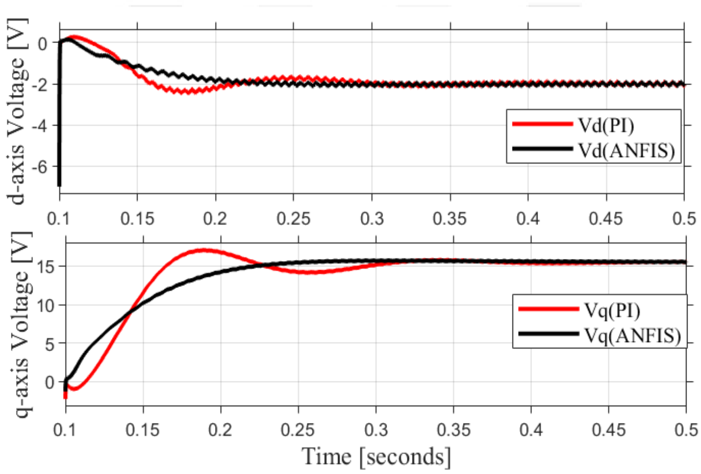

Figure 7.19 : d-q axis voltages at 3000 rpm under 0.10 Nm.

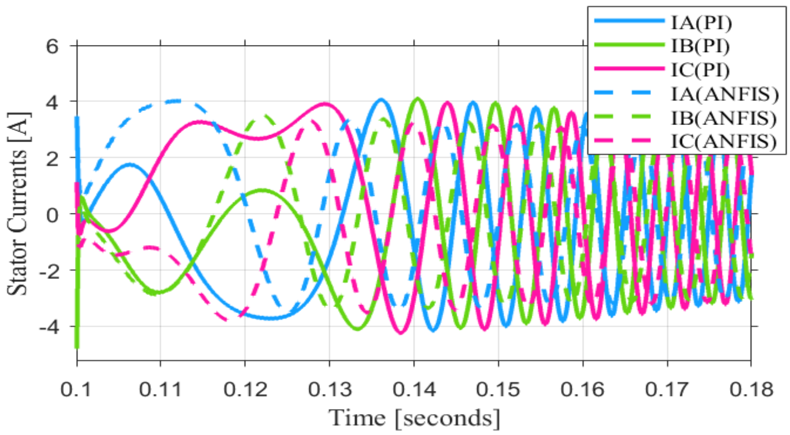

Figure 7.20 : Stator start-up currents at 3000 rpm under 0.10 Nm.

Simulation performance results are given Table 7.1.

Table 7.1 : Simulation performance results.

Controller Type	Conditions	Overshoot(%)	Settling Time(s)	Steady State Error (%)
PI	3000 rpm (No load)	4.57	0.211	0
	2000 rpm (No load)	5.45	0.209	0
	Speed Reversal (No load)	6	0.24	0
	3000 rpm under load	10.53	0.215	0
ANFIS	3000 rpm (No load)	1.6	0.1344	0.17
	2000 rpm (No load)	1.75	0.13	0.2
	Speed Reversal (No load)	2.72	0.23	0.172
	3000 rpm under load	1.33	0.14	0.2

7.2 Experiment Results

In this section, the real-time motor performance results with the both of the PI controller and the ANFIS controller at No-Load condition are illustrated for 2000 rpm and 3000 rpm. Speed reversal characteristics without loading for 3000 rpm are also included. Moreover, the motor is operated under load for 2000 rpm and 3000 rpm. Additionally, two types controllers performance characteristics are compared and examined in terms of overshoot, settling time and steady state error. Performance results are given in Table 7.2.

7.2.1 2000 rpm without the Loading

In the first scenario, the motor operates at a constant speed of 2000 rpm. The motor speed, electromagnetic torque, stator currents, and d-q-axis currents and voltages of a conventional PI controller and an ANFIS controller are presented. Torque response of no-load scenarios is estimated by using torque constant and q-axis current .

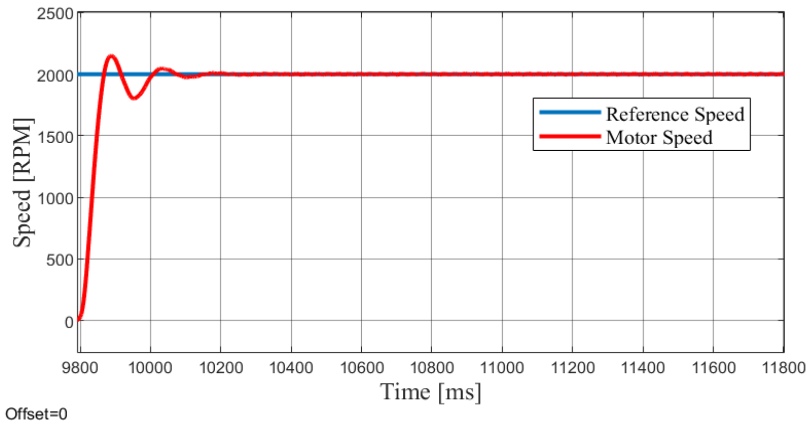

Figure 7.21 : Speed tracking at 2000 rpm without loading (PI Controller).

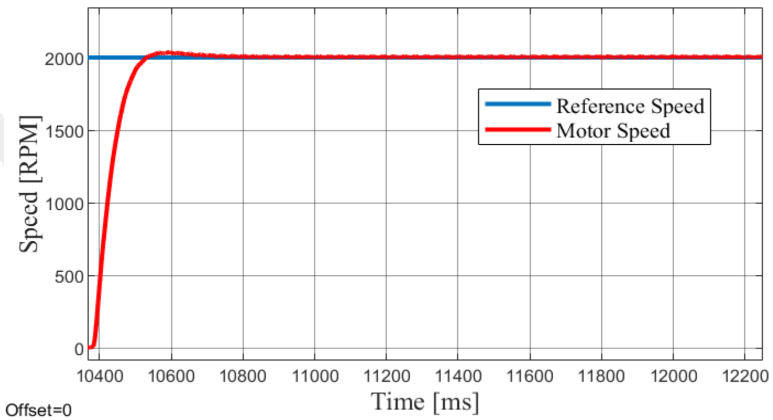

Figure 7.23 : Speed tracking at 2000 rpm without loading (ANFIS Controller).

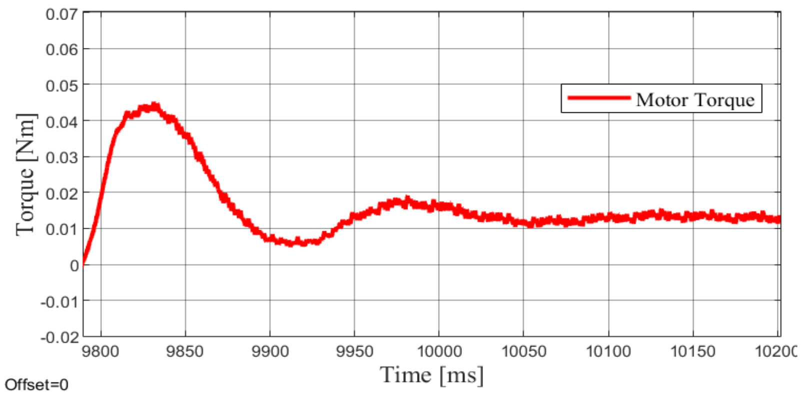

Figure 7.22 : Motor torque at 2000 rpm without loading (PI Controller).

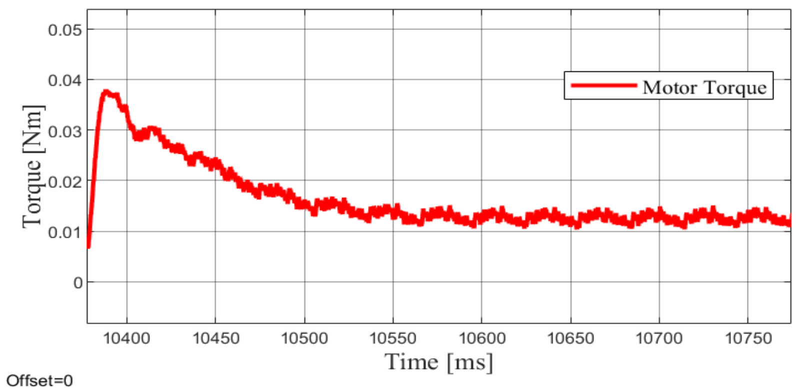

Figure 7.24 : Motor torque at 2000 rpm without loading (ANFIS Controller).

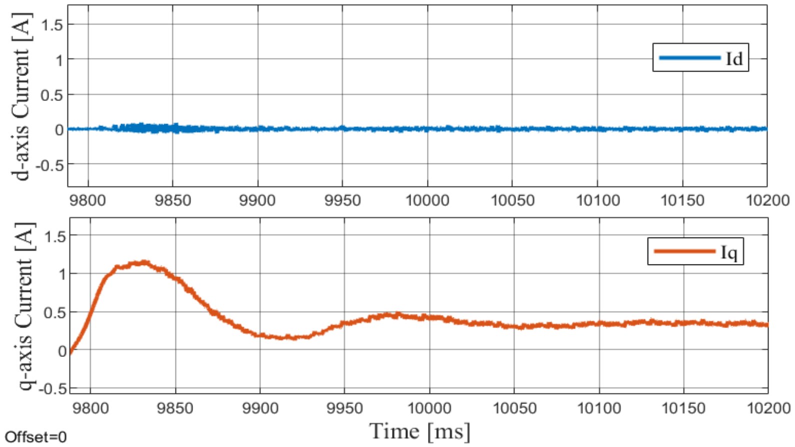

Figure 7.25 : d-q axis currents at 2000 rpm without loading (PI Controller).

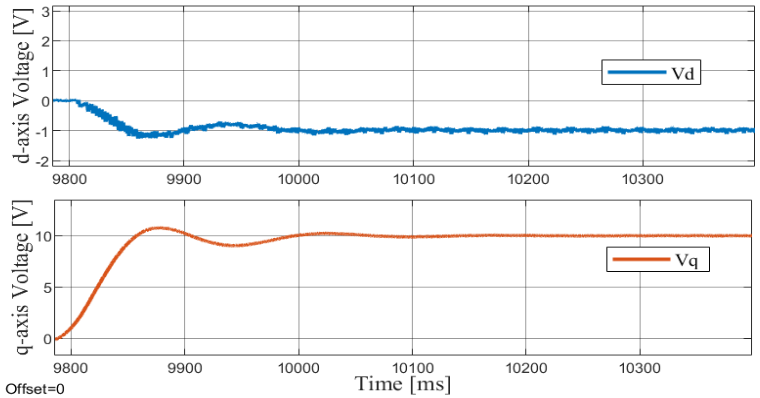

Figure 7.26 : d-q axis voltages at 2000 rpm without loading (PI Controller).

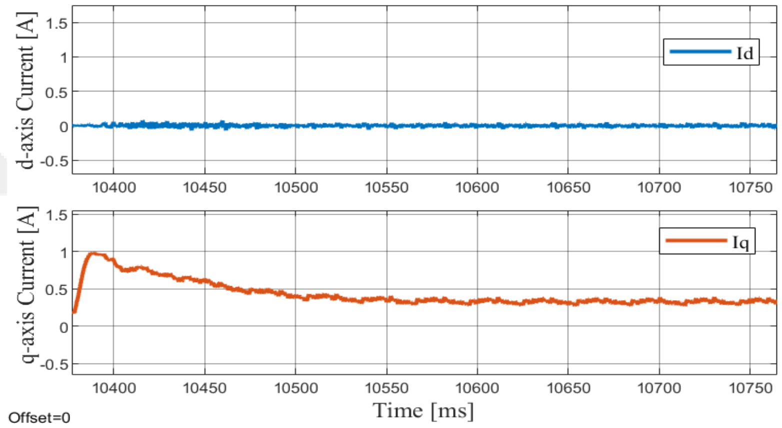

Figure 7.27 : d-q axis currents at 2000 rpm without loading (ANFIS Controller).

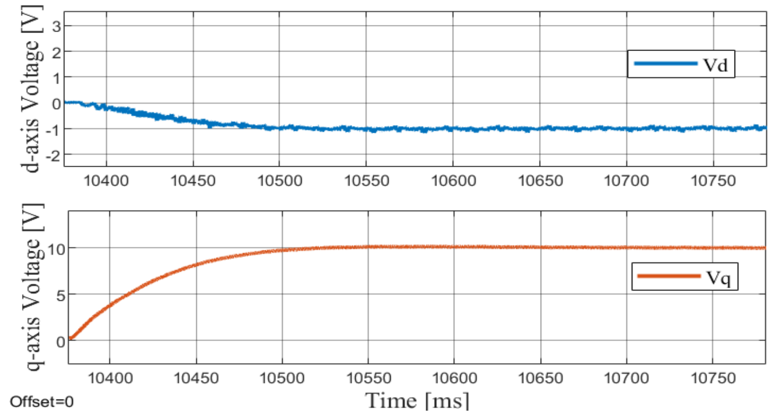

Figure 7.28 : d-q axis voltages at 2000 rpm without loading (ANFIS Controller).

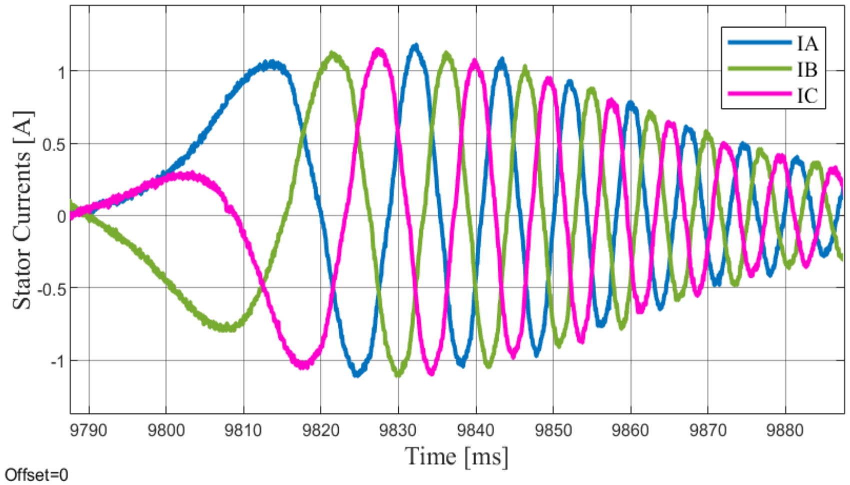

Figure 7.29 : Stator start-up currents at 2000 rpm without loading (PI Controller).

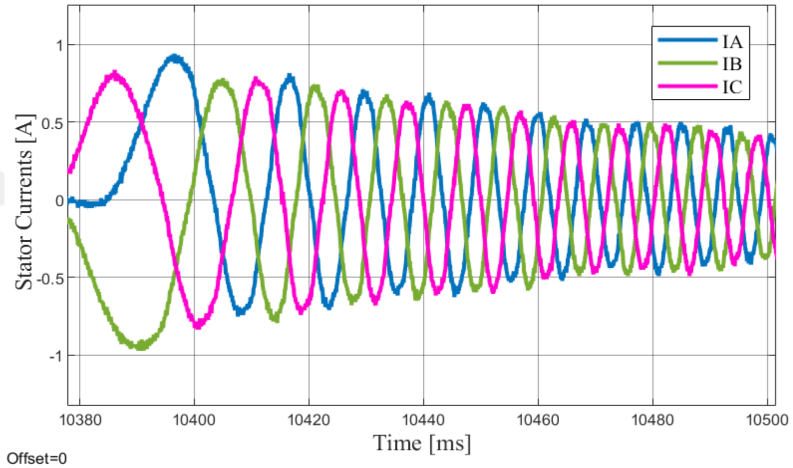

Figure 7.30 : Stator start-up currents at 2000 rpm without loading (ANFIS Controller).

7.2.2 3000 rpm without the Loading

In the second scenario, the motor operates at a constant speed of 3000 rpm. The motor speed, electromagnetic torque, stator currents, and d,q-axis currents and voltages of a conventional PI controller and an ANFIS controller are illustrated. As observed, the ANFIS speed controller allows to design more robust control.

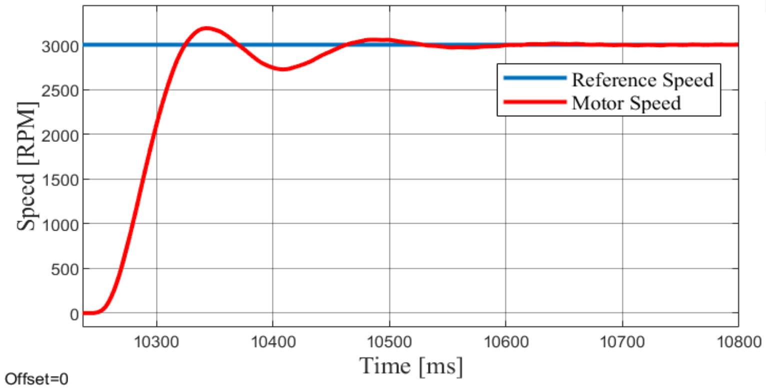

Figure 7.31 : Speed tracking at 3000 rpm without loading (PI Controller).

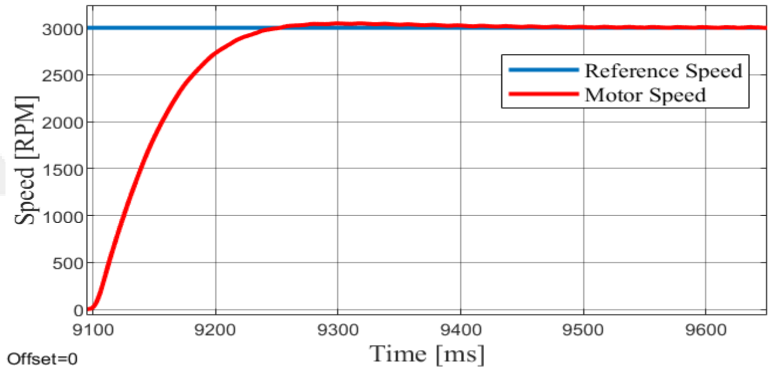

Figure 7.33 : Speed tracking at 3000 rpm without loading (ANFIS Controller).

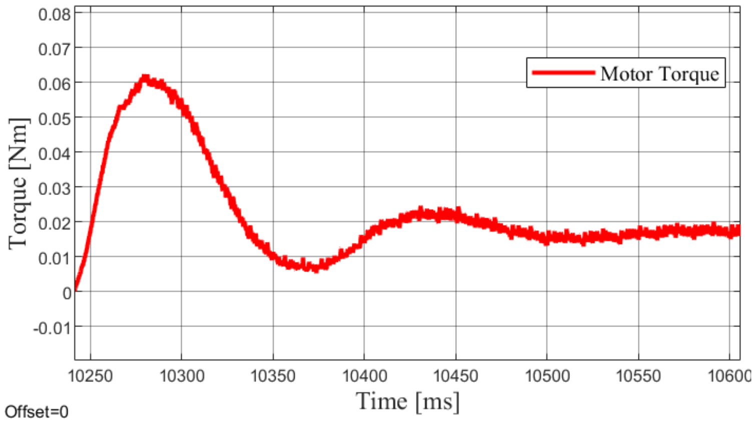

Figure 7.32 : Motor torque at 3000 rpm without loading (PI Controller).

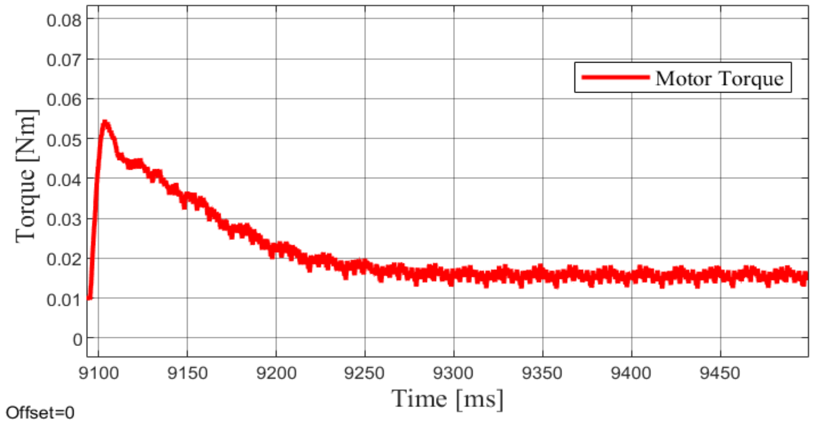

Figure 7.34 : Motor torque at 3000 rpm without loading (ANFIS Controller).

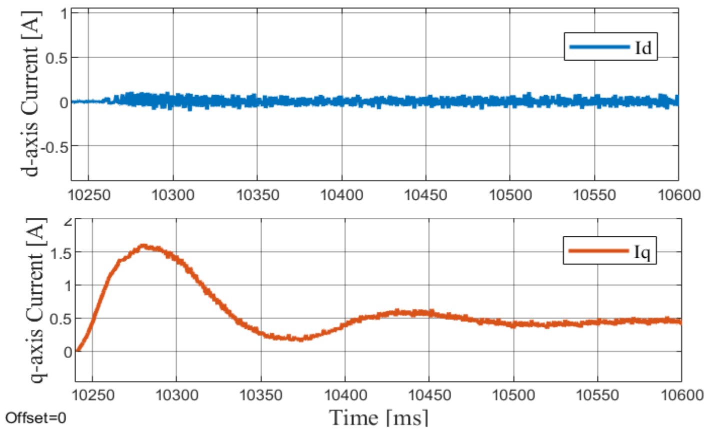

Figure 7.35 : d-q axis currents at 3000 rpm without loading (PI Controller)

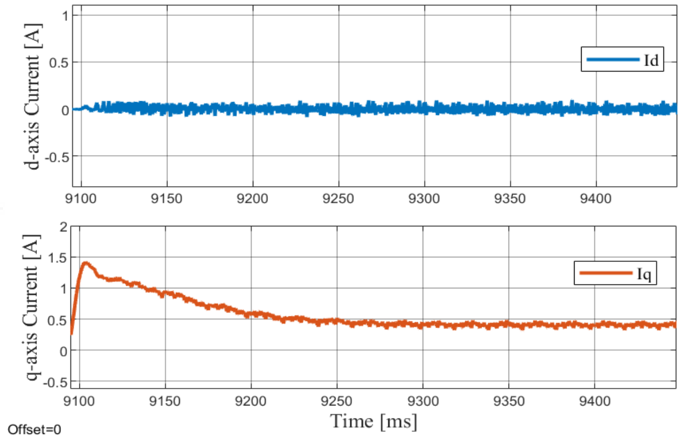

Figure 7.37 : d-q axis currents at 3000 rpm without loading (ANFIS Controller)

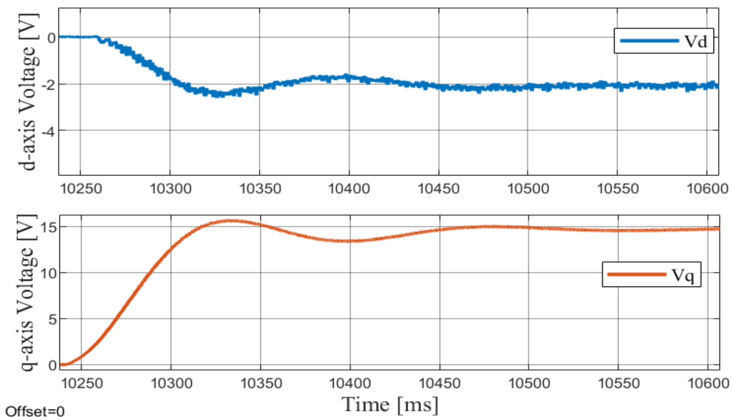

Figure 7.36 : d-q axis voltages at 3000 rpm without loading (PI Controller)

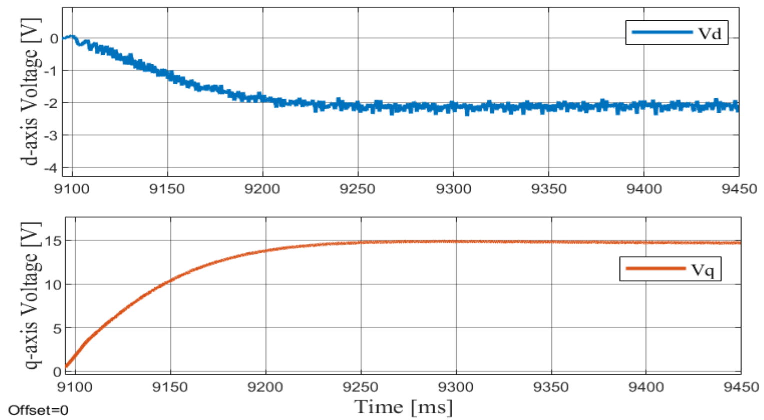

Figure 7.38 : d-q axis voltages at 3000 rpm without loading (ANFIS Controller)

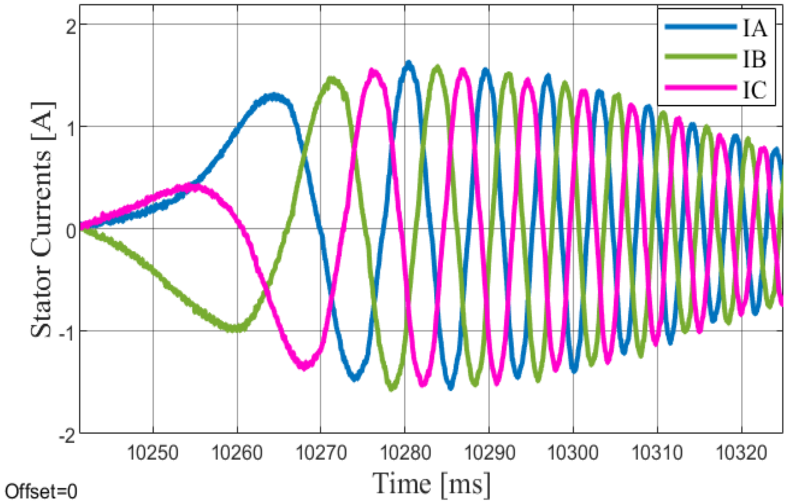

Figure 7.39 : Stator start-up currents at 3000 rpm without loading (PI Controller).

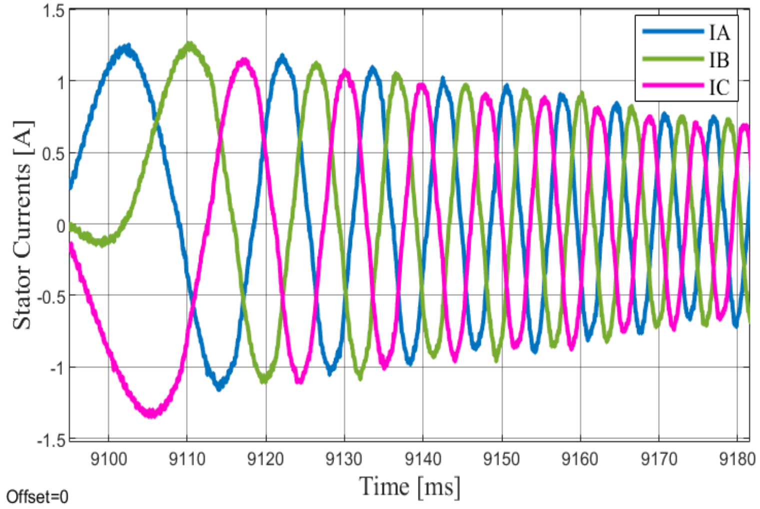

Figure 7.40 : Stator start-up currents at 3000 rpm without loading (ANFIS Controller).

7.2.3 Speed Reversal for 3000 rpm without the Loading

The third scenario is related to obtain speed reversal characteristics of the PMSM. The responses of motor speed, torque, stator currents and d-q-axis currents and voltages during speed reversal operation are given.

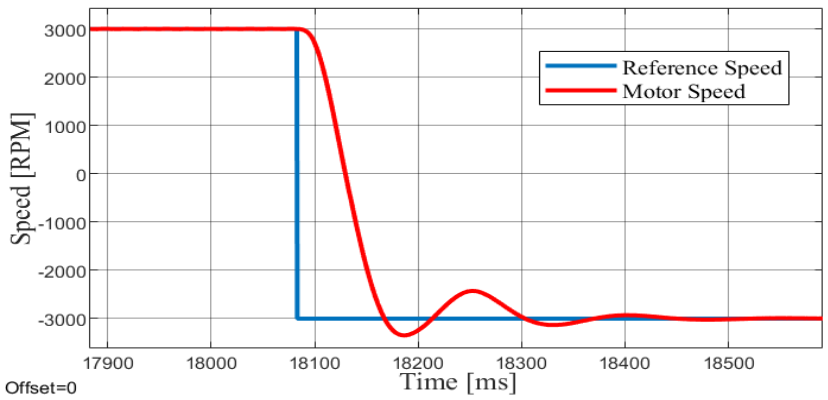

Figure 7.41 : Speed reversal tracking at 3000 rpm without loading (PI Controller)

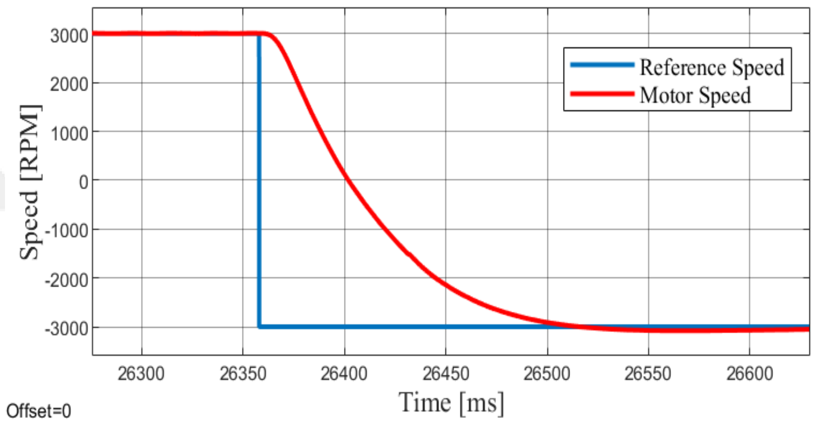

Figure 7.43 : Speed reversal tracking at 3000 rpm without loading (ANFIS Controller)

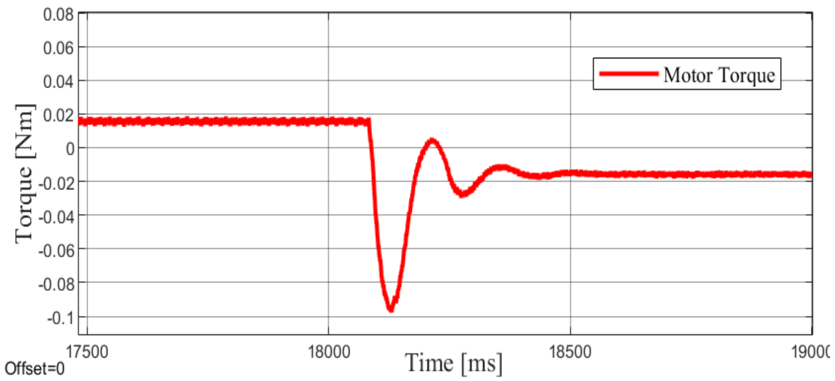

Figure 7.42 : Motor torque of speed reversal at 3000 rpm without loading (PI Controller).

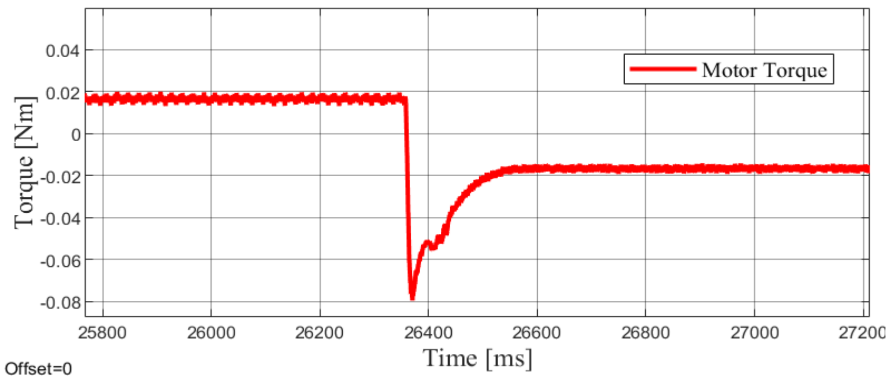

Figure 7.44 : Motor torque of speed reversal at 3000 rpm without loading (ANFIS Controller).

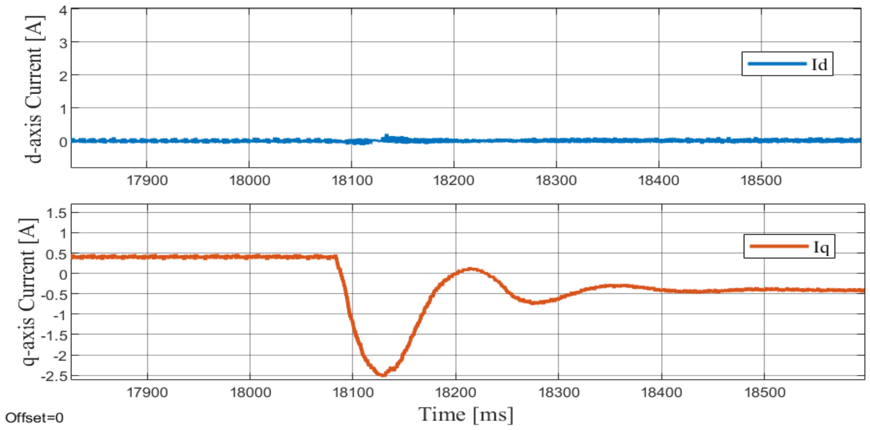

Figure 7.45 : d-q axis currents of speed reversal at 3000 rpm without loading (PI Controller).

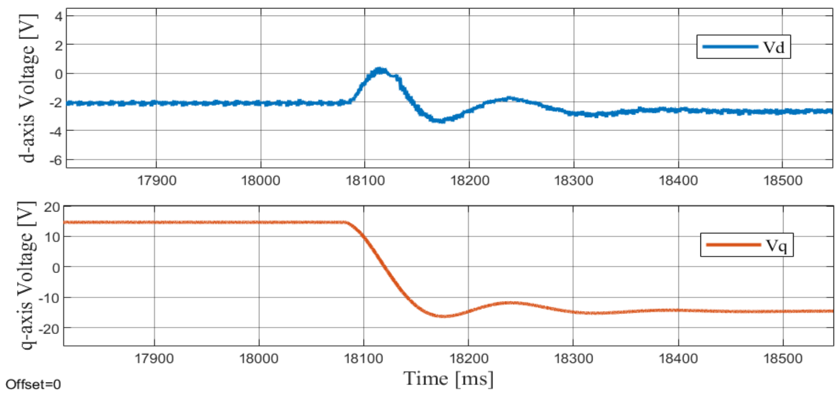

Figure 7.46 : d-q axis voltages of speed reversal at 3000 rpm without loading (PI Controller).

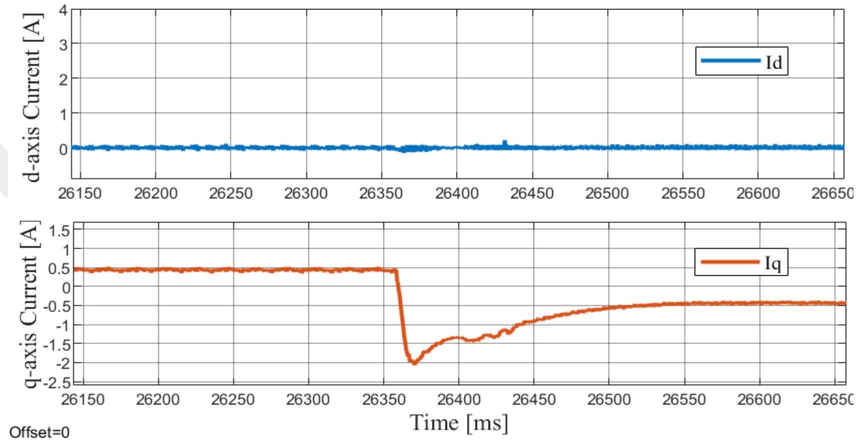

Figure 7.47 : d-q axis currents of speed reversal at 3000 rpm without loading (ANFIS Controller).

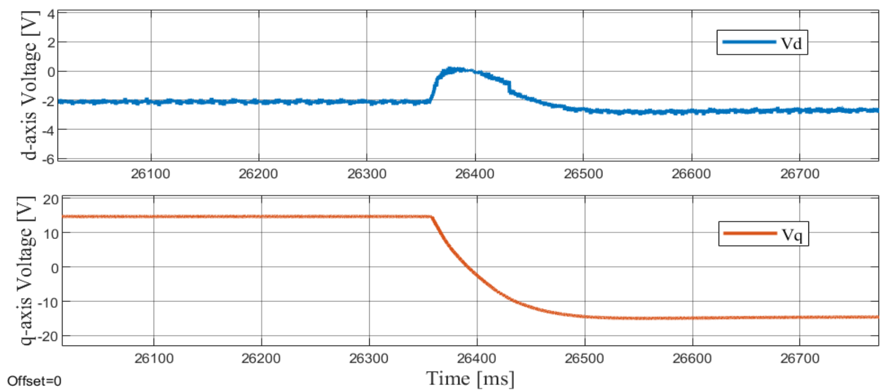

Figure 7.48 : d-q axis voltages of speed reversal at 3000 rpm without loading (ANFIS Controller).

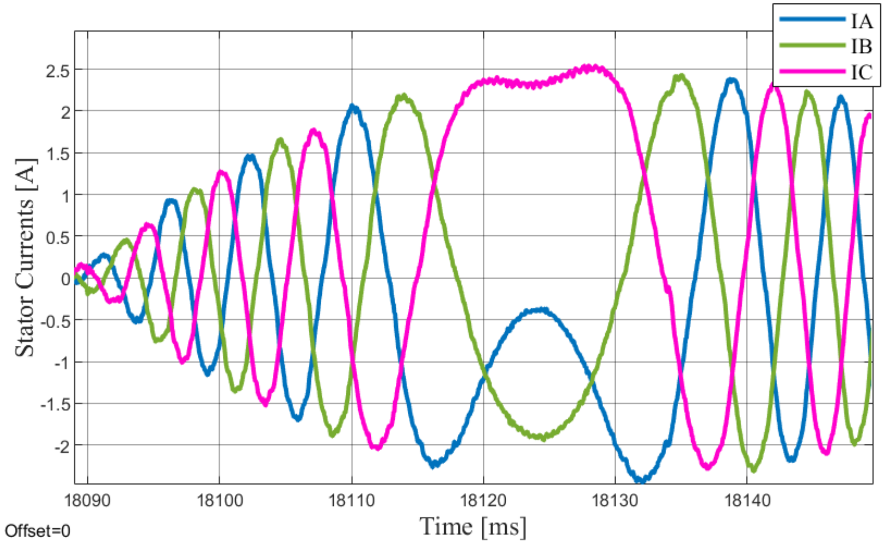

Figure 7.49 : Stator currents of speed reversal at 3000 rpm without loading (PI Controller).

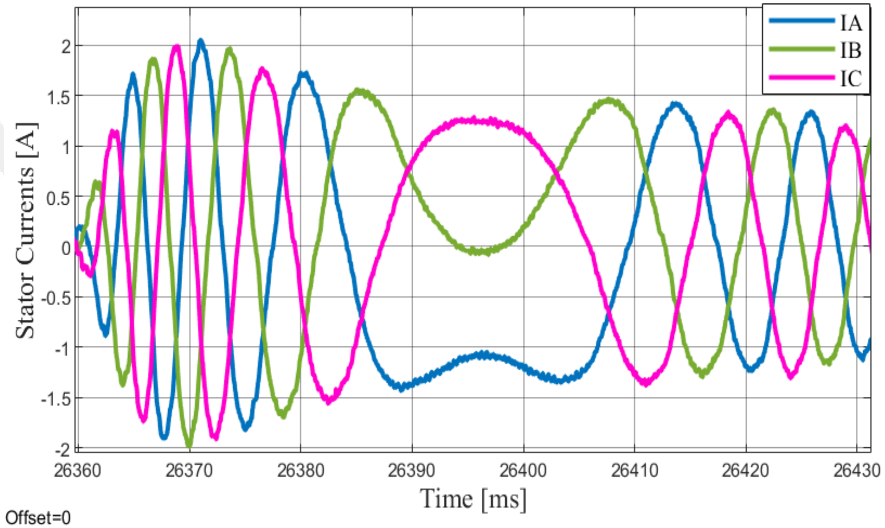

Figure 7.50 : Stator currents of speed reversal at 3000 rpm without loading (ANFIS Controller).

7.2.4 2000 rpm Under the Load

In this scenario, the motor operates at constant speed of 2000 rpm under load. The characteristics of motor speed, torque, stator currents and d-q axis currents and voltages are presented and examined. Loading of the motor is performed with an appropriate testbench. The set-up is integrated with load cells to measure force applied by the motor under load. To obtain motor torque in the test environment, the distance of the motor shaft to reference load cells are considered and the length is multiplied with force found via load cells.

Motor torque characteristic is observed utilizing PLC monitors. The figure is plotted by extracting data using PLC.

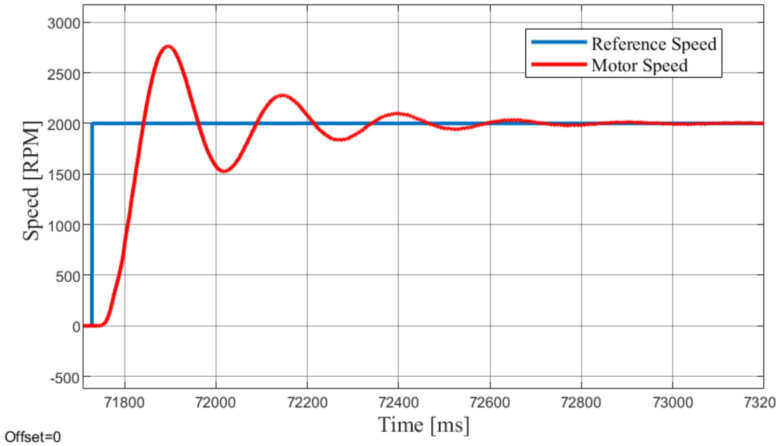

Figure 7.51 : Speed tracking at 2000 rpm under load (PI Controller).

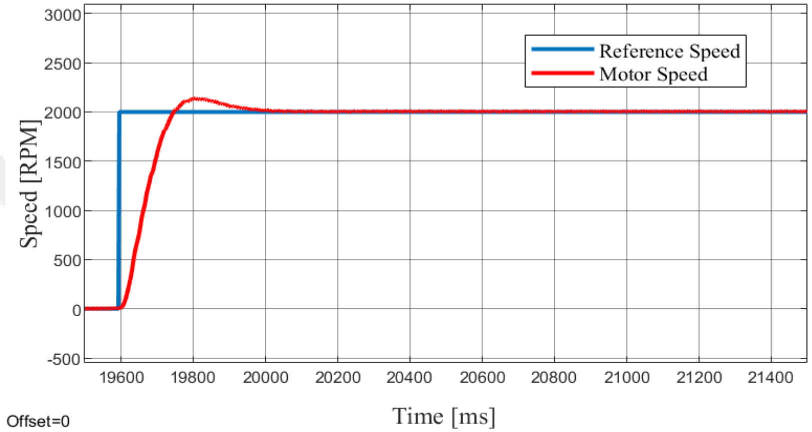

Figure 7.53 : Speed tracking at 2000 rpm under load (ANFIS Controller).

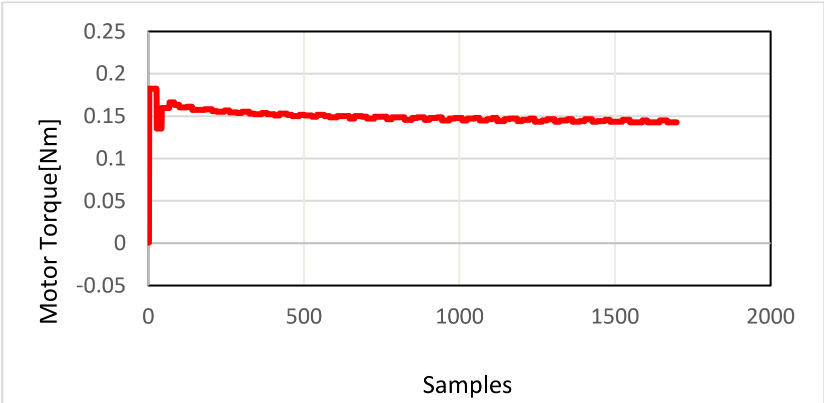

Figure 7.52 : Motor torque at 2000 rpm under load (PI Controller).

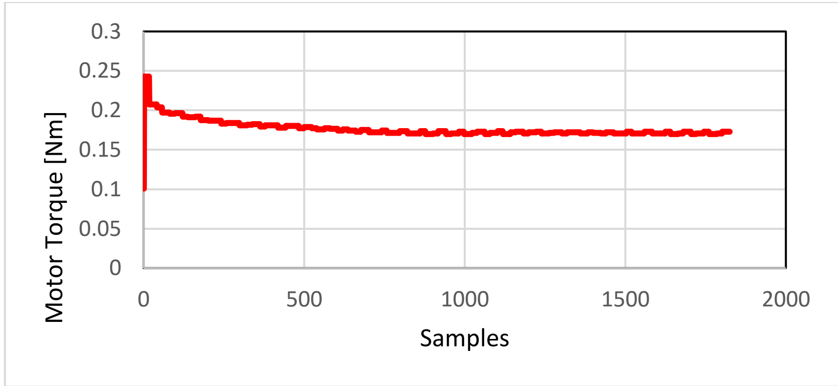

Figure 7.54 : Motor torque at 2000 rpm under load (ANFIS Controller).

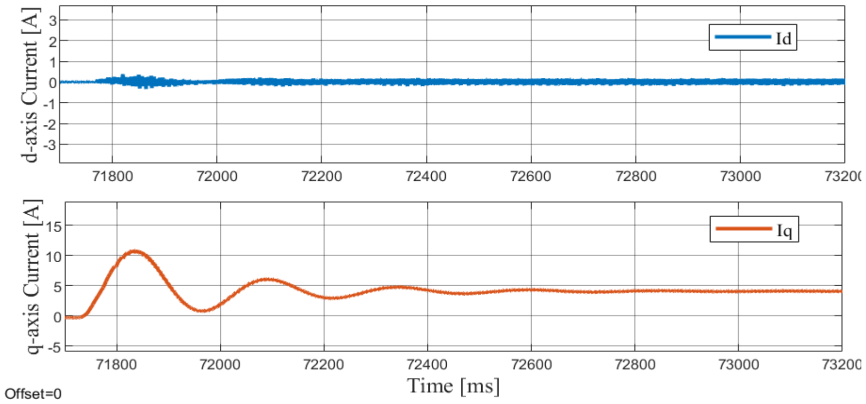

Figure 7.55 : d-q axis currents at 2000 rpm under load (PI Controller).

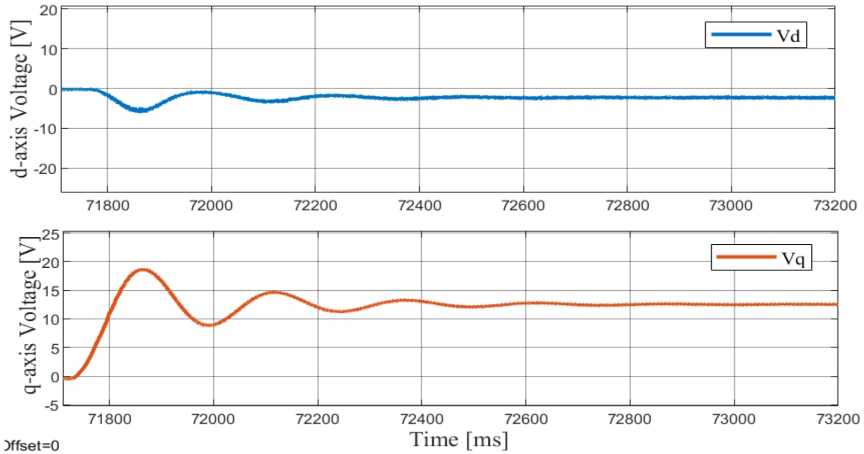

Figure 7.56 : d-q axis voltages at 2000 rpm under load (PI Controller).

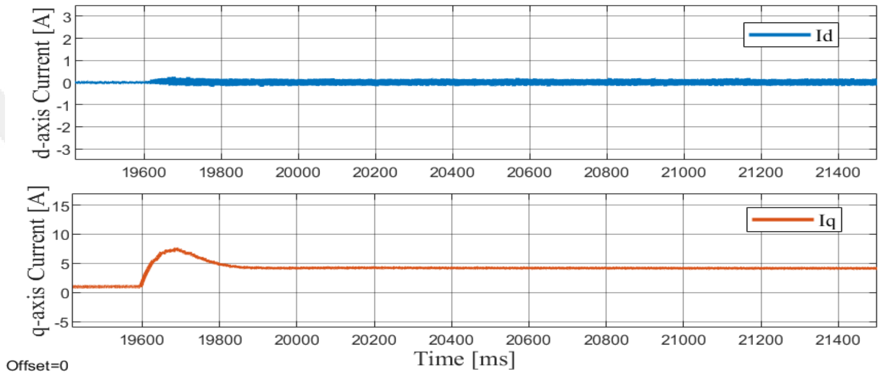

Figure 7.57 : d-q axis currents at 2000 rpm under load (ANFIS Controller).

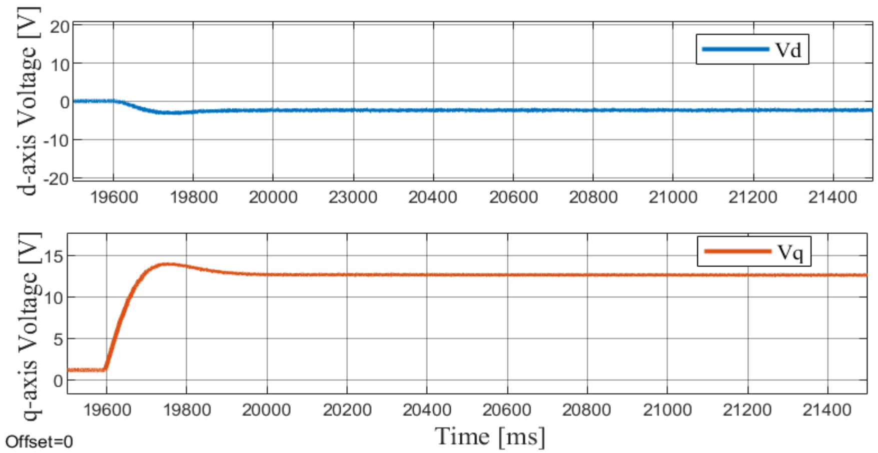

Figure 7.58 : d-q axis voltages at 2000 rpm under load (ANFIS Controller).

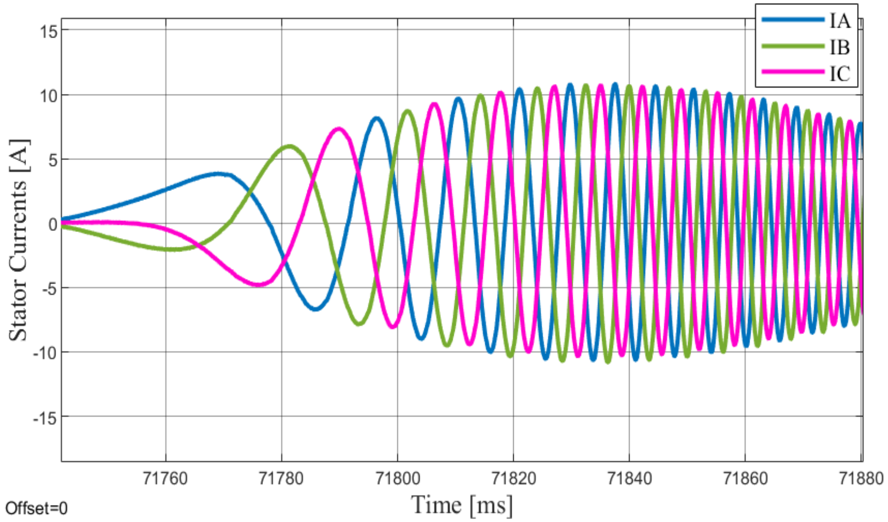

Figure 7.59 : Stator start-up currents at 2000 rpm under load (PI Controller).

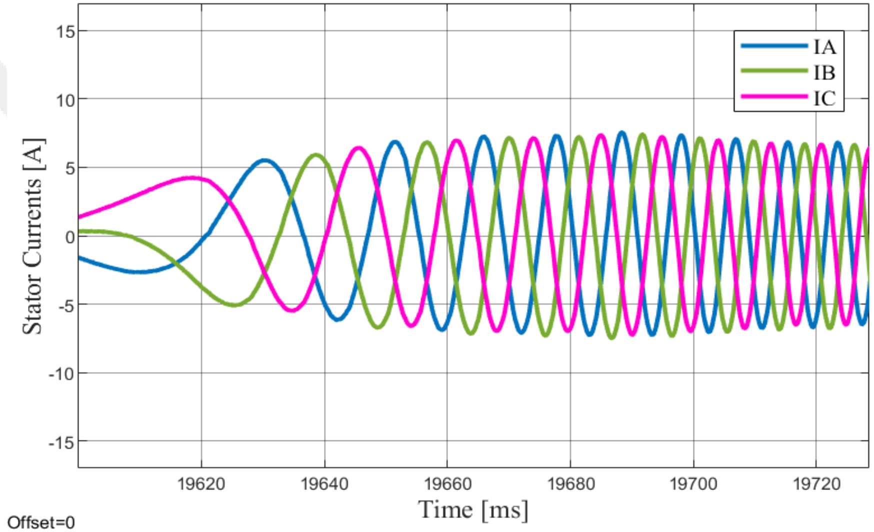

Figure 7.60 : Stator start-up currents at 2000 rpm under load (ANFIS Controller).

7.2.5 3000 rpm Under the Load

The final scenario describes how the PMSM performance changes under the load. In this scenario, the motor operates at constant speed of 3000 rpm under the load. The characteristics of motor speed, torque, stator currents and d-q-axis currents and voltages are illustrated and compared. Loading of the motor requires an appropriate testbench. The set-up is already given.

Obtaining the real-time motor torque characteristic is based on PLC set-up. The dataset of the motor torque response is extracted and imported to Excel and the desired motor response is plotted.

As can be seen from the figures, designed PI Controller is more susceptible to external disturbances. The increased overshoot may cause the desired speed limit to be exceeded or reach the saturation.Therefore, ANFIS provides more reliable operation.

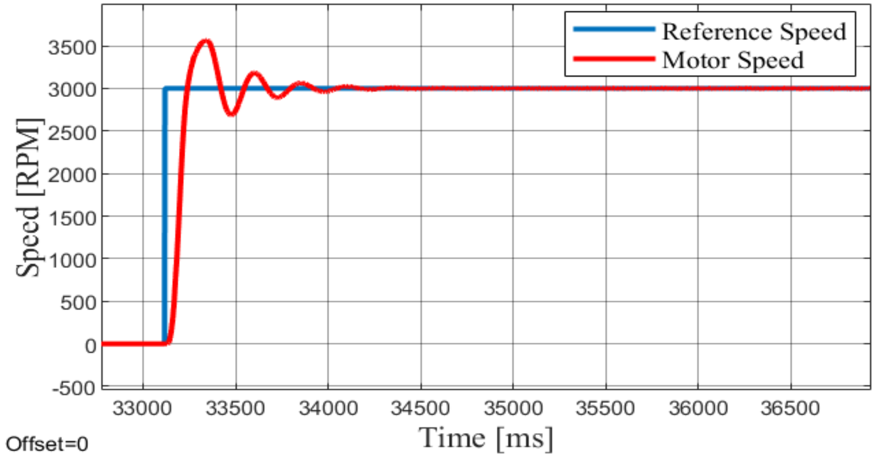

Figure 7.61 : Speed tracking at 3000 rpm under load (PI Controller).

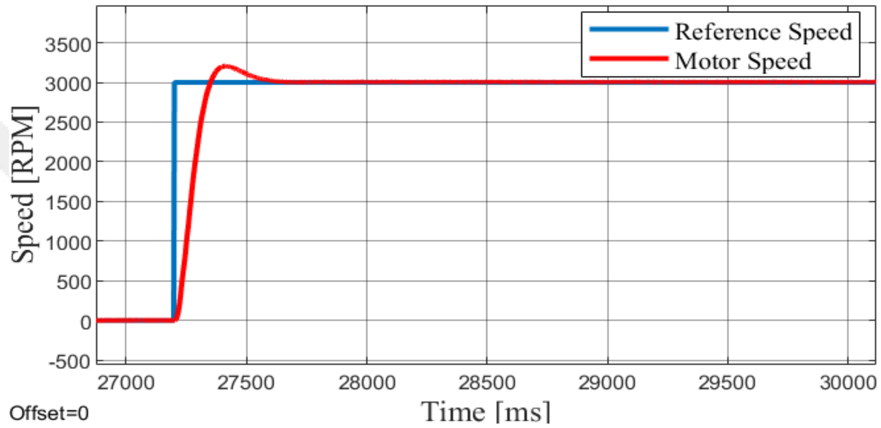

Figure 7.63 : Speed tracking at 3000 rpm under load (ANFIS Controller).

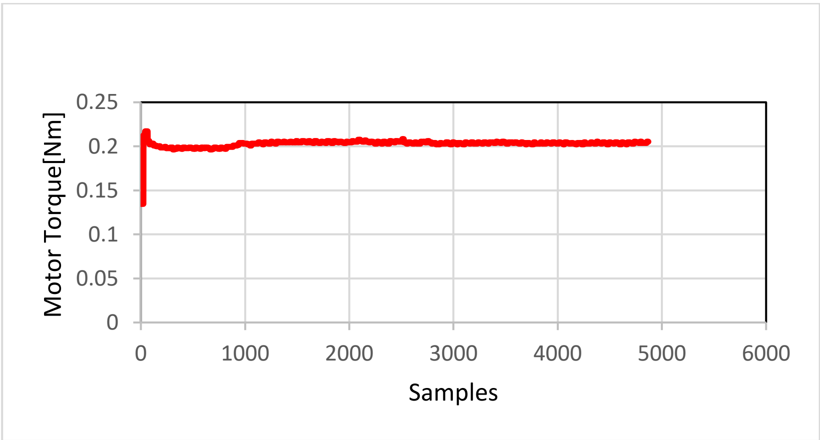

Figure 7.62 : Motor torque at 3000 rpm under load (PI Controller).

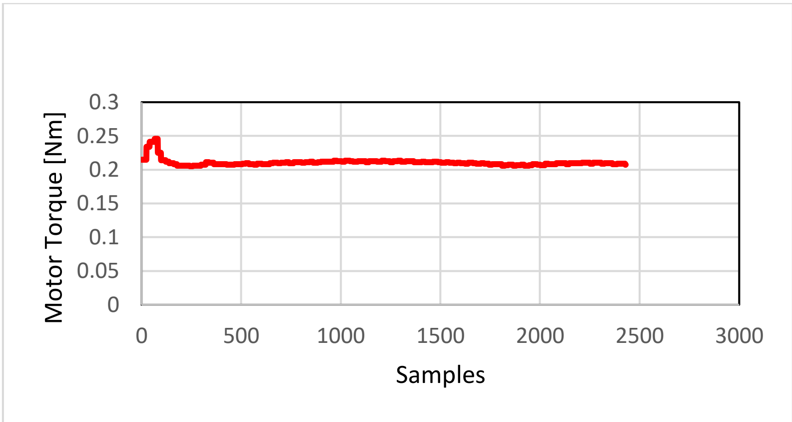

Figure 7.64 : Motor torque at 3000 rpm under load (ANFIS Controller).

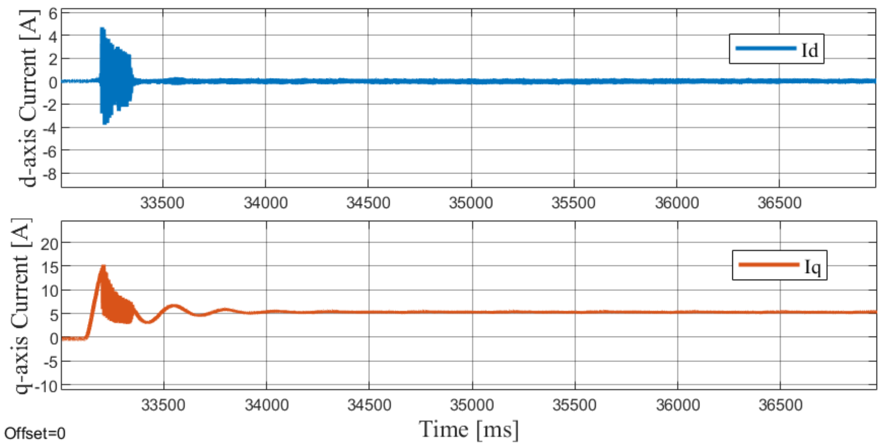

Figure 7.65 : d-q axis currents at 3000 rpm under load (PI Controller).

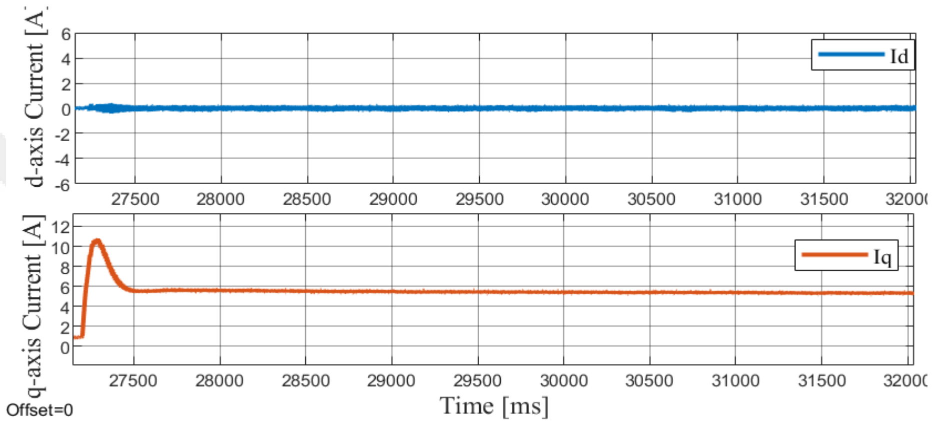

Figure 7.67 : d-q axis currents at 3000 rpm under load (ANFIS Controller).

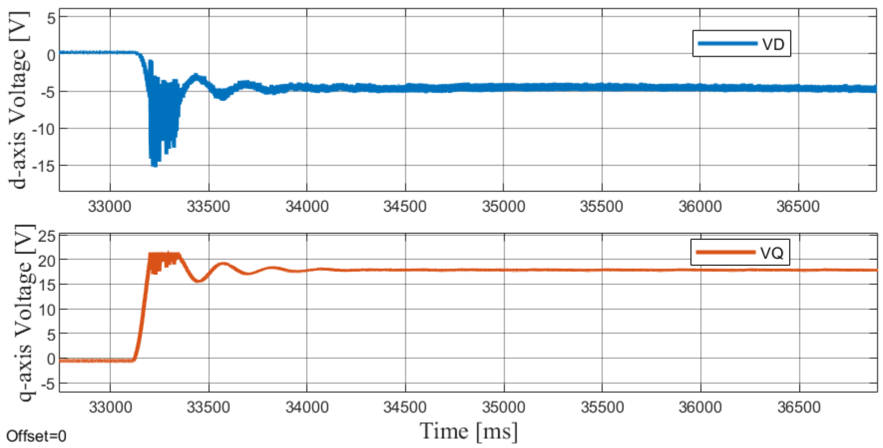

Figure 7.66 : d-q axis voltages at 3000 rpm under load (PI Controller).

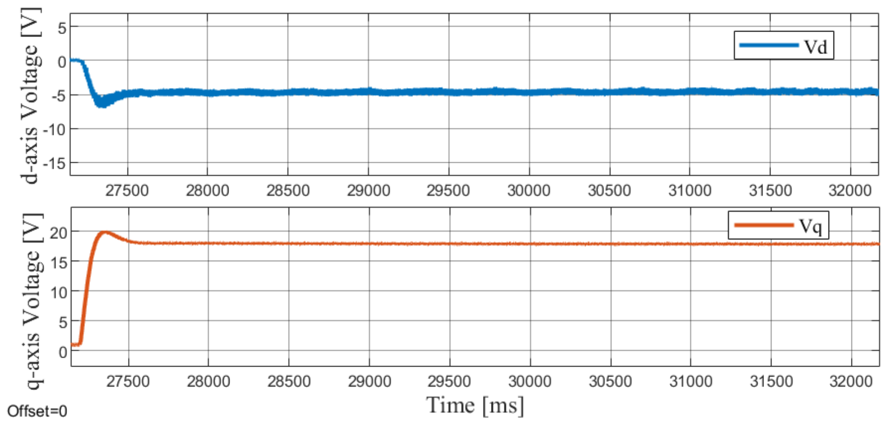

Figure 7.68 : d-q axis voltages at 3000 rpm under load (ANFIS Controller).

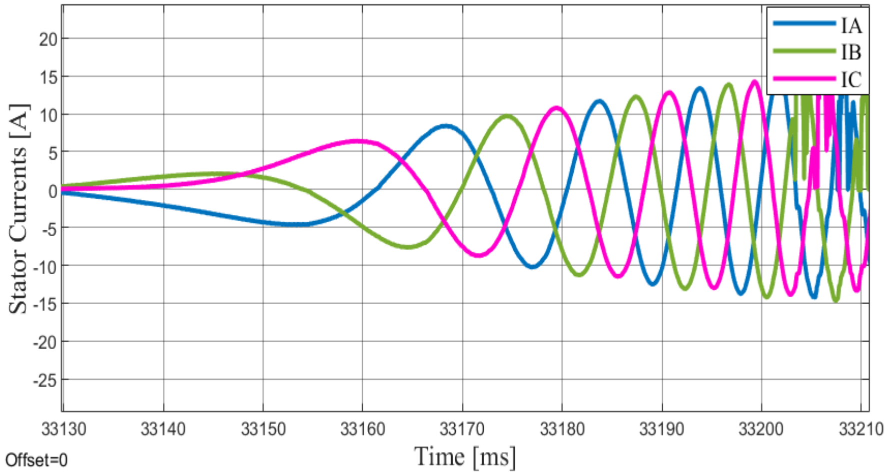

Figure 7.69 : Stator start-up currents at 3000 rpm under load (PI Controller).

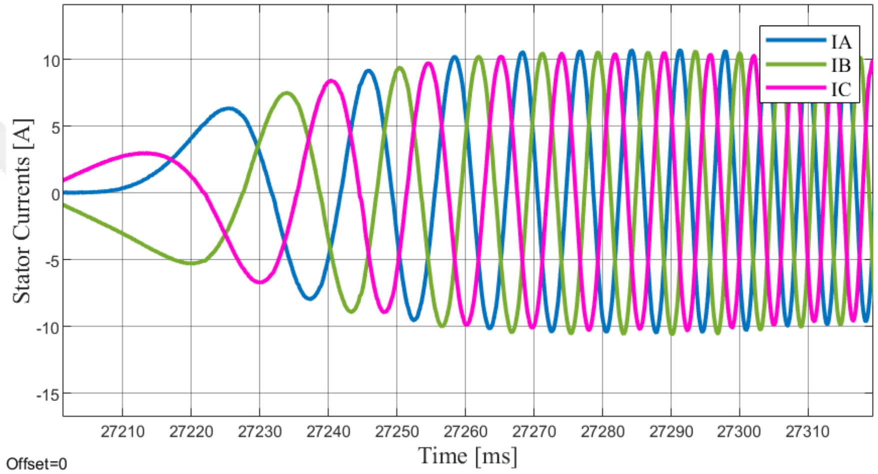

Figure 7.70 : Stator start-up currents at 3000 rpm under load (ANFIS Controller).

Real-time performance results are presented in Table 7.2.

Table 7.2 : Real-time performance results.

Controller Type	Conditions	Overshoot(%)	Settling Time(s)	Steady State Error (%)
PI	3000 rpm (No load)	6.17	0.211	0
	2000 rpm (No load)	7.48	0.208	0
	Speed Reversal (No load)	11.2	0.38	0
	3000 rpm (Under load)	18.9	0.65	0
	2000 rpm (Under load)	36.3	0.77	0
ANFIS	3000 rpm (No load)	1.57	0.136	0.27
	2000 rpm (No load)	1.75	0.135	0.35
	Speed Reversal (No load)	2.79	0.36	0.33
	3000 rpm (Under load)	6.9	0.36	0.39
	2000 rpm (Under load)	6.25	0.31	0.38

8. CONCLUSIONS AND RECOMMENDATIONS

In this thesis, the dynamics of PMSM are modeled using mathematical expressions in MATLAB/Simulink environment. The PMSM is driven with a conventional PI controller and ANFIS controller. The proposed ANFIS system requires the extraction of the training data from a PMSM dynamic model with a conventional PI controller to achieve enhanced motor performance. Implementation of the drive system generally requires intense coding ability and experience. Nevertheless, MATLAB/Simulink supports to build and deploy code into microcontrollers by using Motor Control Blockset and Embedded Coder to generate C code. The experimental results are obtained with non-complex communication interface in Simulink.

Results of the PI and ANFIS controllers are presented under the different speed and loads conditions. The comparative performance analysis is conducted between the ANFIS controller and the PI controller through simulations and testing. Table 8.1 shows Simulation vs. Real-Time performance results for both controllers.

Table 8.1 : Simulation vs. Real-Time performance comparison under no-load.

Type	Condition	Overshoot(%)		Settling Time(s)		Steady State Error (%)	
		Simulation	Test	Simulation	Test	Simulation	Test
PI	3000 rpm (No load)	4.57	6.17	0.211	0.211	0	0
	2000 rpm (No load)	5.45	7.48	0.209	0.208	0	0
	Speed Reversal (No load)	6	11.2	0.24	0.38	0	0
ANFIS	3000 rpm (No load)	1.6	1.57	0.1344	0.136	0.17	0.27
	2000 rpm (No load)	1.75	1.75	0.13	0.135	0.2	0.35
	Speed Reversal (No load)	2.72	2.79	0.23	0.36	0.172	0.33

ANFIS method offers a more robust performance to overshoot in speed. The steady-state error of ANFIS controller is about 0.30% despite the PI controller has no steady state error. Nonetheless, this insignificant error can be ignored as it is too small. In addition, the results show ANFIS design has reduced a settling time compared to the PI controller. However, the part of training data in ANFIS requires more time, and the selection of the number and type of MFs affects the training error. To achieve a better performance result in speed, the speed reference to be trained in ANFIS should cover entire the speed range including motor and generator operation region. In addition, the number of the samples collected should be as large as possible. Therefore, the sampling time of the speed control can be taken in μs.

Table 8.1 indicates that the simulation results of the ANFIS controller are so close to real-time performance results except the settling time of speed reversal characteristics while as the simulation results of the PI controller differs in the overshoot and settling time. The nonlinear system dynamics and the external disturbances lead the difference. On the other hand, the ANFIS controller shows more robust performance as it is adapted and learned the whole motor dynamics and removes the external effects.

Table 8.2 : Real-Time performance results with loading.

Controller Type	Conditions	Overshoot(%)	Settling Time(s)	Steady State Error (%)
PI	3000 rpm (Under load)	18.9	0.65	0
	2000 rpm (Under load)	36.3	0.77	0
ANFIS	3000 rpm (Under load)	6.9	0.36	0.39
	2000 rpm (Under load)	6.25	0.31	0.38

Table 8.2 represents that the real-time performance results with loading. As it is seen obviously, the ANFIS controller has drastically reduced the overshoot (in 2% error band). Moreover, unlike the PI controller the ANFIS controller considerably shortens the settling time Beside the steady-state error, one of the drawbacks of the ANFIS controller in real-time testing is increased torque ripples compared to the PI controller.

In the literature comparison of the performance responses of the proposed ANFIS controller with its counterparts, the similar results are obtained such as reduced settling time and less peak overshoot [11,14].

In the future work, the battery and the Battery Management System ensuring a State of the Charge(SoC) Estimation will be used instead of DC power supply. Kalman filter study for SoC estimation will be applied and this study will be extended in terms of the electrical power generation units. Furthermore, considering the cost the hardware selection will be stand-alone components and coding ability will be improved in case Mathworks modeling interface is insufficient.

REFERENCES

[1] **Marufuzzaman, M., Reaz, M. B. I., Rahman, M. S., & Ali, M. A. M.** (2010). Hardware prototyping of an intelligent current d-q PI controller for FOC PMSM drive. International Conference on Electrical & Computer Engineering (ICECE 2010). Published. https://doi.org/10.1109/icelce.2010.5700559

[2] **Vindel, D., Haghbin, S., Rabiei, A., Carlson, O., & Ghorbani, R.** (2012). Field-oriented control of a PMSM drive system using the dSPACE controller. 2012 IEEE International Electric Vehicle Conference. Published. https://doi.org/10.1109/ievc.2012.6183206

[3] **Shang, H., Zhao, L., & Wang, T.** (2015). Torque Ripple Reduction for Permanent Magnet Synchronous *Motor Based on Learning Control. 2015 2nd International Conference on Information Science and Control Engineering. Published. https://doi.org/10.1109/icisce.2015.226*

[4] **Salem, W. A. A., Osman, G. F., & Arfa, S. H.** (2018). Adaptive Neuro-Fuzzy Inference System Based Field Oriented Control of PMSM & Speed Estimation. *2018 Twentieth International Middle East Power Systems Conference (MEPCON)*. Published. https://doi.org/10.1109/mepcon.2018.8635179

[5] **Zhao, Y., Liu, X., & Zhang, Q.** (2019). Predictive Speed-Control Algorithm Based on a Novel Extended-State Observer for PMSM Drives. *Applied Sciences*, *9*(12), 2575. https://doi.org/10.3390/app9122575

[6] **Aghili, F.** (2018). Optimal Feedback Linearization Control of Interior PM Synchronous Motors Subject to Time-Varying Operation Conditions Minimizing Power Loss. *IEEE Transactions on Industrial Electronics*, *65*(7), 5414–5421. https://doi.org/10.1109/tie.2017.2784348

[7] **Hu, J., Qiu, Y., & Lu, H.** (2016). Adaptive robust nonlinear feedback control of chaos in PMSM system with modeling uncertainty. *Applied Mathematical Modelling*, *40*(19–20), 8265–8275. https://doi.org/10.1016/j.apm.2016.04.019

[8] **Chen, J., Yao, W., Ren, Y., Wang, R., Zhang, L., & Jiang, L.** (2019). Nonlinear adaptive speed control of a permanent magnet synchronous motor: A perturbation estimation approach. Control Engineering Practice, 85, 163–175. https://doi.org/10.1016/j.conengprac.2019.01.019

[9] **Qian, J., Ji, C., Pan, N., & Wu, J.** (2018). Improved Sliding Mode Control for Permanent Magnet Synchronous Motor Speed Regulation System. *Applied Sciences*, *8*(12), 2491. https://doi.org/10.3390/app8122491

[10] **Liu, X., Yu, H., Yu, J., & Zhao, L.** (2018). Combined Speed and Current Terminal Sliding Mode Control With Nonlinear Disturbance Observer for PMSM Drive. *IEEE Access*, *6*, 29594–29601. https://doi.org/10.1109/access.2018.2840521

[11] **Shanthi, R., Kalyani, S., & Devie, P. M.** (2020). Design and performance analysis of adaptive neuro-fuzzy controller for speed control of permanent magnet synchronous motor drive. *Soft Computing*, *25*(2), 1519–1533. https://doi.org/10.1007/s00500-020-05236-5

[12] **Yu, J., Chen, B., Yu, H., Lin, C., & Zhao, L.** (2018). Neural networks-based command filtering control of nonlinear systems with uncertain disturbance. *Information Sciences*, *426*, 50–60. https://doi.org/10.1016/j.ins.2017.10.027

[13] **Wang, M. S., & Tsai, T. M.** (2017). Sliding Mode and Neural Network Control of Sensorless PMSM Controlled System for Power Consumption and Performance Improvement. Energies, 10(11), 1780. https://doi.org/10.3390/en10111780

[14] **Yilmaz, M.** (2015). Limitations/capabilities of electric machine technologies and modeling approaches for electric motor design and analysis in plug-in electric vehicle applications. *Renewable and Sustainable Energy Reviews*, *52*, 80–99. https://doi.org/10.1016/j.rser.2015.07.033

[15] **Wenping Cao, Mecrow, B. C., Atkinson, G. J., Bennett, J. W., & Atkinson, D. J.** (2012). Overview of Electric Motor Technologies Used for More Electric Aircraft (MEA). *IEEE Transactions on Industrial Electronics*, *59*(9), 3523–3531. https://doi.org/10.1109/tie.2011.2165453

[16] **Cakin, U., Kaçan, Z., Aydogan, Z. A., & Kuvvetli, I.** (2020). Initial Sizing of Hybrid Electric VTOL Aircraft for Intercity Urban Air Mobility. *AIAA AVIATION 2020 FORUM*. Published. https://doi.org/10.2514/6.2020-3173

[17] **Url-1** < https://www.mathworks.com/help/mcb/getting-started-with-mcb.html > , date retrieved 10.12.2021.

[18] **Sebastian, T., Slemon, G., & Rahman, M.** (1986). Modelling of permanent magnet synchronous motors. *IEEE Transactions on Magnetics*, *22*(5), 1069–1071. https://doi.org/10.1109/tmag.1986.1064466

[19] **Jahns, T. M., Kliman, G. B., & Neumann, T. W.** (1986). Interior Permanent-Magnet Synchronous Motors for Adjustable-Speed Drives. *IEEE Transactions on Industry Applications*, *IA-22*(4), 738–747. https://doi.org/10.1109/tia.1986.4504786

[20] **Pillay, P., & Krishnan, R**. (1988). Modeling of permanent magnet motor drives. *IEEE Transactions on Industrial Electronics*, *35*(4), 537–541. https://doi.org/10.1109/41.9176

[21] **Pillay, P., & Krishnan, R.** (1989). Modeling, simulation, and analysis of permanent-magnet motor drives. I. The permanent-magnet synchronous motor drive. *IEEE Transactions on Industry Applications*, *25*(2), 265–273. https://doi.org/10.1109/28.25541

[22] **Morimoto, S., Tong, Y., Takeda, Y., & Hirasa, T.** (1994). Loss minimization control of permanent magnet synchronous motor drives. *IEEE Transactions on Industrial Electronics*, *41*(5), 511–517. https://doi.org/10.1109/41.315269

[23] **Wijenayake, A., & Schmidt, P.** (1997). Modeling and analysis of permanent magnet synchronous motor by taking saturation and core loss into account. *Proceedings of Second International Conference on Power Electronics and Drive Systems*. Published. https://doi.org/10.1109/peds.1997.627416

[24] **Jang-Mok Kim, & Seung-Ki Sul.** (1997). Speed control of interior permanent magnet synchronous motor drive for the flux weakening operation. *IEEE Transactions on Industry Applications*, *33*(1), 43–48. https://doi.org/10.1109/28.567075

[25] **Bose, B. K.** (2002). *Modern Power Electronics and AC Drives*. Prentice Hall.

[26] **Mademlis, C., & Margaris, N.** (2002). Loss minimization in vector-controlled interior permanent-magnet synchronous motor drives. *IEEE Transactions on Industrial Electronics*, *49*(6), 1344–1347. https://doi.org/10.1109/tie.2002.804990

[27] **Xu, J. X., Panda, S., Pan, Y. J., Lee, T., & Lam, B**. (2004). A Modular Control Scheme for PMSM Speed Control With Pulsating Torque Minimization. *IEEE Transactions on Industrial Electronics*, *51*(3), 526–536. https://doi.org/10.1109/tie.2004.825365

[28] **Onoda, S., & Emadi, A.** (2004). PSIM-Based Modeling of Automotive Power Systems: Conventional, Electric, and Hybrid Electric Vehicles. *IEEE Transactions on Vehicular Technology*, *53*(2), 390–400. https://doi.org/10.1109/tvt.2004.823500

[29]**Url-2**< https://www.mathworks.com/help/physmod/sps/ug/ac6-pm-synchronous-3hp-motor-drive.html > , date retrieved 10.12.2021.

[30] **Url-3 <**http://www.mathworks.com/access/helpdesk/help/toolbox/physmod/ powersys/powersys.html>, date retrieved 10.12.2021.

[31] **Xi, X., Meng, Z., Li Yongdong, & Li Min.** (2006). On-line estimation of permanent magnet flux linkage ripple for PMSM based on a Kalman filter. *IECON 2006 - 32nd Annual Conference on IEEE Industrial Electronics*. Published. https://doi.org/10.1109/iecon.2006.347875

[32] **Alsayid, B., Daud, A.-K., & Zaidan, A.** (2012). Simulation and Digital Control of Speed for Permanent Magnet Synchronous Motor with Space Vector Modulation. European Journal of Scientific Research, 68(2), 235–245.

[33] **Hu, D., Alsmadi, Y. M., & Xu, L.** (2015). High-Fidelity Nonlinear IPM Modeling Based on Measured Stator Winding Flux Linkage. *IEEE Transactions on Industry Applications*, *51*(4), 3012–3019. https://doi.org/10.1109/tia.2015.2407864

[34] **Yadav, D., & Verma, A.** (2018). Behaviour Analysis of PMSM Drive using ANFIS Based PID Speed Controller. *2018 5th IEEE Uttar Pradesh Section International Conference on Electrical, Electronics and Computer Engineering (UPCON)*. Published. https://doi.org/10.1109/upcon.2018.8596845

[35] **Kusagur, A., Kodad, S. F., and Ram, B. V. S.** (2010). Modeling, Design and Simulation of an Adaptive Neuro-Fuzzy Inference System (ANFIS) for Speed Control of Induction Motor, *International Journal of Computer Applications*, 6(12), 29–44

[36] **P., A. A.& Punitharaji, R.** (2013). Transient Stability Enhancement of Grid by Using Fuzzy Logic Based Statcom, *IOSR JEEE*, 6(1), 6–13

[37] **Chi, S.** (2007). Position-sensorless control of permanent magnet synchronous machines over wide speed range. Thesis for the degree of Doctor, Department of Electrical and Computer Engineering, Ohio State University, Ohio

[38] **Levron, Y., Belikov, J., & Baimel, D.** (2018). A Tutorial on Dynamics and Control of Power Systems with Distributed and Renewable Energy Sources Based on the D-Q0 Transformation. *Applied Sciences*, *8*(9), 1661. https://doi.org/10.3390/app8091661

[39] **Url-4** < https://www.mathworks.com/help/physmod/sps/ref/pmsm.html> , date retrieved 10.12.2021.

[40] **Xudong Wang, Risha Na, & Ning Liu.** (2009). Simulation of PMSM field-oriented control based on SVPWM. *2009 IEEE Vehicle Power and Propulsion Conference*. Published. https://doi.org/10.1109/vppc.2009.5289523

[41] **Aydogmus, O., & Sünter, S.** (2012). Implementation of EKF based sensorless drive system using vector controlled PMSM fed by a matrix converter. *International Journal of Electrical Power & Energy Systems*, *43*(1), 736–743. https://doi.org/10.1016/j.ijepes.2012.06.062

[42] **Url-5 <** https://www.mathworks.com/help/mcb/ref/averagevalueinverter.html>, date retrieved 10.12.2021.

[43] **MathWorks** (2020). *Motor Control Blockset Getting Started Guide.*

[44] **Negnevitsky, M.** (2002). Artificial Intelligence: A Guide to Intelligent Systems, 1st ed., Addison Wesley, Pearson Education Limited.

[45] **Kumbasar, T**. (2019). Fuzzy Modeling & Control [Slides]. Retrieved from https://kontrol.itu.edu.tr

[46] **Hamarsheh, Q.** (2021). Neural Networks and Fuzzy Logic [Slides]. Retrieved from https://www.philadelphia.edu.jo/academics/qhamarsheh

[47] **Alasvandi, M., Moussavi, S., Morad, E., & Rasouli, E.** (2019). ANFIS based IMC PID Controller for Permanent Magnet DC Motor. *Proceedings of the 16th International Conference on Informatics in Control, Automation and Robotics*. Published. https://doi.org/10.5220/0007840402350242

[48] **Nour, M. & Too, S. Y. M.** (2006). Adaptive Fuzzy Logic Speed Controller with Torque Adapted Gains Function for PMSM Drive. Journal of Engineering Science and Technology, 1(1), 59–75.

[49] **Premkumar, K., & Manikandan, B.** (2014). Adaptive Neuro-Fuzzy Inference System based speed controller for brushless DC motor. *Neurocomputing*, *138*, 260–270. https://doi.org/10.1016/j.neucom.2014.01.038

[50] **Jilani, A., Murawwat, S., & Jilani, S. O.** (2015). Controlling Speed of DC Motor with Fuzzy Controller in Comparison with ANFIS Controller. *Intelligent Control and Automation*, *06*(01), 64–74. https://doi.org/10.4236/ica.2015.61008

APPENDICES

APPENDIX A: Datasheets
APPENDIX B: Schematic
APPENDIX C: Overview

APPENDIX A

HIGH POWER DENSITY

Teknic's industrial-grade NEMA 23 motors are more powerful than similarly sized motors because of the combination of fully sintered, high temperature, Neodymium-Iron-Boron magnets and an optimized stator design. This means that you can match existing performance specifications with smaller (and less expensive) motors or get more power without increasing motor size.

GREATER CONTINUOUS CAPACITY

Several innovations combine to provide more continuous motor performance. The ribbed motor housing and internal construction provide a better thermal path from the stator to free-air and the front mounting face, resulting in significantly more thermal conductivity than other motors. Additionally, the FEA-optimized electromagnetic design ensures that this motor is a more efficient converter of electrical to mechanical power (i.e., high motor constant) which means that less motor power is lost to extraneous heating.

LOW DETENT = SMOOTHER MOTION

Special attention was paid to the interaction of the rotor's magnetic field with the stator's tooth design with regard to detent (or cogging) torque. Low detent torque enables the smoothest motion possible—which minimizes motor heating and improves the motor's continuous capacity. The magnetic design also assures a sinusoidal torque constant for minimization of torque ripple when using sinusoidal vector drive

FEA DESIGNED SHAFTS

Finite element analysis is used to reduce stress concentrations on machined areas of the shaft (such as the fillet where the shaft exits the bearing assembly). This allows the use of oversized bearings without reducing shaft strength. The result is rugged, load-bearing capability.

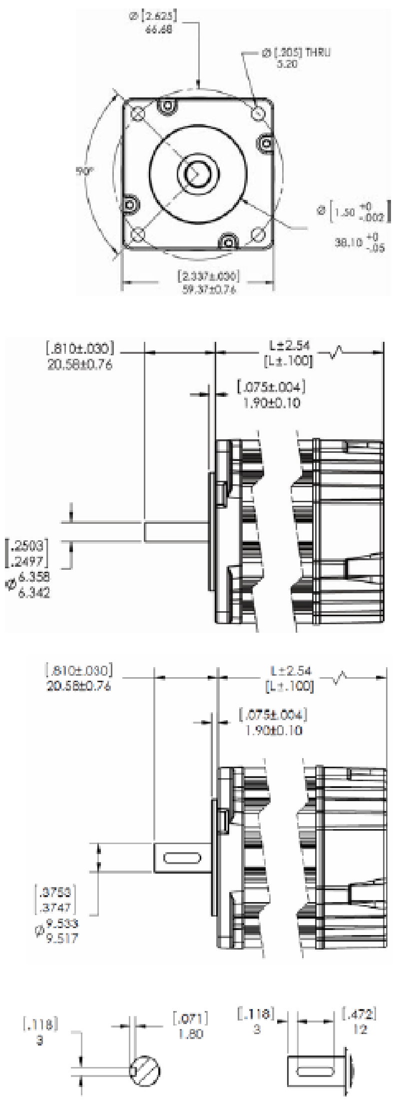

"L" Dimension

M-231x	70.94 mm	2.79 in.
M-232x	89.92 mm	3.54 in.
M-233x	108.97 mm	4.29 in.
M-234x	128.02 mm	5.04 in.

Figure A.1: Teknic 2310P motor size.

Molex® Mini-Fit Jr.™

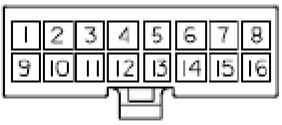

(Wire Entry View)

Mating Housing P/N:	39-01-2161	
Mating (Male) Contact P/N:	39-00-0049 (24 AWG)	39-00-0082 (16 AWG)
Crimp Tool P/N:	11-01-0198	

Pin	Color	Signal	Pin	Color	Signal
1	DRAIN x3	P DRAIN	9	16AWG BLK	PHASE R
2	N/A	N/A	10	16AWG RED	PHASE S
3	GRN	COMM S-T	11	16AWG WHT	PHASE T
4	GRN/WHT	COMM R-S	12	RED	+5VDC IN
5	GRY/WHT	COMM T-R	13	BRN	ENC I
6	DRAIN x1	E DRAIN	14	ORN	ENC B
7	BLK	GND	15	BLU	ENC A
8*	BLU/WHT	ENC A~	16*	ORN/WHT	ENC B~

** Although all terminals in the connector are populated, this signal complement is available only in motor models configured with a differential encoder*

Figure A.2: Molex-Mini-Fit connector pins.

SPECIFICATIONS		
GENERAL	Insulation Rating:	Class H, 180°C
	Motor Poles:	8
	Standard Shaft Diameter:	0.375 in., 9.5 mm
	Motor Pigtail Type:	Space saving, single-exit, DualShield™
	Motor Pigtail Length:	16 in ± 1 in., 431.8 mm ± 25.4 mm.
ENVIRONMENTAL	Shock:	2.0 G
	Vibration:	0.5 G
	Max External Deceleration:	250,000 rad/s²
	Max Case Temperature:	85°C
	Max Winding Temperature:	155°C
	Storage Temperature:	-20 to 85°C
	Humidity, non-condensing:	0-95%
	Operating Conditions:	No direct fluid wash-down or submerged use
ENCODER	Type:	Floating optical disk; single-ended or differential signals
	Resolution(s):	2000, 4000, 8000, 16000 counts/rev (post-quad)
	Index Pulse Repeatability:	± 1 count for resolutions ≥ 4,000 counts/rev³
	Current Draw, Loaded:	180mA @ 5VDC, all signals loaded with 200Ω load
	Current Draw, Unloaded:	125mA @ 5VDC
COMMUTATION	Commutation Type:	120° spaced, optical commutation sensors
MECHANICAL LOADING	Bearing Type:	Oversized, single-row, deep groove, radial with non-contacting lubrication seals.
	Bearing Life vs. Load:	Depending on the specific motor model, typical bearing life is approximately 3.2 x10⁹ to 5.0 x10⁹ revolutions (based on 5 lb axial and 25 lb radial loads, centered 1.0 inch from front bearing surface). For more detailed loading information, contact Teknic.

Figure A.3: Industrial-Grade NEMA 23 Motor family specifications.

APPENDIX B

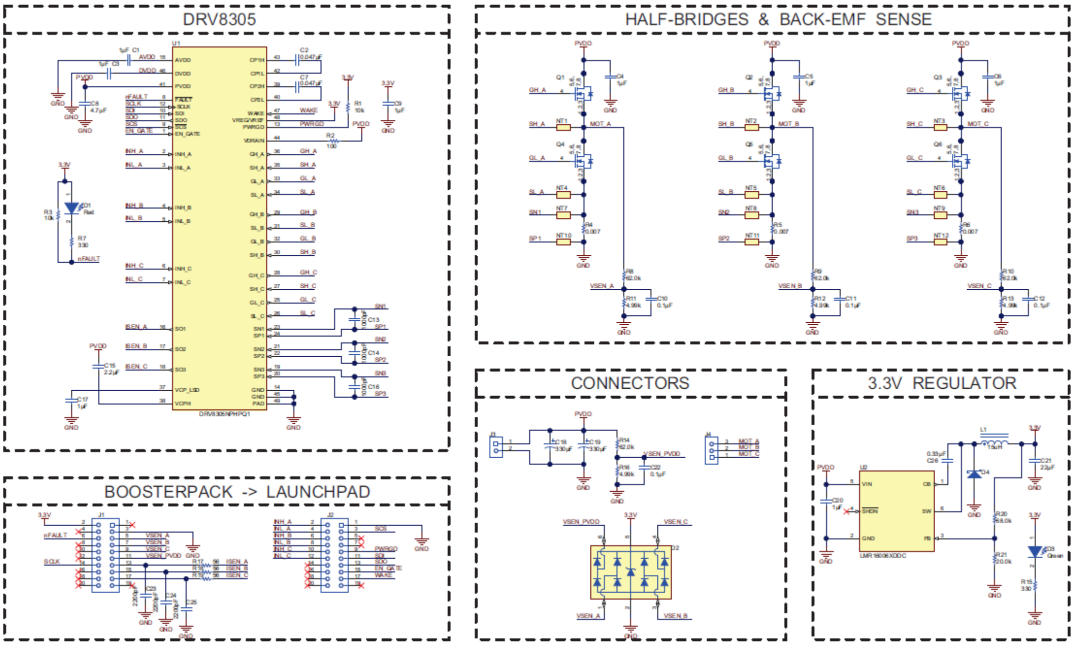

Figure B.1: BOOSTXL-DRV8305EVM schematic.

APPENDIX C

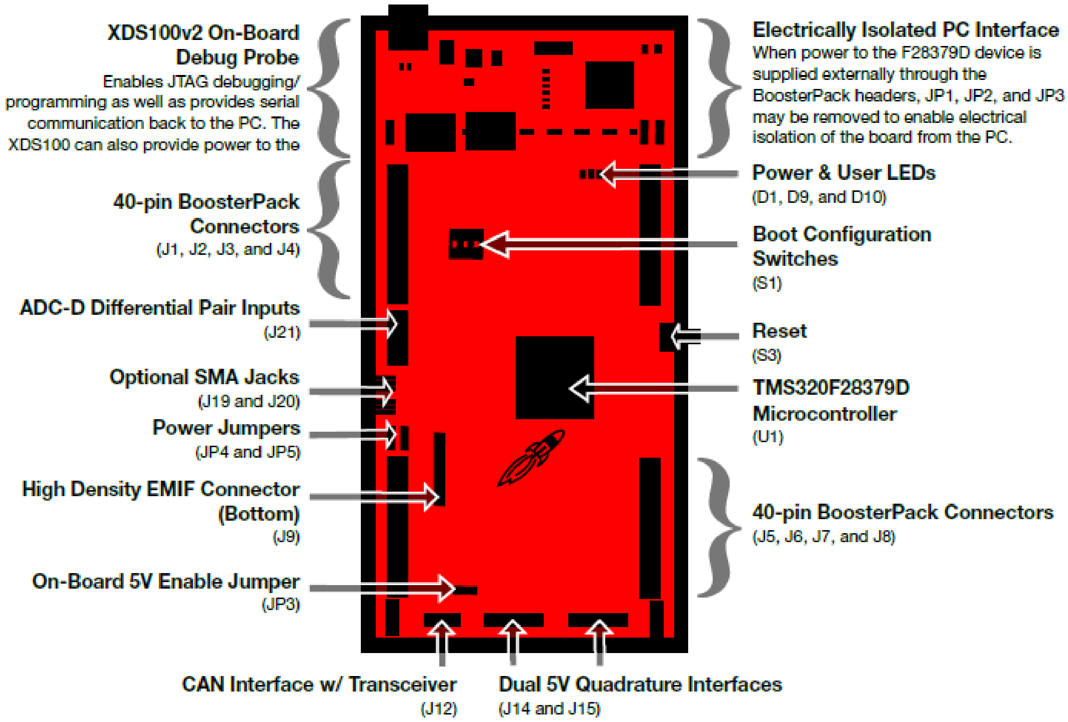

Figure C.1: LaunchXL-F28379D overview.

CURRICULUM VITAE

Name Surname : Ipek Kuvvetli

EDUCATION :

- **B.Sc.** : 2017, Istanbul Technical University, Faculty of Electrical and Electronics Engineering, Electrical Engineering Department
- **B.Sc.** : 2019, Istanbul Technical University, Faculty of Electrical and Electronics Engineering, Control and Automation Engineering Department

PROFESSIONAL EXPERIENCE AND REWARDS:

- Double Major Programme
- Honours degree(3rd) -BSc in Electrical Engineering
- Turkish Aerospace Industries (Flight Control Law Engineering)-2017,…

PUBLICATIONS, PRESENTATIONS AND PATENTS:

- **Cakin, U., Kaçan, Z., Aydogan, Z. A., & Kuvvetli, I.** 2020: Initial Sizing of Hybrid Electric VTOL Aircraft for Intercity Urban Air Mobility. *AIAA AVIATION 2020 FORUM.* Published. https://doi.org/10.2514/6.2020-3173
- **Kuvvetli, I., Tap, A.,& Ergene, L.,T.** 2021:PI Based ANFIS Controller Design for PMSM Drives. International Conference – ELECO, November 25-27, Bursa, Turkey.